SIMPLE NUMERICAL MODELS FOR FLUVIALLY-DOMINANT RIVER DELTAS

BY

MATTHEW J. CZAPIGA

DISSERTATION

Submitted in partial fulfillment of the requirements
for the degree of Doctor of Philosophy in Civil Engineering
in the Graduate College of the
University of Illinois at Urbana-Champaign, 2018

Urbana, Illinois

Doctoral Committee:

Professor Gary Parker, Chair
Professor Marcelo Garcia
Professor Jim Best
Professor Rafael Tinoco
Professor David Mohrig, University of Texas, Austin
Professor Enrica Viparelli, University of South Carolina

ABSTRACT

Morphodynamic numerical models of 2D fan deltas can predict evolution delta area and extension rates, but these models have struggled to estimate channel features such as width and depth. A re-analysis of recent bankfull hydraulic geometry data provides an empirical closure for the formative, bankfull Shields Number. This closure improves on previous models that assumed a constant value for this term or used a biased regression scheme.

By including this extra constraint, 1D models can simultaneously predict channel width and channel elevation changes, where the former is predicted based on physically-based trends of rivers near morphodynamic-equilibrium. New, juvenile channels are formed at the delta periphery and we find that young channels relate to a formative bankfull Shields number that linearly scales to our empirical relation. A new distributed Exner formulation is included that accounts for channel and floodplain elevations along with a geometric mean delta elevation. This addition allows for a basement incision modelling, which is relevant for river deltas growing into shallow, low slope basins, which commonly erode into the pre-delta surface. The incision submodel includes a below-capacity sediment transport framework and a rate-law function for cohesive sediment erosion. Hindcast model runs compared against the evolution of Wax Lake Delta, Louisiana, USA suggest the new features improve the model's ability to predict width and depth trends over a 35-year period.

A second model is introduced that investigates the effect of juvenile channels on the ability to export sediment from the delta topset. This model convolves a spatial bifurcation rate and flow losses related to juvenile channels to induce declining sediment transport down delta; the model is normalized by upstream variables and all variables are defined by only two parameters. Results are compared against volumetric changes of the Wax Lake Delta topset and the model reasonably well predicts channel properties. An exploration of parameter space for these variables indicates the conditions necessary for sediment trapping in any generic fluvially-dominant delta.

To Mom and Dad

TABLE OF CONTENTS

CHAPTER 1: INTRODUCTION

River deltas lie at the interface between a river and a receiving basin. As such, the morphology and growth rate of deltas rely on a bevy of characteristics relative to both environments [Galloway, 1975; Orton and Redding, 1993]. This type of landform is therefore a complex feature, spanning terrestrial and marine research fields. More than one third of the world's population lives within 100km of the nearest coast [Syvitski et al., 2005] and with sea level rise predicted at rates of 2.8-9.8 mm/ year [IPCC 2013], the coastline will necessarily migrate landward. Rivers are the most important and efficient mechanism for transporting terrestrial sediment to the coast [Syvitski, 2003] and, by definition, deltas are the last major terrestrial features where sediment can be sequestered. A recent map of elevation difference in the Louisiana coastline between 1932 and 2010 shows land loss everywhere – except near modern active channels [Couvillion et al., 2011]. In particular, the Atchafalaya and Wax Lake Deltas, both distributaries of the Atchafalaya River and Mississippi River, are particular hot spots for sediment deposition. This is the case, despite the fact that Wax Lake Delta only first appeared (in terms of subaerial land) in 1973 [Roberts et al., 1980; Wellner et al., 2005]. The adjacent Louisiana coastline developed by past deltaic deposits of the Mississippi River [Frazier, 1967] is now sinking. Therefore, the design of plans to maintain the coastline with impending sea level rise is directly related to our understanding of deltas; both how they develop as juvenile deltas, e.g. Wax Lake Delta, and how they respond as mature deltas, e.g. Mississippi River Delta.

The number and co-dependence of pertinent variables leads to complexity in understanding generalities in deltaic systems. Allogenic forces, i.e. those that are external to a specified deltaic system, such as land uplift/subsidence, sea level rise, or anthropogenic effects, add additional complexity. Starting with the end-member paradigms suggested by Galloway [1975], i.e. river-dominated, tide-dominated and wave-dominated deltas, the complexity of the analysis can be reduced by making assumptions regarding the delta's general environment. Syvitski and Saito [2007] establish a precedent for the development of such paradigms through mass collection of delta metrics. As expected, the river discharge (either maximum or monthly average) and marine energy (waves and tides) are significant in correlating different delta metrics. However, the comparative strength of these variables is a function of time and space. For example, at any given point in time, the relative strength of discharge must decrease basin-ward due to backwater, bifurcation, and frictional effects. Over time, the relative strength of discharge may approach that of the receiving basin (tide, waves) at the delta-basin interface. For example, Ta et al. [2002] demonstrates how the Mekong delta evolved from a tidally dominated system toward a joint tidally and wave dominated delta in the late Holocene.

The Syvitski and Saito [2007] dataset allows distinctions between relatively important, or conversely unimportant, variables. Some of these distinctions are obvious, e.g. the effect of total discharge into the delta is generally more influential toward its morphology than, for example, the wind shear during storm events. However, ancillary forces can be important in specific conditions; in congruence with the previous example, Geleynse et al. [2015] show that wind direction and magnitude can play a major role on the temporal position of the delta shoreline at Wax Lake Delta. Either numerical models must account for all the variables that affect a given process, or select based on physical insight and setting which variables or feedbacks are most necessary to get an appropriate solution. Proper modelling of all the variables can provide more detailed results, but requires more parameterization and comes at a computational cost. The time scale of morphological changes for a river ranges from a single flood event to thousands of years, so the type of model used should be selected based on the research goal.

We seek to model the evolution of a river delta, i.e. the Wax Lake Delta, over engineering (10s of years) and geologic time scales (up to 1000s of years). We focus on geometrically defined models that model delta evolution by assuming a fixed geometry of the delta accommodation space and assess a shock-condition at the delta foreset to account for new delta growth, e.g. Swenson et al. (2000). We seek to improve prediction of the most basic morphodynamic characteristics of deltas including the spatial and temporal evolution of channel width, channel depth, the number of channels, and the rate of delta growth, i.e. progradation rate. Herein, we develop several numerical models based on a 1.5D approach, which solves uniform flow or the steady, shallow water equations in one dimension along with additional equations to estimate channel width. A necessary equation to model channel width is a predictor for bankfull Shields number. Chapter 2 uses a major axis regression scheme to improve an empirical predictor for this term. Chapter 3 modifies several existing numerical models and investigates which features are necessary to reproduce historic delta morphodynamics; a key modification include a framework which accounts for incipient, juvenile channels at the delta periphery, thereby allowing the typical shoaling pattern observed in channels toward the delta/basin boundary. Chapter 4 develops a morphodynamic modelling framework that relaxes the assumption of a single, lumped channel in favor of an implicit network of identical channels. This model is solved through an analytical closure reliant on two input parameters to understand the sediment trapping efficiency as a result of channel bifurcation.

Much of our work is focused toward modelling of Wax Lake Delta, Louisiana, USA (WLD) as it provides a real-world example of a growing delta with quantifiable change over a geologically short period. This delta has been well documented in the recent past; sediment was first routed to modern-day WLD in 1941 when the Wax Lake Outlet Channel was constructed to protect nearby Morgan City, Louisiana from flooding [Wellner et al., 2005]. Roberts et al. [1997] concluded that the major building block of the young

WLD is sand, setting a precedent for the role of sand in the formation of man-made deltas through engineered diversions [Nittrouer et al., 2011]. Therefore, it represents a rich source of past measurements for model validation and an important analogue for understanding land-building processes through delta morphodynamics in other locations.

References

1. Couvillion, B. R., Barras, J. A., Steyer, G. D., Sleavin, W., Fischer, M., Beck, H., & Heckman, D. (2011). Land area change in coastal Louisiana from 1932 to 2010.
2. Frazier, D. E., 1967, Recent deltaic deposits of the Mississippi River: their development and chronology: Gulf Coast Association of Geological Societies Transactions, v. 27, p. 287-315
3. Galloway, W.E., 1975. Process Framework for Describing the Morphologic and Stratigraphic Evolution of Deltaic Depositional Systems, in Deltas, M.L. Broussard, ed., Houston Geological Society, 87-98.
4. Geleynse, N., Hiatt, M., Sangireddy, H., & Passalacqua, P. (2015). Identifying environmental controls on the shoreline. *Journal of Geophysical Research:Earth Surface*, *120*, 877–893. http://doi.org/10.1002/2014JF003408
5. IPCC. (2013). Climate change 2013: The physical science basis.*Report*, U.N. Intergovernmental Panel on Climate Change, http://www.climatechange2013.org/
6. Nittrouer, J. A., Best, J. L., Brantley, C., Cash, R. W., Czapiga, M., Kumar, P., & Parker, G. (2012). Mitigating land loss in coastal Louisiana by controlled diversion of Mississippi River sand. *Nature Geoscience*, *5*(8), 534.
7. Roberts, H. H., Adams, R. D., & Cunningham, R. H. W. (1980). Evolution of Sand-Dominant Subaerial Phase, Atchafalaya Delta, Louisiana. AAPG Bulletin, 64(2), 264–279.
8. Roberts, H. H., Walker, N., Cunningham, R., Kemp, G. P., & Majersky, S. (1997). Evolution of sedimentary architecture and surface morphology: Atchafalaya and Wax Lake Deltas, Louisiana (1973-1994). Gulf Coast Association of Geological Societies Transactions, 47, 477–484.
9. Swenson, J. B., Voller, V. R., Paola, C., Parker, G., & Marr, J. G. (2000). Fluvio-deltaic sedimentation: A generalized Stefan problem. European Journal of Applied Mathematics, 11(5), 433–452.
10. Syvitski, J. P., Peckham, S. D., Hilberman, R., & Mulder, T. (2003). Predicting the terrestrial flux of sediment to the global ocean: a planetary perspective. *Sedimentary Geology*, *162*(1-2), 5-24.
11. Syvitski, J. P., Vörösmarty, C. J., Kettner, A. J., & Green, P. (2005). Impact of humans on the flux of terrestrial sediment to the global coastal ocean. *Science*, *308*(5720), 376-380.
12. Syvitski, J. P. M., & Saito, Y. (2007). Morphodynamics of deltas under the influence of humans. Global and Planetary Change, 57(3-4), 261–282. http://doi.org/10.1016/j.gloplacha.2006.12.001

13. Ta, T.K.O., Nguyen, V.L., Tateishi, M., Kobayashi, I., Saito, Y., Nakamura, T., (2002). Sediment facies and late Holocene progradation of the Mekong River delta in Bentre Province, southern Vietnam: an example of evolution from a tide-dominated to a tide- and wave dominated delta. Sedimentary Geology 152, 313–325.
14. Wellner, R., Beaubouef, R., Van Wagoner, J., Roberts, H., & Sun, T. (2005). Jet-plume depositional bodies—the primary building blocks of Wax Lake Delta.

CHAPTER 2 : BANKFULL DEPTH VERSUS SLOPE AND GRAINSIZE – RESOLVING A MAJOR DISCREPANCY

Abstract

Many characteristics of alluvial rivers, including hydraulic geometry and sediment transport during periods of morphological activity, can be related to the bankfull Shields number. Recent papers have used regression analysis on large data sets of bankfull hydraulic geometry to formulate a predictive relation for bankfull Shields number as a function of reach-averaged channel slope and characteristic bed grain size. These results show different regression fits; the relationship for bankfull Shields stress is therefore still ambiguous. We propose a new relation via multivariate major axis regression, a symmetric, error-in-variables regression scheme, which improves on previous attempts by introducing error in both the dependent variable and independent variables. We discuss the use of typical ordinary least squares, Bayesian, and error-in-variables regressions to inform the use of regression statistical methods to quantify hydraulic geometry. The results reported here back previous claims that bankfull shear velocity is rather invariant to median bed material.

Introduction

The mobility of sediment in rivers is classically characterized in terms of a dimensionless number known as the Shields number (e.g. Garcia, 2008). We define the Shields number τ^* as

$$\tau^* = \frac{\tau_b}{\rho g R D_{50}} \quad (1)$$

where τ_b denotes bed shear stress (Pa), ρ denotes water density (kg/m^3), g denotes gravitational acceleration (m/s^2), R denotes the submerged specific gravity of sediment (-), and D_{50} denotes the median size of the bed sediment (m). The Shields number appears in many sediment transport equations (e.g. see Garcia, 2008). Here we focus on estimating the bankfull Shields number τ^*_{bf} of a self-formed alluvial river channel, i.e. the Shields number at incipient conditions for the flow to leave the confines of its channel and spill onto its floodplain. The bankfull condition of interest here is representative of reach-scale river morphology, rather than the specific details of local flow and channel conditions.

River structure is classically characterized through hydraulic geometry relations, as first introduced by Leopold and Maddock (1953) and Leopold and Wolman (1957). These relationships characterize general trends in regard to river channel structure, as illustrated by e.g. Parker (1978), Dade and Friend (1998), Mueller et al. (2005) and Phillips and Jerolmack (2016). Among such relations, empirical predictors of bankfull Shields number in particular have proved useful in a variety of contexts, including sediment management (Parker et al., 1998), river restoration (Wilkerson and Parker, 2011), calculation of meander bend migration (Eke et al. 2014), estimation of paleochannel characteristics (Paola and Mohrig 1996) and estimation of "bankfull" discharge in submarine channels (Konsoer et al. 2013).

The wide applicability of bankfull Shields number motivates the quest for the most accurate predictive relation that can be obtained from available data. Such a relation is normally cast in dimensionless form in order to maximize generality. Recently two such predictors have been proposed. The predictor of Trampush et al. (2014) was developed with (among other things) the reconstruction of paleochannel hydraulics in mind. The predictor of Li et al. (2015, 2016) was developed for (among other things) the modeling of self-formed river width, in the context of the response of river long profile to sea level rise. It was also used by Eke et al. (2015) in a 2D model of river meander migration.

The two relations of Trampush et al. (2014) and Li et al. (2015, 2016) were developed using partially overlapping data sets. They are broadly similar in structure, with bankfull Shields number depending on channel slope and dimensionless characteristic bed material grain size. They are different, however, in one essential way. In the relation of Trampush et al. (2014), bankfull Shields number is nearly independent of bed slope, so that it can be estimated for paleochannels using a characteristic grain size

alone. In the relation of Li et al. (2015, 2016; the latter provides a modest correction to the former), however, bankfull Shields number depends on both characteristic grain size and channel slope. The goals of this paper are to: 1) provide a thorough re-analysis to resolve this discrepancy, 2) develop a revised closure for bankfull Shields number relative to slope and grain size, and 3) provide an interpretation of the resulting relationship in the context of previous and current methods.

Relations of Trampush et al. and Li et al.

In both the work of Trampush et al. (2014) and Li et al. (2015, 2016), a large data set of bankfull hydraulic geometry measurements was used to obtain regression-based predictors for relations for bankfull Shields number. Li et al. (2015, 2016) used a data set modified from Wilkerson and Parker (2011) (W&P); 11 sets are removed from, and 16 sets are added to the W&P dataset resulting in 230 river reaches with characteristic bed material grain size ranging from fine sand to coarse gravel. Trampush et al. (2014) used a data set with 541 river reaches that includes 207 points from the Wilkerson and Parker (2011) data set and 334 more reaches pertaining to gravel-bed rivers. One potential explanation for the difference in regression results is the differences in the data sets themselves.

The dimensionless variables in question can be evaluated through field measurement of three variables that relate to the basic structure of river channels: bankfull depth H_{bf}, reach-averaged bed slope S, and reference grain size D_{50} (median bed material grain size). Bankfull bed shear stress $\tau_{b,bf}$, is estimated using the assumptions of normal flow and of a wide rectangular channel, respectively;

$$\tau_{b,bf} = \rho g H_{bf} S \tag{2}$$

Between (1) and (2), bankfull Shields number can be estimated as

$$\tau^*_{bf} = \frac{H_{bf} S}{R D_{50}} \tag{3}$$

The Shields number along with bankfull water and sediment discharge directly relate to self-formed river channel structure. (Parker, 2004, Parker et al. 2007, Wilkerson and Parker, 2011). The estimate of bankfull Shields number given by eq. (3) is seen to require estimates of H_{bf}, S, and D_{50}. Here we relate this Shields number to bed slope S and grain size D_{50} .For the sake of generality, we render grain size D_{50} dimensionless as follows;

$$D_* = \left(\frac{Rg}{\nu^2} \right)^{1/3} D_{50} \tag{4}$$

The predictors for bankfull Shields number presented in Li et al. (2015, 2016) and Trampush et al. (2014) are of identical form, but have substantially different dimensionless coefficients and exponents. The equations in question can be expressed in either of the following equivalent forms:

$$\tau_{bf}^{*} = \lambda_0 S^{\lambda_1} D_{*}^{\lambda_2} \tag{5}$$

$$\log \tau_{bf}^{*} = \gamma_0 + \gamma_1 \log S + \gamma_2 \log D_{*} \tag{6}$$

where

$$\lambda_0 = 10^{\gamma_0}, \quad \lambda_1 = \gamma_1 \quad , \quad \lambda_2 = \gamma_2$$

In evaluating these relations, submerged specific gravity R is assumed to be 1.65, i.e., the value for quartz in water at the Earth's surface); gravitational acceleration g is set to 9.81 m/s^2; and kinematic viscosity ν is assumed to be the value for clear water at 20°C, i.e. 1.0^{-6} m^2/s. The values of these coefficients as presented in each paper are listed in Table 2-1; they are the direct values of Li et al. (2016) (column 4), and the values of Trampush et al. (2014) translated into the forms of Eq. (5) (column 1). The results from these papers along with data from Trampush et al. (2014) are shown in Figure 2-1.

Table 2-1: Regression results of Eq. (5) using previous methodologies applied to two data sets.

Coefficient	Trampush et al. (2014) Methodology		Li et al. (2015, 2016) Methodology	
	Tr. Data[*,†]	W&P[‡] Data	Tr. Data[†]	W&P Data
λ_0	17.4	23.9	613	502
λ_1	0.083	0.099	0.513	0.434
λ_2	-0.767	-0.783	-0.934	-0.951

[*] Regression values from Trampush et al. (2014), then carried into form of Eq. (5)
[†] Tr. Data from Trampush et al. (2014)
[‡] W&P Data from Wilkerson and Parker (2008); data set used by Li et al. (2015, 2016)

As seen from the above, the relation for bankfull Shields number presented in either paper is fully dimensionless. However, the papers used different methods. Li et al. (2015) first arranged the parameters into the three dimensionless terms contained in Eq. (5), and then performed a multivariate ordinary least squares linear regression in log (base 10) space. Trampush et al. (2014), on the other hand used bankfull depth (H_{bf}), median grain size diameter (D_{50}), and reach-averaged bed slope (S) as primary variables for regression. They then performed a Bayesian analysis, nominally equivalent to ordinary least squares (OLS) linear regression in logarithmic space, to determine log(S) as a function of log(H_{bf}) and log(D_{50}). The result can then be algebraically manipulated in a straightforward way into the form of Eq. (5).

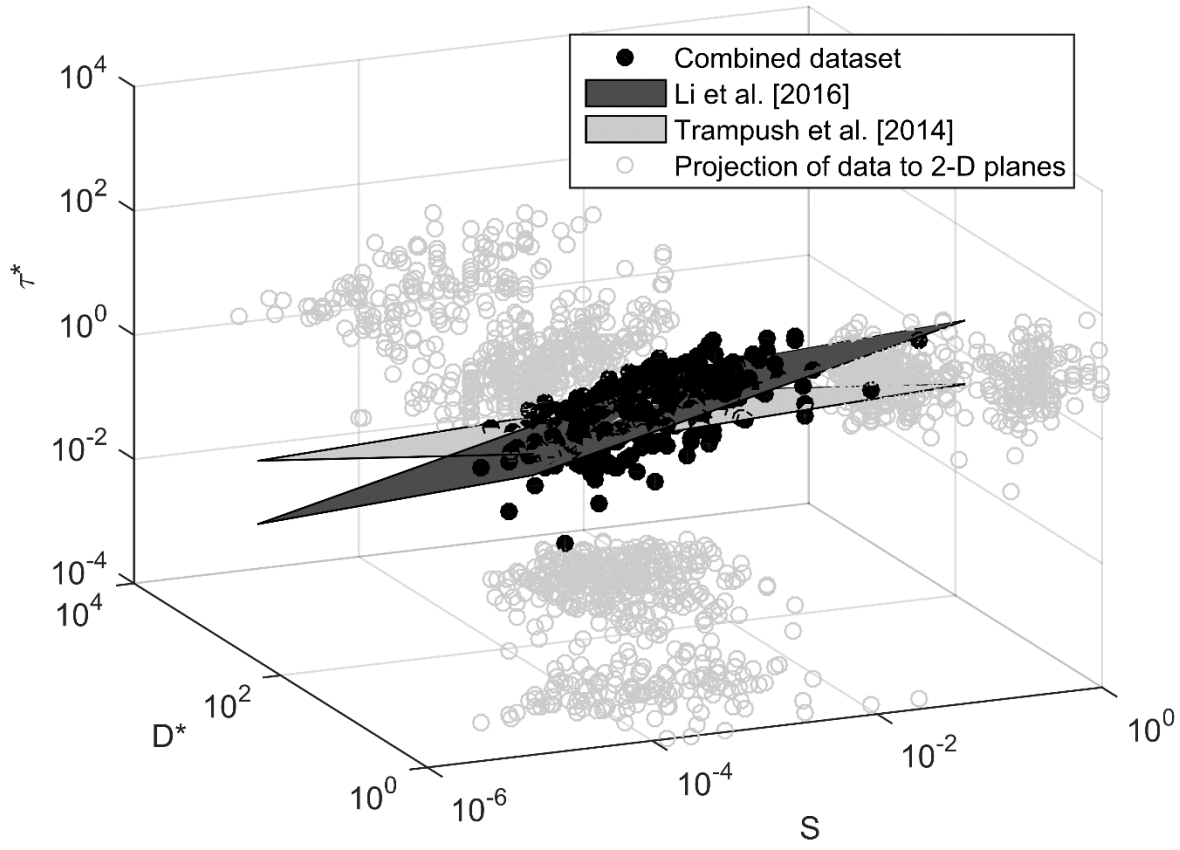

Figure 2-1: Comparison of results from Trampush et al. (2014) and Li et al. (2016) using the data set from Trampush et al. (2014). Filled planes are computed from relations presented by Trampush et al. (2014) and Li et al. (2016). Data are plotted in black solid circles; the hollow gray circles are projections of the data onto each of the 2-D planes.

Thus Trampush et al. (2014) started from a model of the core variables S, H_{bf}, and D_{50}, as in Eq. (7).

$$Log\, S = \alpha_0 + \alpha_1 Log\, D_{50} + \alpha_2 Log\, H_{\mathrm{bf}} \tag{7}$$

They used this form, in part, to develop a predictive relationship for paleoslopes versus measureable quantities in the rock record. Li et al. (2015, 2016) regress on the dimensionless parameters, as in Eq. (6).

The regression form used by Li et al. (2015, 2016) induces some spurious correlation, since D_{50} and S are contained in the definition of τ^*_{bf} (Eq. 3). Thus, these two parameters appear on both sides of the regression relation (Eqs. (5) and (6)). However, the authors compared their regression against a similar regression free of spurious correlation to find similar results and concluded that any potential effects of spurious correlation was minimal. However, because the Trampush et al. (2014) parameterization of Eq.

(7) does not have any direct potential for spurious correlation, it will be used in the rest of this manuscript.

Here we isolate: 1) effects of the data set; 2) difference in regression scheme; 3) methodology, i.e. Bayesian OLS multivariate linear regression of Trampush et al. (2014) versus frequentist OLS linear regression of Li et al. (2015, 2016); and 4) effect of the order of regression (in relation to the core components).

While our results have implications for predicting paleoslopes, this manuscript will focus on the trends in relationship between the three dimensionless parameters, which is of first order importance in predicting self-formed channel morphodynamics, e.g., Kim et al. (2009).

Methodology: Discrepancy in the Order of Regression

Trampush et al. (2014) used a Bayesian approach, in which they assumed that the prior distributions for coefficients α_0, α_1, and α_2 (Eq. 7) and an error term are normally distributed. This method results in a posterior probability distribution of values for each coefficient. The mode of the posterior distribution is the maximum a posteriori (MAP), which represents the most likely value for each of the regressed coefficients. Trampush et al. (2014) used the median of the posterior distribution, which is equivalent to the mode when the posterior distribution is normally distributed. The frequentist method of Li et al. (2015, 2016) results in a single value for each coefficient that reduces the cumulative sum of square residuals between data points and their respective predicted value. Here this is referred to as the least square error (LSE), equivalent to the maximum likelihood estimator (MLE) when data are normally distributed (Bingham and Fry, 2010). This equivalence is significant because the logarithmic-transformed variables $\log(H_{bf})$, $\log(S)$, and $\log(D_{50})$ are all approximately normally distributed (Trampush et al. 2014), so the Li et al. (2015, 2016) method should produce the MLE in the course of computing LSE. Additionally, MLE and MAP are closely related as both result in the most likely estimator. MAP implies a Bayesian scheme with assumed prior distributions for each of the coefficients being regressed. Therefore, if prior distributions are uniform, i.e. all possible outcomes are initially equally likely, then MAP and MLE are equivalent. The same result can be achieved if data overwhelm any effects of the priors on the results (Hoff, 2009). Trampush et al. (2014) use a "very wide normal distribution" as their prior distributions. If this distribution approaches uniformity, then it should be expected that the methods of Trampush et al. (2014) and Li et al. (2015, 2016) would both produce the same result equivalent to the MLE result, but as previously noted, this is not the case. We elaborate on the reasons for this below.

An alternative explanation could relate to the order of regression. Trampush et al. (2014) specify their regression function as:

$$S = f\left(H_{bf}, D_{50}\right) \tag{8}$$

The form in Li et al. (2015), on the other hand, is $\tau^*_{bf} = f(S, D^*)$. It can be recast in the same form as Trampush et al. (2014):

$$\tau^*_{bf} = \frac{H_{bf} S}{R D_{50}} = \beta S^m D_*^n \tag{9}$$

thus

$$H_{bf} = R\beta S^{m-1} D_*^n D_{50} \tag{10}$$

or in general, since H_{bf} is on only one side,

$$H_{bf} = f(S, D_{50}) \tag{11}$$

The diverging methodologies of these two papers can be summarized into three categories: 1) use of Bayesian vs. Frequentist regression techniques, 2) different data sets, and 3) different order of regressions.

As noted above, in this particular instance, Bayesian and frequentist LSE regressions should be equivalent. A typical OLS frequentist multivariate regression carried out in form of Eq. (7) and shows identical results to the median of Bayesian regression of the same form (Trampush et al. 2014). As we are concerned only with the general trends as identified by median or mean regression coefficients here, frequentist least-squares regression techniques can be taken as acceptable moving forward.

A second step concerns the effects of the difference in data sets. Table 2-1 compares results of Eq. (5) via the methodologies of Li et al. (2015, 2016) and Trampush et al. (2014) against both data sets. The results in Column 2 of Table 2-1 differ modestly from those in Column 4 of Table 2-1, indicating that the data sets, while overlapping, are different enough to result in differing regression results. However, Table 2-1 makes it clear that the contrast between results of each paper cannot be attributed predominantly to different data sets. The largest differences clearly arise from the regression details and not through the data.

As a third step, we look at the effect of the order of regression on the coefficients ultimately obtained for the final relation, Eq. (5), through algebraic manipulation from two different initial regressions. The initial regressions use either H_{bf} or S as the dependent or response variable; S is the response variable in Eqs. (7) and (8), and H_{bf} is the response variable in Eqs. (11) and (12):

$$Log\, H_{bf} = \beta_0 + \beta_1 Log\, D_{50} + \beta_2 Log\, S \tag{12}$$

As the methodology and form of regression are set, this isolates the effect of the variable order on coefficient values in Eq. (5) through regression and algebraic manipulation of Eq. (7) and Eq. (12), respectively. Table 2-2 presents these results compared with results of Li et al. (2016) (second column) and an equivalent form of Trampush et al. (2014) (third column).

Table 2-2: Results for Eq. (5) from different initial regressions, i.e. S versus D_{50} and H_{bf} and H_{bf} versus S and D_{50}.

		Eq. (5) results via initial regression:			
		Eq.(7) – $S = f(H_{bf},D_{50})$		Eq. (12) – $H_{bf} = f(S,D_{50})$	
Coefficient	Li et al. (2016) Result	Tr. Data*	W&P Data	Tr. Data	W&P Data
λ_0	502	17.4	23.9	598.9	507.5
λ_1	0.434	0.083	0.099	0.51	0.43
λ_2	-0.951	-0.767	-0.783	-0.93	-0.95

* Values taken directly from Trampush et al. (2014); this result is equivalent to Eq. 8 in their paper.

Table 2-2 implies that the order of regression, i.e. the choice for dependent variable, has a significant impact on the regressed coefficients in the form of Eq. (5). The Trampush et al. (2014) methodology can, as a reasonable approximation, replicate the results of Li et al. (2015, 2016) when performing the initial regression on Eq. (12) rather than Eq. (7), as done in their paper. Regardless of the data set, regressing S versus H_{bf} and D_{50} yields coefficients in Eq. (5) that are substantially different than those obtained from regressing H_{bf} versus S and D_{50}. These results do not indicate, however, which form, if either, provides the most appropriate representation of the data. However, for situations where a response variable can be selected, the regression relation should be set up to solve for this variable.

As the Trampush et al. (2014) dataset does not include the full W&P dataset, we make a modified dataset that includes non-W&P data from Trampush et al. (2014) plus the Li et al. (2015) data; this data is used for regressions given below,, and is referred to as the combined dataset.

Results with Multivariate Major Axis Regression

The regressions from Li et al. (2015, 2016), Trampush et al. (2014), and the preceding examples shown herein use some equivalent of Ordinary Least Squares (OLS) regression, which minimizes the sum of vertical (y-axis) squared residuals as the objective function. There are, however, several alternative techniques. Major Axis Regression (MA) and Reduced Major Axis (RMA) regression are two forms of Error-In-Variables (EIV) regression that are typically used where significant error exists in both the dependent and independent variables, e.g. McArdle (2003).

Parker et al. (2007) and Wilkerson and Parker (2011) have performed regressions on bankfull variables that are similar to the ones given here. They intentionally chose to use OLS instead of Reduced Major Axis (RMA) regression. Parker et al. (2007) justified this by noting that RMA method fails when there is poor correlation between the dependent variable and independent variables, i.e. $y \cong x^0$. In fact, coefficients in an EIV regression can never equal zero (McArdle 1988); Parker et al. (2007) show this in a similar example. Since RMA was not appropriate for the specific example of bankfull discharge as a function of bankfull depth, the authors chose to use OLS regressions exclusively for consistency.

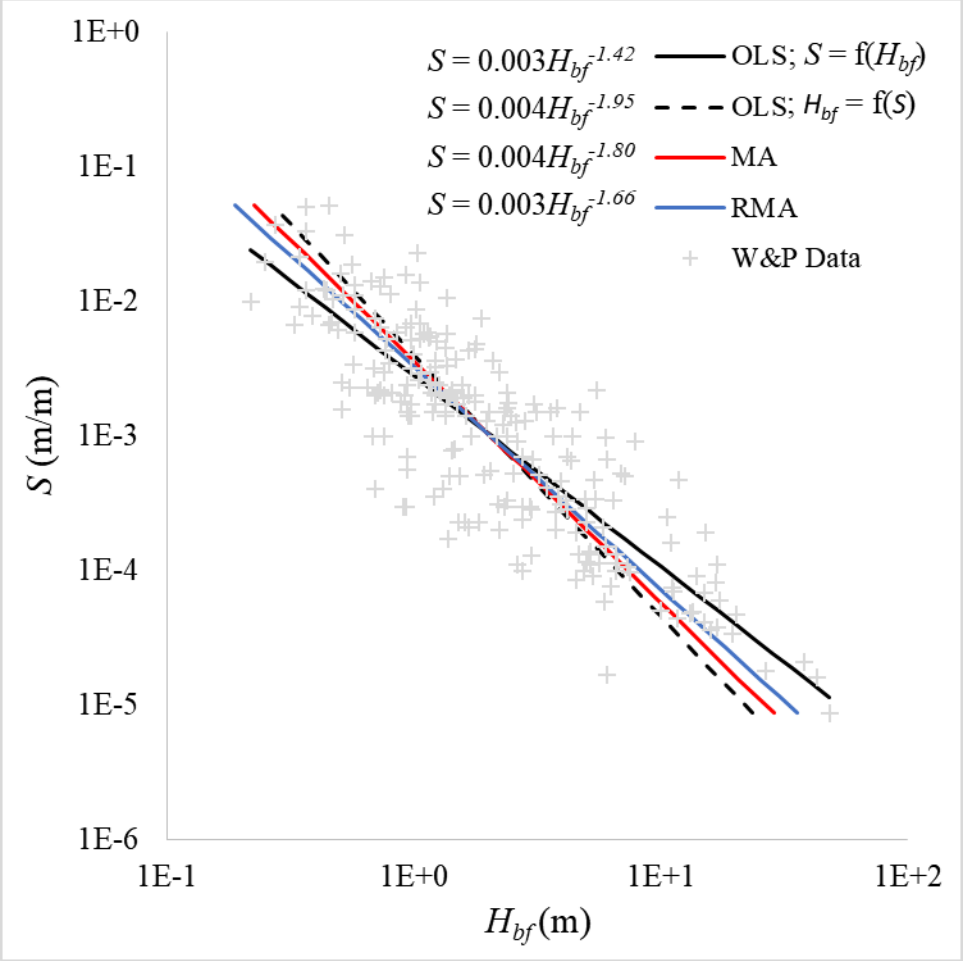

Figure 2-2: Example plot of bankfull depth H_{bf} versus reach-averaged bankfull slope, S, showing regression results for typical Ordinary Least Squares and Error-in-Variables techniques. Data set from Wilkerson and Parker (2011), denoted here as W&P; the same data were used in Li et al. (2015, 2016).

In order to explore this issue, and for purposes of comparison, a form simplified to bivariate regression relating S and H_{bf} is shown in Figure 2-2, above. In this example calculation, the data set consists of values of S and H_{bf} from the Wilkerson and Parker (2011) data set with one regressed against another. The figure includes two OLS regressions, i.e. for $S = f(H_{bf})$ and $H_{bf} = f(S)$, and two types of EIV regressions,

RMA and MA regression. While OLS regression uses an objective function that minimizes the sum of vertical residual squares, MA minimizes the sum of orthogonal residual squares, and RMA minimizes the sum of triangular areas computed through the product of vertical and horizontal deviations from the regressed line. OLS regression tends to bias towards a more nearly horizontal slope (McArdle, 2003); the steeper OLS regression line would become more horizontal if the axes were inverted.

In Figure 2-2, it can be seen that the order of regression is important for OLS regression; the result for S versus H_{bf} is substantially different than the transformed result for H_{bf} versus S. The order of regression plays no role in the result for MA and RMA; MA uses orthogonal distance, which is equivalent irrespective of regression order, and RMA is computed from a combination of both OLS results. In addition, the result for MA is close to that for RMA, and both are bracketed by the two OLS results.

Based on Figure 2-2, a central question becomes whether EIV techniques like RMA or MA are more appropriate than OLS techniques for the stated goal of quantifying the relationship between τ^*_{bf}, S, and D^* in the form of Eq. (5). Smith (2009) discusses the situations where RMA should be selected over OLS regression and comments on the implied distribution of error in each regression type. It is noted therein that OLS regressions imply asymmetry that depends on the selection of the dependent variable, reflecting our findings presented in Table 2-2. The author concludes that OLS should be considered the baseline regression scheme, but RMA is more appropriate when, for example, the selection of variable seems arbitrary or the objective is to define a mutual, codependent relationship underlying the reaction between variables. We argue that both these conditions apply to a regression between H_{bf}, S, and D_{50}, and indeed EIV techniques provide symmetrical solutions (e.g. McArdle (1998), McArdle, (2003), Smith (2009)), so rectifying the divergence in past solutions for Eq. (5).

For further analysis, we thus adopt the Multivariate Major Axis (MA) regression applied through principal component analysis regression. For the case of regression with three variables, the first principal component hyperplane aligns with a line that minimizes the orthogonal distance of the data to the hyperplane axis. Therefore, this line is equivalent to the MA objective function that minimizes the sum of squared perpendicular distance between points and the regressed line (McArdle, 1988). We use the MA method in part because implementation of this method for multiple regression is quite simple, whereas a closed form of multivariate RMA is only feasible under certain conditions (Goodman and Tofallis, 2003). However, it must be noted that assumptions differ among OLS, RMA, and MA. First, as previously noted, both EIV regressions (MA and RMA) are symmetric as they include error on both sides of the regression model, while OLS regressions have only one error term. MA assumes that the magnitude of errors in the dependent and independent variables are equivalent. RMA uses a ratio relative to the variances on dependent and independent variables. For MA, this ratio is equal to one because error values

for dependent and independent variables are assumed identical and because the ratio for OLS is constrained to be either 0 or ∞ (McArdle 1988).

In our analysis, variables are mean-centered prior to regression. As a preliminary step, we also tested several other conditions that include interaction terms, i.e. the product of independent variables, as well as different variable treatments, including variable standardization. The interaction variables $H_{bf}D_{50}$ and SD_{50} are small in OLS regressions, irrespective of the regression order, but these terms may become significant when performed in MA regression. Further details are included in the Appendix.

In Table 2-3, we show the results for the coefficients in Eq. (5) obtained by applying MA to Eqs. (7) or (12) (same result). The MA regressions include bias correction for log-transformed variables by applying a factor relative to the mean square error of regressed variables (Newman, 1993). Table 2-3, using the combined data set, shows a useful result. In Eq. (5), i.e. $\tau_{bf}^{*} = \lambda_0 S^{\lambda_1} D_{*}^{\lambda_2}$, the value of slope exponent λ_1 (0.365) falls between the Trampush (0.083) and Li (0.434) values, and λ_2 (-0.876) also falls between the Trampush (-0.767) and Li (-0.951) values. Similarly to Figure 2, the MA multivariate regression is bounded by the two OLS multivariate regressions offered by Trampush et al. (2014) and Li et al. (2015, 2016). The MA result is given below, and is plotted in Figure 3:

$$\tau_{bf}^{*} = 182 S^{0.365} D_{*}^{-0.876} \tag{13}$$

Three factors argue for the MA results as being superior to past OLS results: 1) the MA coefficients in Table 2-3 are similar for both data sets; 2) the results are independent of the order of regression, i.e. regressing from Eq. (7) versus Eq. (12); and 3) as shown in Figure 2-2, MA is bracketed by the two OLS results obtained by reversing the dependent and independent variable.

Table 2-3: Coefficients for relation noted in Eq. (13).

Coefficient	Combined Data
λ_0	182
λ_1	0.365
λ_2	-0.876

The coefficient of determination R^2 and root mean square error (RMSE) for each regression form are included in Table 2-4. In that table, RMSE is seen to be minimized with MA regression, while R^2 is seen to be similar to past OLS regression results. Results from Eq. (7) are algebraically manipulated to Eq. (12) , so as to solve for $\log(H_{bf})$. The correlation coefficient, R^2, is computed after this translation but has an

RMSE value comparable to values in Table 2-4 for the case where RMSE is computed directly from Eq. (7).

Table 2-4: Comparison of Root mean square error (RMSE) and R^2 values with OLS and MA regressions.

	OLS		MA
	$S = f(H_{bf},D_{50})$ Regression	$H_{bf} = f(S,D_{50})$ Regression	
RMSE	0.322	0.245	0.211
R^2	0.376	0.640	0.621

The relation in Eq. (13) is plotted in D_* vs. τ^*_{bf} space along discrete slope horizons ranging from 10^{-6} to 10^{-1} in Figure 2-3. Data from the combined dataset is separated between the slope horizons and included below.

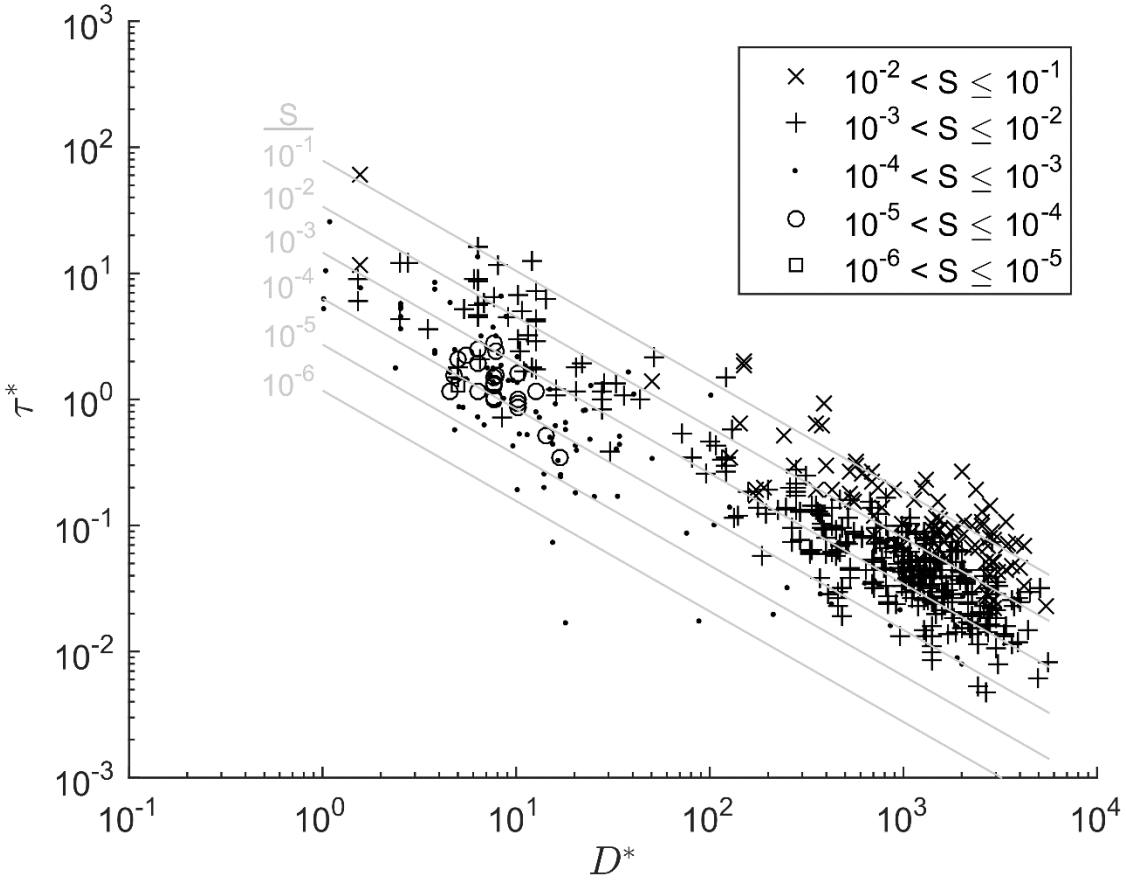

Figure 2-3: Results from Eq. (13) are plotted with the Trampush et. al [2014] dataset. The data is segmented by bed slope ranges, and relation results are presented for specified values of slope. This figure suggests that an order of magnitude change in slope results in a change in τ^*_{bf} that is much less than an order of magnitude. To read this figure for a predicted τ^*_{bf}, find a selected value of D^* and follow a vertical path to the appropriate slope horizon as labeled in the legend, and then follow a horizontal path to the τ^*_{bf} value on the y-axis. The same result can be computed directly from Eq. (13) as well.

Discussion

The MA regression is more appropriate for statistical inference than the OLS regression, as the former reduces bias in estimation of the data trends. However, MA only shows slight improvement in the magnitude of RMSE. While there are modest differences between the OLS regressions and the MA result presented herein (Tables 2-4 and 2-5), these differences would be amplified when extrapolating beyond the bounds of the regressed data set (Smith 2009).

The symmetric regression obtained with MA lies between OLS results presented by the two papers, but has exponents on slope *S* and dimensionless grain size *D** that are closer to the exponents presented by Li et al. (2016). The new MA results slightly weaken the claim of Li et al. (2015, 2016) that bankfull shear velocity is nearly independent of grain size. Li et al. (2016) report normalized bankfull shear velocity as Eq. (14) below; note that $\tilde{u}_{bf}^{*} \sim D_{*}^{0.0245}$. The modified versions of Eq. (14) obtained through MA regression takes the form of Eq. (15) below for combined data set.

Li et al. (2016) result:

$$\tilde{u}_{bf}^{*} = \frac{u_{bf}^{*}}{\left(Rg\nu\right)^{1/3}} = 22.4\,S^{0.217} D_{*}^{0.0245} \tag{14}$$

MA regression with combined dataset:

$$\tilde{u}_{bf}^{*} = 13.5\,S^{0.183} D_{*}^{0.062} \tag{15}$$

Note that the exponent on D_{*} has increased from 0.0245 to 0.062.

The regression relation of Trampush et al. (2014) for Eq. (5), i.e. $\tau_{bf}^{*} = \lambda_0 S^{\lambda_1} D_{*}^{\lambda_2}$ suggests that the role of slope S is very weak in the relation for τ_{bf}^{*}. In this relation, the exponent on *S* (λ_1 = 0.083) is significantly smaller than than the exponent on D_* (λ_2 = -0.737); the ratio of these exponents has magnitude $|\lambda_1/\lambda_2|$ = 0.11. The MA regression has the same trend for the exponents of D_* and *S*, but the difference is less extreme. In the case of MA regression, the same ratio has magnitude $|\lambda_1/\lambda_2|$ = 0.42, so the role of slope cannot be considered completely negligible.

However, as illustrated in Figure 3, there is still significant scatter in the results, similar to the results of past research. Bankfull hydraulic geometry has historically exhibited significant scatter in predictive relations, going back to Leopold and Wolman (1953). Li et al. (2015) suggest the scatter could relate to a factor not included in the regressions, i.e. bank material and, implicitly, the bank strength resisting bank

erosion. Pfeiffer et al. (2017) proposed that this scatter could be related to sediment supply to the river. The physical interpretation of this scatter therefore remains an open question. Indeed, it cannot be characterized by the regression scheme itself. In actuality, the presence of scatter is the crux of the issue addressed by this paper. As the variance in the covariates approaches zero, the regression results become invariant to the regression method (McArdle, 2003). The MA regression reduces bias so as to give a better estimate of the average trend within the scattered dataset. However, a more accurate regression could result from an appropriately expanded data set as well.

The final relations presented herein can be applied directly within numerical models to characterize general trends of streamwise variation of channel depth, width, grainsize and slope (either bed slope or water surface slope), as in e.g. Parker et al. (2007) and Li et al. (2015). Scatter in the dataset does not invalidate clear general trends. However, when applying our relations to a specific river, it would be more appropriate to use reference values from data of the given channel as the anchor for the general trends of a larger data set, as in Li et al. (2015). Channel evolution predicted through this method converges to the predictions of Eq. (13) as the selected reference values move closer to the regressed surface represented by that equation (Figure 3).

The results of this paper have focused on understanding the general relationships between τ^*_{bf}, D^*, and S. The relations themselves have multiple uses including the prediction of paleoslopes via regression of the core variables H_{bf}, S, and D_{50} as in Eq. (7), (Trampush et al., 2014). Since our log-scaled variables are all normally distributed, the method presented herein can be used to evaluate mean coefficients, median coefficients, and maximum likelihood estimator for trends in paleoslope given rock outcrop measurements of H_{bf} and D_{50}. However, one might rather have a probability density function of paleoslope for every pair of measured values. In this case, a symmetric regression applied through Bayesian methods would be useful. It is worth pointing out that the convergence of frequentist OLS and the Bayesian scheme nominally equivalent to OLS here (when regressing on the same model, e.g. Eq. (7)) was somewhat coincidental. These methods converged because the variables are normally distributed and priors in the Bayesian model were chosen to be nearly uniform. If either of these conditions were not satisfied, the results might diverge.

Discussions can be found in other scientific fields as to the appropriateness and applicability of various regression techniques, e.g. McArdle (1988), McArdle (2003), Warton (2006), and Smith (2009). Historically, bankfull hydraulic geometry regressions have been done with OLS regression. This method may be appropriate when the dependent variable(s) are subject to much less error than the independent variable, or if one variable is seen as a response to another (McArdle 2003). When this is not the case, however, a symmetric regression scheme may give more appropriate predictions. Parker et al. (2007), and

Wilkerson and Parker (2011) by extension, were right to forgo the use of symmetric regression schemes with highly uncorrelated variables. In addition, symmetric and asymmetric regression converge as bivariate or multivariate correlation increases (McArdle 2003). Outside of these two end-member scenarios, there are many situations where symmetric EIV regressions such as MA or RMA might be more appropriate. All hydraulic geometry variables can be expected to have measurement error, which fulfills one important criterion for the selection of symmetric regression. Additional conditions that could suggest use of symmetric EIV regression include: 1) when there is ambiguity in selection of the dependent/response variable, i.e. when it is unclear whether one variable is a response to another, and 2) when it is believed that error in the independent variables are significant.

The above comments may be useful in the selection of a regression style in future research involving regression relationships among hydraulic geometry variables. In many cases, the differences between symmetric and asymmetric regression types may be minimal, but the results shown herein indicate how notably different conclusions are possible simply due to the selection of different regression schemes.

Conclusions

The bankfull Shields number of alluvial rivers provides a useful quantification of channel characteristics. We show regression results for this parameter and two other dimensionless parameters for the median bed material grain-size and reach-averaged bed slope. More specifically, we obtain a relation for bankfull Shields number τ^*_{bf} as a function of channel slope S and dimensionless grain size D^* (also shown in Eq. (13) and 2-3):

The trends in this relationship can be used in self-formed channel morphodynamic models (e.g. Li et al., 2015, 2016) or for prediction of paleoslopes (e.g. Trampush et al., 2014), among other applications. The mode of Bayesian regression results and frequentist regression results happen to converge in the examples described above. However, results could differ if variables are not normally distributed or if non-uniform priors are used and priors are not overwhelmed by data in Bayesian regression. We note that past regressions of this type have used asymmetric regression techniques, such as ordinary least squares regression, and mean regression results depend on the selection of the response/dependent variable. We apply a symmetric regression scheme, which accounts for errors in the dependent and independent variables and produces results that do not depend on selection of the dependent variable. Herein we implement this with Major Axis (MA) regression. This type of scheme is more appropriate for our application to hydraulic geometry because there is no obvious choice for the “response” variable, and all terms are measured with error and natural variance. The discussion in this paper may be useful in future research on the determination of hydraulic geometry relations from regression schemes. The reader may

refer to e.g. McArdle (1988), McArdle (2003), Warton (2006) and Smith (2009) for more detailed discussion on methodology, and for guidance in selecting a regression type.

Acknowledgements

This chapter is the topic of a journal article in review at Journal of Hydraulic Research with coauthors Brandon McElroy and Gary Parker. The authors thank Hongbo Ma, Tian Dong, and Rina Schumer for their comments and advice in developing this manuscript.

Funding

This research was partially supported by the United States National Science Foundation, through Award Numbers 1209427 (WSC-Category 2) 1135427 (FESD Type I) and by the University of Wyoming School for Energy Resources.

Notation List

D_{50} = Median grain size [m]

D^* = van Rijn's dimensionless grain size [-]

g = Gravitational acceleration, 9.81 [ms^{-2}]

H_{bf} = Bankfull depth [m]

R = Submerged specific gravity, 1.65 [-]

S = Reach-averaged bed slope [-]

u^*_{bf} = Bankfull shear velocity [ms^{-1}]

v = Kinematic viscosity, 1e-6 [m^2s^{-1}]

ρ = Density of water, 1000 [kg/m^3]

τ_b = Bed shear stress [Pa]

τ^*_{bf} = Bankfull Shields number, [-]

$\tilde{u}^*_{bf}$ = Normalized Bankfull Shear velocity, [-]

References

1. Bingham, N.H., & Fry, J.M. (2010) *Regression – Linear Models in Statistics*. Springer-Verlag.
2. Dade, W. B., & Friend, P. F. (1998). Grain-size, sediment-transport regime, and channel slope in alluvial rivers. *The Journal of Geology*, *106*(6), 661-676.
3. Eke, E., Parker, G., & Shimizu, Y. (2014) Numerical modeling of erosional and depositional bank processes in migrating river bends with self-formed width: morphodynamics of bar push and bank pull. *J. Geophys. Res. 119* (7), 1455–1483.
4. Goodman, T., & Tofallis, C. (2003). Neutral data fitting in two and three dimensions. (Business School Working Papers; Vol. UHBS 2003:9). University of Hertfordshire.
5. Hoff, P.D. (2009). A First Course in Bayesian Statistical Methods. *Springer*. DOI 10.1007/978-0-387-92407-6
6. Kim, W., Mohrig, D., Twilley, R., Paola, C. & Parker, G. (2009). Land building in the delta of the Mississippi River: is it feasible? *Eos*, *90*(42).
7. Konsoer, K., J. Zinger, & G. Parker (2013), Bankfull hydraulic geometry of submarine channels created by turbidity currents: Relations between bankfull channel characteristics and formative flow discharge, *J. Geophys. Res. Earth Surf., 118*(216–228), doi:10.1029/2012JF002422.
8. Leopold, L.B., & Maddock, Jr., T. (1953). The hydraulic geometry of stream channels and some physiographic implications. *In Professional paper 252*. U.S. Geological Survey,Washington, DC.
9. Leopold, L.B., & Wolman, M.G., 1957. River channel patterns; braided meandering and straight. *USGS Prof. Paper, vol. 282-B*. US. Geological Society, Washington, DC.
10. Li, C., Czapiga, M. J., Eke, E. C., Viparelli, E., & Parker, G. (2015). Variable Shields number model for river bankfull geometry: bankfull shear velocity is viscosity-dependent but grain size-independent. *Journal of Hydraulic Research*, *1686*(January), 1–13. http://doi.org/10.1080/00221686.2014.939113
11. Li, C., Czapiga, M. J., Eke, E. C., Viparelli, E., & Parker, G. (2016). Closure to "Variable Shields number model for river bankfull geometry: Bankfull shear velocity is viscosity-dependent but grain size-independent" by Li, C., Czapiga, M. J., Eke, E. C., Viparelli, E., & Parker, G, *J. Hydraulic Res. 53*(1), 2. *Journal of Hydraulic Research, 54*(2). http://doi.org/10.1080/00221686.2015.1137088
12. Paola, C., & Mohrig, D. (1996). Palaeohydraulics revisited: palaeoslope estimation in coarse-grained braided rivers. *Basin Research, 8*(3), 243-254.
13. Mohrig, D., Heller, P.L., Paola, C., & Lyons, W.J. (2000). Interpreting avulsion process from ancient alluvial sequences: Guadalope-Matarranya system (northern Spain) and Wasatch

Formation (western Colorado). *GSA Bulletin, 112*(12): 1787–1803. Doi: https://doi.org/10.1130/0016-7606(2000)112<1787:IAPFAA>2.0.CO;2

14. McArdle, B.H. (1988). The structural relationship: regression in biology. *Can. J. Zool. 66*, 2329-2339.
15. McArdle, B. H. (2003). Lines, models, and errors: regression in the field. *Limnology and Oceanography 48*, 1363–1366.
16. Mueller, E. R., Pitlick, J., & Nelson, J. M. (2005). Variation in the reference Shields stress for bed load transport in gravel-bed streams and rivers. *Water Resources Research, 41*(4).
17. Newman, M.C. (1993). Regression analysis of log-transformed data: Statistical Bias and Its Correction. *Environmental Toxicology and Chemistry. 12*, 1129-1133.
18. Parker, G. (1978). Self-formed straight rivers with equilibrium banks and mobile bed. Part 2. The gravel river. *Journal of Fluid Mechanics, 89*(1), 127-146.
19. Parker, G. (2004). 1D sediment transport morphodynamics with applications to rivers and turbidity currents, Copyrighted e-book at http://vtchl.uiuc.edu/people/parkerg/morpho dynamics/ebook.htm.
20. Parker, G., Paola, C., Whipple, K., Mohrig, D., Toro-Escobar, C., Halverson, M., & Skoglund, T. (1998). Alluvial fans formed by channelized fluvial and sheet flow: application. *J. Hyd. Eng., 124*(10), 12-20.
21. Parker, G., Wilcock, P., Paola, C., Dietrich, W.E., & Pitlick, J. (2007). Physical basis for quasi-universal relations describing bankfull hydraulic geometry of single-thread gravel bed rivers. *J. Geophys. Res. Earth 112*(F4), 21.
22. Pfeiffer, A. M., Finnegan, N. J., & Willenbring, J. K. (2017). Sediment supply controls equilibrium channel geometry in gravel rivers. *Proceedings of the National Academy of Sciences*, *114*(13), 3346-3351.
23. Phillips, C. B., & Jerolmack, D. J. (2016). Self-organization of river channels as a critical filter on climate signals. *Science*, *352*(6286), 694–697. http://doi.org/10.1126/science.aad3348
24. Smith, R.J. (2009). Use and misuse of the reduced major axis for line-fitting. *American journal of Physical Anthropology. 140*, 476-486.
25. Trampush, S. M., Huzurbazar, S., & McElroy, B. (2014). Empirical assessment of theory for bankfull characteristics of alluvial channels. *Water Resources Research*, *50*(12), 9211-9220.
26. Van Rijn, L. C. (1984). Sediment transport, part I: bed load transport. *J. Hydraulic Eng., 110*(10), 1431-1456.
27. Warton, D.I., Wright, I.J., Falster, D. S., & Westoby, M. (2006). Bivariate line-fitting methods for allometry *Biol. Rev., 81*, 259–291, doi:10.1017/S1464793106007007.

28. Wilkerson, G.V., & Parker, G. (2011). Physical basis for quasi-universal relationships describing bankfull hydraulic geometry of sand-bed rivers. *J. Hydraulic Eng. 7*(1), 739–753.

CHAPTER 3 : NUMERICAL MODELS OF THE MORPHODYNAMICS OF WAX LAKE DELTA: THE ROLES OF JUVENILE CHANNELS, INCISION INTO CONSOLIDATED MUD, AND OVERBANK PROCESSES

Abstract

River deltas exist in a state of flux and require sufficient sedimentation to maintain their planform during period of sea level rise. The Wax Lake Delta is an important analogue for understanding delta evolution due to its fast progradation; the delta has been well measured in recent years and is one of a few areas along coastal Louisiana actively gaining land area. Many models are available to understand delta growth in a variety of complexities, but model selection largely depends on the desired question. Here we focus on a simple model framework and include several new features to improve morphodynamic modelling for channel dimensions. We compare our new model to a group of past models to understand how new model features affect the morphodynamic changes. The full model presented here includes a new distributed Exner equation, variable Shields number equation and framework for dealing with pre-delta basement substrate and under-developed channels at the periphery. The new model can better characterize depth and estimates channel area well, but computes a different spatial trend in width in comparison to field data. A leave-one-out analysis explains difference in delta models and observations are included to guide future modelling efforts.

Introduction

Characteristic morphodynamic features of deltas

River deltas represent a complex balance of hydrology, geomorphology, oceanography, and biology. Modelling the evolution of river deltas strongly depends on the question to answer. The simplest delta models characterize areal growth rates of the delta given boundary conditions for inflow water discharge, inflow sediment discharge, and the geometry of the basin to fill. Swenson et al. (2000) introduced a major advancement for simple models by modifying a Stefan problem, which predicts the propagation of a phase boundary through time, into a 1D river delta with moving shoreline. This framework has been expanded to include other features, including analytical closures for an upstream alluvial-bedrock transition (Lorenzo-Trueba et al. 2009, 2010) or for delta evolution with hyperpycnal runout turbidity currents (Lai and Capart, 2009). Time-stepping 1D models predict delta evolution in confined basins, e.g. Parker, 2004 (e-book), Parker et al. (2007). Many two-dimensional models include assumptions for a single channel that implicitly migrates across the fan (e.g., Kim et al., 2009a; Viparelli et al., 2011) or a single channel that explicitly avulses due to environmental controls (e.g., Sun et al., 2002). More complex models include channel networks. A recent novel model by Liang et al. (2015) generates a channel network without directly solving the Navier-Stokes or Shallow Water Equations through a stochastic parcel-based cellular routing scheme for water and sediment rather than traditional modelling of detailed hydrodynamics.

Many others use Delft3D software to model the specifics of how different characteristics affect the overall development of deltas, e.g. sand/mud concentration (Edmonds and Slingerland, 2010, Burpee et al. 2013), sediment cohesion (Caldwell and Edmonds, 2014), wind (Gelensye et al., 2015), or vegetation (Nardin et al. 2016). Models like Delft3D can resolve complex hydrodynamics and morphodynamics along with sub-functions to estimate ancillary components, but these models require a considerable computational cost. Geometric delta models are computationally efficient and requires less parameterization, but use many simplifying assumptions that may not capture the desired physics. For example, a common assumption of past geometric delta models is uniform, normal flow, which is a highly simplified model of the hydrodynamics of flow into a receiving basin which may be subject to tidal effects. However, these models, e.g. Kim et al. (2009a), have been successful in estimating the progradation rate of fluvially-dominated deltas because the assumption properly accounts for the long-term flux of sediment to the delta-basin boundary. We hereby refer models of the type of Kim et al. (2009a) as 1D morphodynamic models.

1D morphodynamic models have been effective for predicting progradation rates, but have not been able to replicate down-delta trends in channel width and depth. We seek to modify an existing framework for

quasi-steady lumped-channel fan delta models with an algorithm for self-formed channel geometry, as well as a treatment for incision to bedrock, so as to improve capabilities of these models.

Modelling channel width change

Modelling channel width variation, and indeed channel hydraulic geometry in general, can be accomplished by imposing, among other things, a closure for the channel bankfull Shields number (e.g. Parker et al. 1998, Parker et al. 2008). The Parker et al. (2008) model uses a constant channel-forming Shields number value, which has been shown to over predict bankfull depth as it varies downstream in the Fly River, Papua New Guinea by Li et al. (2015). The Li et al. (2015) model computes a steady state solution of a single channel, assuming uniform flow. The formative bankfull Shields number relates to the dimensional shear stress applied to the bed during bankfull conditions. However, since river channels erode or deposit on their boundaries to select their own width, this value is co-dependent on river structure. As such, this term allows for modelling of channel width, rather than assuming a fixed width in time. Precisely how width is selected is still not completely understood. Parker (1978a; 1978b) first offered a theory for the physical development of self-formed channels. Paola (1992) hypothesized a constant Shields number. Parker et al. (1998) use a sparse dataset to assume a value for bankfull Shields number, e.g. in form of Eq. (1), where C is a prescribed constant, and develop a model for width and depth closures based on this idea. Parker et al. (2007) and Wilkerson and Parker (2011) assemble datasets of bankfull channel characteristics for gravel and sand, respectively. These authors develop empirical relations that suggest quasi-universal laws for bankfull geometry in the separate sub-types of alluvial rivers. Li et al. (2015) show that the bankfull Shields number can be predicted with only reach-average channel slope S and dimensionless grainsize, D_*, as in Eq. (2). Dimensionless grainsize is defined by Van Rijn, 1984 as $D^* = \left(Rg / \nu^2 \right)^{1/3} D_{50}$, where R is submerged specific gravity, assumed 1.65, g is gravitational acceleration (9.81 Nm^{-2}), ν is kinematic viscosity, and D_{50} is median bed material grain size. Czapiga et al. (2018) modestly adjust these results by including more data and changing the regression scheme. Li et al. (2015) apply their new formulation and compare with results of Parker et al. (2008) for the Fly River Delta. Their variable Shields number formulation improves on the Parker et al. (1998) formulation by reducing the effect of over-deepening and over-narrowing downstream.

$$\tau_{bf}^{*} = C \tag{1}$$

$$\tau_{bf}^{*} = \beta S^{m} D_{*}^{n} \tag{2}$$

The variable Shields number relations, i.e. Czapiga et al. (2018), Li et al. (2015, 2016), Trampush et al. (2014) were empirically derived from a large dataset of rivers. Both constant and slope-dependent Shields

number closures relate to a well-developed channel at its intrinsic bankfull geometry. We suggest that this methodology is not valid at the delta periphery, where new channels form as the delta progrades (e.g. Shaw et al. 2014). Past 1D models of river deltas that have so-called self-formed channels e.g. Kim et al. (2009a) do not accurately account for the process of channel evolution toward the mature bankfull condition development, i.e. they do not follow morphology patterns identified by Shaw et al. 2016a. Here we include the concept of a juvenile channel, and relate the bankfull Shields number of a juvenile channel to its mature counterpart.

Added features considered here

We start from two past 1D morphodynamic models that include self-formed channel width and constant formative Shields number closure. The base models include a uniform, normal flow model developed by Kim et al. (2009a) and a steady, shallow water hydraulics model by Parker and Sequieros (2006) (PS). Several features are incorporated into both models. Models that use the shallow water equations for hydraulics, i.e. backwater models, will require a new, distributed Exner equation that simultaneously accounts for both channel and floodplain/island morphodynamics, and treat the problem in terms of average delta elevations, rather than channel bed elevations. Specifically, sediment continuity is computed over the average delta and sediment is allocated to cause morphodynamic change in channel and floodplain elevations. This allows us to model channel elevation below the water surface elevation while maintaining a net-depositional environment. Implementations with the constant formative Shields number and variable Shields number relation by Czapiga et al. (2018) are considered with and without accounting for incipient channel formation at the delta periphery, i.e. juvenile channels. Due to the presence of a confining basement layer consisting of consolidated shelf clay at Wax Lake Delta (Shaw et al. 2013), we include additional equations for bedrock-alluvial transitions after Viparelli et al. (2014), and a rate-excess law closure for erosion of the consolidated clay basement material (e.g. Garcia, 2008, eq. 4-35).

We define juvenile channels as those with banks that are entirely inundated for at least some threshold percentage of time. Hoyal and Sheets (2009) describe morphodynamic differences between upstream and downstream channels in their experiments, and note the juvenile channels are much wider and shallower than the mature channels upstream. Chatanantevet and Lamb (2014) observe a continuous shoaling pattern in their experiments where flow velocity in channel is slowed and water ostensibly leaves over the subaqueous channel banks. Subaqueous channel banks are ubiquitous in Wax Lake Delta (e.g., Shaw et al., 2013; Wellner et al., 2006; Carle, 2013), and are likely common in deltas in general. Viparelli et al. (2011) relate vegetation type to inundation rate. Carle (2013) note that vegetation types are correlated to inundation rates, which provides a link between radial length from the delta apex and inundation rate.

Geleynse et al. (2015) compute shoreline extent at different conditions; their results show 50-65% of WLD's radial topset extent is inundated during floods. Hiatt and Passalacqua (2015) show flow lost in WLD channels to the islands via tie-channels and overbank flow. Hiatt and Passalacqua (2017) model the effect of bank roughness on flow confinement with subaqueous banks.

Application to Wax Lake Delta

In so far as we validate our model (presented below) with field measurements at WLD in coastal Louisiana, USA, it is of value to introduce the site. This site represents a micro-tidal and rapidly prograding delta with >30 years of collected data via bathymetric surveys before and after initial deposition, along with aerial imagery to estimate the temporal changes to delta topset extent, channel widths and inter-channel widths.

While WLD is the stimulus for our research, our methodology will not be specific to WLD, so it can be representative of generic deltaic growth. The Kim et al. (2009a) model provides a simple framework for modelling the morphodynamic evolution of WLD, and the authors used their model to infer potential growth of river diversions in coastal Louisiana. Due to several simplifying assumptions, including a uniform flow condition, the Kim et al. (2009a) results are not directly comparable with bathymetric data. Here we find that this restriction is largely removed when the normal flow assumption is relaxed and gradually varied flow is considered. We must also investigate how recent scientific advancements affect the predictions made by Kim et al. (2009a). In particular, the assumptions for uniform flow and spatially constant bankfull Shields number are relaxed herein; juvenile channels are also be included for a downstream portion of the delta. All conditions are validated against generalized bathymetry measured from Wax Lake Delta over a period of 35 years.

We have identified several key features that current morphodynamic delta models of this type do not address, but it is unclear which features are necessary to reproduce the basic morphodynamics in a growing fluvially-dominated delta. Therefore, we have modified the existing framework of past models to test the importance of accounting for under-developed channels, bedrock/basement interaction effects and the effect of constant versus variable formative Shields number. We also assess when the assumption of uniform flow is acceptable.

Methodology

Our model considers a 2D fan delta, but follows the 1D moving-boundary framework as illustrated in Figure 3-1. There are four elevations modelled, channel bed elevation η_c, floodplain elevation η_f, basement elevation η_{base} and the geometric average delta elevation $\overline{\eta}$. The physical model space can be described in polar coordinates such that the radial distance from the delta apex to any given point is r and

the angle of the delta topset is θ. The topset has an assumed topset angle θ_0 and the radial extent of the delta topset is denoted as s_s, while the radial distance to the foreset-bottomset transition is s_b. The basement is assumed to be a specified constant-slope plane.

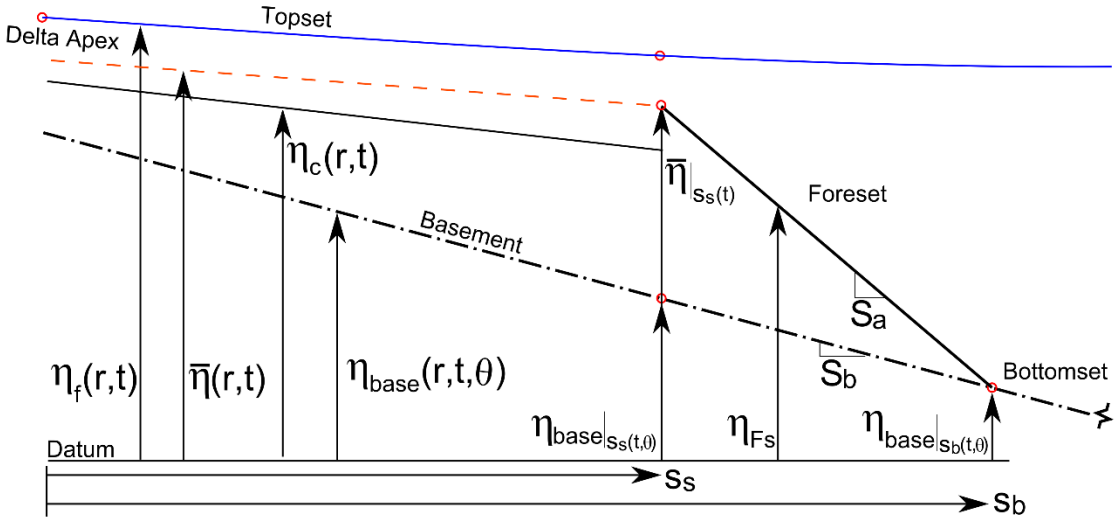

Figure 3-1: A schematic profile of the cross-section of delta model domain. The delta is separated into topset, foreset, and bottomset areas, where the slopes of foreset and basement are assumed. The model tracks four separate elevations representing the pre-delta basement η_{base}, channel η_c, floodplain η_f /water surface ξ (they are equivalent), and geometric average delta elevation $\overline{\eta}$. Foreset slope and the basement slope are assumed to have values that do not vary in time. The length of delta topset is shown as ss and the length from apex to foreset-bottomset transition is s_b, both of which can increase as the delta evolves.

The topset is assumed to have a pie-shaped planform, the down-delta slope of which can vary. Because the slopes of the topset and basement can differ, the elevation η_{base} is also a function of θ according to simple geometric relation. A representative flood inundation length scale r_{flood}, is defined such that a representative flood inundates channel banks for $r > r_{flood}$ (Figure 3-2). This demarcates the transition to juvenile channels. As channel banks become more subaqueous, channel confinement decreases and discharge leaves the channel via overbank flow, e.g. Hiatt and Passalacqua (2015), Shaw et al. (2016a). The model assumes channels at radial length $r \leq r_{flood}$ possess fully confining banks and resemble mature bankfull channel architecture. Conversely, channels at radial length $r > r_{bank}$ are in varying degrees of a transitional state between the incipient channel form where flow is nearly axisymmetric up to the condition where the representative flood no longer inundates the banks.

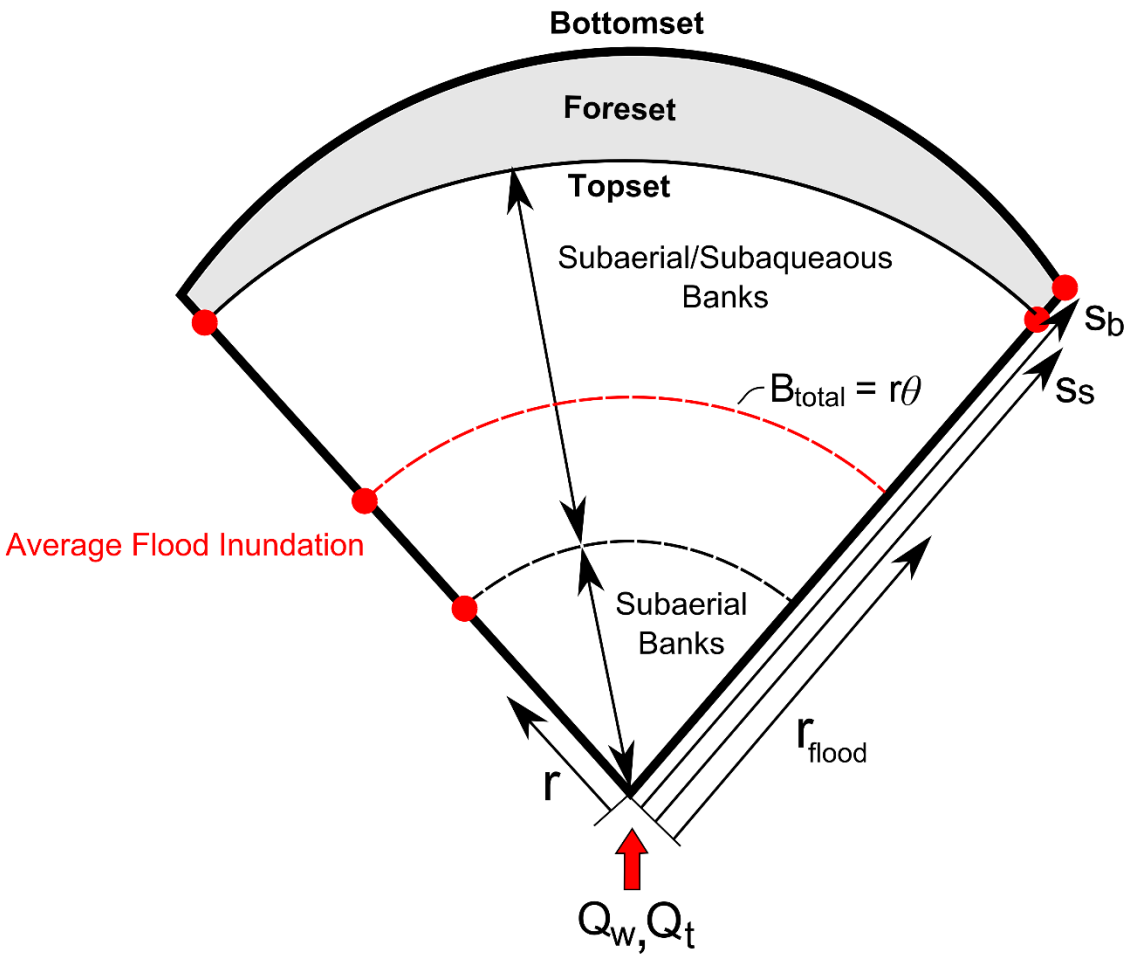

Figure 3-2: Schematic of model domain in plan view, showing along-delta coordinate r, inundation length rflood, delta angle θ, total delta width B_{total}, distance to shoreline ss and distance to topset-basement break s_b. The model has an inflow water and sediment discharge as Qw and Qt, respectively. The input water discharge is distributed evenly at the delta periphery, but not necessarily so for the sediment flux. The topset contains areas with subaerial and subaqueous banks and the overbank inundation of a typical flood is identified as occurring downstream of r_{flood}.

Equations for water mass and momentum and sediment conservation are written in dimensionless form relative to the current extent of the delta topset. The model assumes all bed material load leaving the delta topset is captured within the delta foreset; this implies that the delta progrades. We use appropriate assumptions regarding the shape of the delta foreset and the pre-delta elevation to compute delta extension as bed material load aggrades the delta. The dimensionless spatial coordinate $\hat{r}$ scales the radial distance from the delta apex r against the radial extent of the delta apex s_s, i.e. from apex to topset-foreset transition.

$$\hat{r} = \frac{r}{s_s} \tag{3}$$

$$\hat{t} = t \tag{4}$$

$$\frac{\partial}{\partial r} = \frac{1}{s_s}\frac{\partial}{\partial \hat{r}} \tag{5}$$

$$\frac{\partial}{\partial t} = -\frac{\dot{s}_s}{s_s}\frac{\partial}{\partial \hat{r}} + \frac{\partial}{\partial \hat{t}} \tag{6}$$

Below Capacity Transport relation

A framework of interest for models that use the shallow water equations for hydraulics concerns the interactions between channel beds and a confining basement layer. This framework must account for declining sediment loads as bed material is winnowed away, leaving only bare basement surface. Typical sediment transport equations relate the normalized bed shear stress, i.e. Shields' stress to the sediment transport rate. Therefore, the equations implicitly assume that there is always sediment available to be moved; this is clearly not the case as a channel incises into a non-fluvial basement layer. Shaw et al. (2013) show the Wax Lake Outlet feed channel and most of the delta channels have relatively little sediment on the channel bottom; the authors suggested that a method developed by Sklar and Dietrich (2004) for erosion of bedrock due to particle abrasion could be modified for delta application at WLD. Zhang et al. (2015) use part of the framework of Sklar and Dietrich (2004) in their bedrock incision model and imply that the aerial fraction of cover of the bedrock by alluvium, p_c, increases with thickness of alluvial cover. These authors assume a macro-roughness height representative to the scale of the intrinsic bumpiness of the bedrock. When the bed elevation η_c is greater than the basement elevation η_{base} plus the macro-roughness height, the bed is fully alluviated; when channel elevation is less than a macro-roughness height above the bedrock/basement, $p_c < 1$ and a below capacity transport condition prevails. The capacity sediment flux Q_{tc} is the value predicted when the bed is fully alluvial, and the actual sediment flux $Q_t = p_c Q_{tc}$ decreases as p_c decreases, i.e. as the bed becomes deficient in alluvium. Viparelli et al. (2014) use this form for the lower Mississippi River and substitute the macroroughness height for a representative dune height, L_{ac}. We use this formulation as in Eqs. (7) and (8).

$$Q_t = p_c Q_{t,c} \tag{7}$$

$$p_c = \begin{cases} 1, & \eta_c \geq \eta_{base} + L_{ac} \\ p_{c,min} + \dfrac{\eta_c - \eta_{base}}{L_{ac}}, & \eta_c < \eta_{base} + L_{ac} \end{cases} \quad (8)$$

Most previous authors have applied this methodology to bedload transport, but we apply it here to a total bed material load condition that includes suspended transport of the bed material As Shaw et al. (2013) elaborate, this methodology relates local transport conditions to the transport capacity and local availability of sediments. When sediment is travelling in suspension, the transport capacity is not necessarily limited by a local decrease to cover fraction. However, there are currently no simpler means to qualify below capacity transport conditions. Ignoring the spatial lag between sediment entrainment and advection length can affect local details, but the mean sediment transport rate in the delta will not be affected. In the future, this implementation should be revisited using a more sophisticated methodology accounting for entrainment and deposition of bed sediment.

Distributed Exner Equation

The modeled delta width is divided into two regions for channelized and non-channelized area. Non-channel regions are denoted as a floodplain here and marked with subscript *f*. Since channel width B_c is modeled and total accommodation width B_{total}, measured normal to the axial coordinate *r* is specified (Figure 3-3), floodplain width B_f is passively determined as the difference between B_c and B_{total}. We assume channel and floodplain areas have characteristic elevations separated by local channel depth, Eq. (9), and the geometric average elevation $\overline{\eta}$ of the delta as in Eq. (10)

$$\eta_f = \eta_c + H_{bf} \quad (9)$$

$$B_{total}\overline{\eta} = B_c\eta_c + B_f\eta_f \quad (10)$$

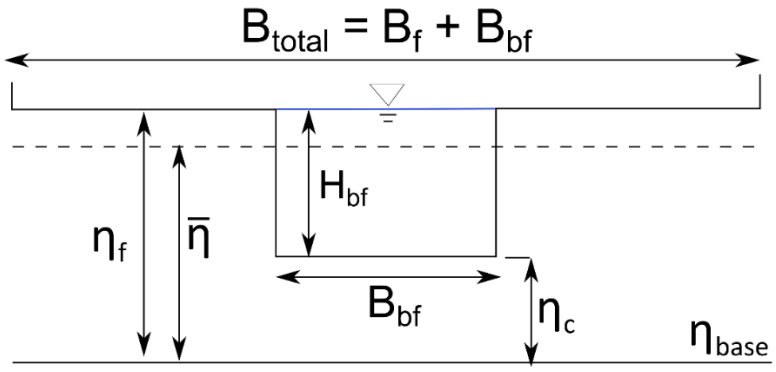

Figure 3-3: Schematic for a distributed Exner equation of sediment conservation at any arbitrary cross section in the delta. The total width is composed of channel B_{bf} and floodplain B_f. The basement elevation η_{base} represents the pre-delta elevation, and the channel elevation η_c is separated from the floodplain elevation ηf by bankfull depth H_{bf}.

Water and sediment move through the channel, but are implicitly distributed across the entire delta topset. The Exner equation is computed with the average delta elevation $\bar{\eta}$. We modify the typical Exner equation to include an intermittency factor I_f (as in e.g. Parker, 2004, Parker et al., 2008) and a proportional unit deposition of washload material for every unit of sand deposited Ω (as in e.g. Kim et al. 2009a). The percent cover p_c is included in the Exner equation, Eq. (11), similarly to Viparelli et al. (2014) and is also included within the sediment flux Q_t via Eq. (7). The dimensionless form of distributed Exner equation, derived in accordance with Eqs. (3) ~ (6), is shown in Eq. (12).

$$\left(1-\lambda_p\right) p_c B_{total}\left(\frac{\partial \bar{\eta}}{\partial t}+\sigma\right)=-I_f\left(1+\Omega\right)\frac{\partial Q_t}{\partial r} \tag{11}$$

$$\left(1-\lambda_p\right) p_c B_{total}\left(\frac{\partial \bar{\eta}}{\partial \hat{t}}-\frac{\dot{s}_s}{s_s}\frac{\partial \bar{\eta}}{\partial \hat{r}}+\sigma\right)=-I_f\left(1+\Omega\right)\frac{\partial Q_t}{\partial \hat{r}} \tag{12}$$

Change in the average delta elevation is proportionally distributed to predict changes in floodplain and channel elevations. Discrete changes in the terms in Eqs. (9) and (10) obey Eqs. (14) and (13), respectively. Additionally, since the delta is divided into one channel and one floodplain area, an increase in channel width relates to an equal and opposite decrease in floodplain width as in Eq. (15).

$$\left(\bar{\eta}+\Delta\bar{\eta}\right)B_{total}=\left(\eta_c+\Delta\eta_c\right)\left(B_{bf}+\Delta B_c\right)+\left(\eta_f+\Delta\eta_f\right)\left(B_f+\Delta B_f\right) \tag{13}$$

$$\eta_f+\Delta\eta_f=\eta_c+\Delta\eta_c+H_{bf} \tag{14}$$

$$\Delta B_c = -\Delta B_f \tag{15}$$

These relations can be manipulated into Eqs. (16) and (17) that predict change in channel and floodplain elevations at any arbitrary location.

$$\Delta \eta_c = \overline{\eta} + \Delta \overline{\eta} - \eta_c H \frac{B_c - \Delta B_f}{B_{total}} \tag{16}$$

$$\Delta \eta_f = \overline{\eta} + \Delta \overline{\eta} - \eta_f H \frac{B_f + \Delta B_f}{B_{total}} \tag{17}$$

Juvenile Channels

As the formative, bankfull Shields number formulation of Eqs. (1) and (2) relate to river channels, these equations should not be directly applied to the condition of incipient channel form. We make a first-order hypothesis that the bankfull Shields number of an incipient channel scales linearly to its mature counterpart, i.e. Eq.(18), where γ is a decay factor that ranges on (0,1) and $\tau^*_{bf,mature}$ is the value representative of the mature channel structure.

$$\tau^*_{bf} = \gamma \tau^*_{bf,mature} \tag{18}$$

Incipient channel formation directly relates to absence of subaerial bank structure, which reduces channel confinement. Shaw et al. (2016) has shown typical flow patterns in the distal end of Wax Lake Delta where channels are bordered by subaqueous banks. Hiatt and Passalacqua (2015) measure discharge at several cross-sections down two channels at WLD to show that approximately 40% of the flow is lost during an inter-flood period. Flow so lost is incorporated through an additional parameter ε that represents the portion of flow maintained in the channel as in Eq. (19), where Q_w is the bankfull discharge in the channel and $Q_{w,tot}$ is the discharge of the feed channel. It can be shown in the Appendix that values for γ and ε are approximately equal at the delta periphery, so we assume they are equal in this framework as a first-order assumption. Flow loss from the channels are also incorporated when deriving equations for hydraulics.

$$Q_w = \varepsilon Q_{w,tot} \tag{19}$$

The delta inundation varies significantly throughout the year, with peak inundation occurring during floods normally related to the spring (Gelensye et al., 2015). The distributed Exner framework discussed above requires the floodplain elevation to be exactly H_{bf} above the bed elevation, so subaqueous bank

development cannot be directly modelled here. It is assumed, however, that the channel intrinsically migrates across the floodplain, as in Kim et al. (2009a). We also use an intermittency factor of flooding (I_f < 1), and model with a single representative flood discharge. Measurements from Gelenyse et al. (2015) show the typical inundation length scale of floods range from 35 – 50% of the full topset length; from these results we assume a value for $r_{flood} = 0.5 s_s$, where s_s is the radial distance from delta apex to the topset-foreset break. Therefore, τ_{bf}^*, takes the form of Eq. (20) or Eq (21), depending whether a constant value or a slope-dependent relation is used.

$$\tau_{bf}^* = \gamma \tau_{bf,const,sand}^* \tag{20}$$

$$\tau_{bf}^* = \gamma \beta S^m D_*^n \tag{21}$$

Here, since we apply the model to a sand-bed delta, we use $\tau_{bf,const,sand}^* = 1.86$ after Parker (2004) when applying Eq. (20), and use β = 182, n = -0.87, m = 0.365 from Czapiga et al. (2018) when applying Eq. (21).

We assume an exponential decay function for γ and allow ε to range from (0,1] with specified rate coefficients, as in Eqs. (22) and (23). The rate coefficients are computed from field data at WLD; as detailed in the appendix, k_τ is scaled via depth measurements and k_{Qw} is estimated from discharge measurements of Hiatt and Passalacqua (2015). The function for γ takes form of Eq. (22); when γ = 1, the bankfull Shields number approaches its mature value.

$$\gamma = \begin{cases} 1, & r < r_{flood} \\ exp\left(-k_\tau \hat{r}\right), & r \geq r_{flood} \end{cases} \tag{22}$$

$$\varepsilon = \begin{cases} 1, & r < r_{flood} \\ exp\left(-k_Q \hat{r}\right), & r \geq r_{flood} \end{cases} \tag{23}$$

$$\frac{\partial \gamma}{\partial \hat{t}} = \frac{\partial \varepsilon}{\partial \hat{t}} = 0 \tag{24}$$

Both parameters are defined to be temporally constant in dimensionless space according to Eq. (24), implying a condition of self-similarity. The dimensioned domain expands over time as the delta progrades, resulting in a decreased streamwise gradient for both γ and ε. The boundary separating mature and juvenile, r_{flood}, channels must propagate at the speed of delta propagation, so channels at a given dimensioned distance from the delta apex mature over time.

An alternative method can also consider temporal evolution in γ, which takes the forms of Eq. (25).

$$\frac{\partial \gamma}{\partial t} = C_1 \frac{v_{s,fine}}{H_{bf}} \left(\gamma_{max} - \gamma \right) \tag{25}$$

$$\frac{\partial \gamma}{\partial \hat{t}} = C_1 \frac{v_{s,fine}}{H_{bf}} \left(\gamma_{max} - \gamma \right) + \frac{\dot{S}_s}{s_s} \hat{x} \frac{\partial \gamma}{\partial \hat{r}} \tag{26}$$

The maximum value $\gamma_{max} = 1$, corresponds to a mature channel structure, C_1 is a fitting coefficient, and $v_{s,fine}$ is the settling velocity of fine grained material (assumed to be 63 microns here). This equation includes a representative timescale for fine material to fall one channel depth, which is considered a proxy for the timescale of levee development, which acts to confine flow and increase streamwise transport capacity. Less mature channels develop the fastest and this effect augments through basinward shoaling, which reduces H_{bf} near the periphery. The derivative is defined in physical space, and γ, ε assume an initial value defined by Eqs. (22) and (23), respectively. This equation translated to dimensionless space takes the form of Eq. (26). The first term in the right hand side of this equation is always positive, and the second term is initially negative as the assumed initial condition considers channels to be immature at the delta periphery.

Over time, as γ increases, the slope of γ decreases and eventually approaches a value corresponding to a spatially mature channel at all nodes. We now consider conditions just basinward of the topset-foreset break; Shields stress can be recast as Eq. (27). Shields stress can be estimated here by assuming unconfined flow and zero-gradient conditions for channel depth H_{bf} and friction slope S_f. This form creates a minimum value, by using in-channel properties at the topset-foreset break and applying them assuming channel width expands to the delta topset arc length, so encompassing the entire delta width. The parameter γ_{min} can be defined from this minimum shear condition as in Eq. (28).

$$\tau_{bf}^{*} = \frac{\rho U^2}{Cz^2 \rho RgD} \tag{27}$$

$$\gamma_{min} = \frac{Q_{w,tot}^2}{Cz^2 RgD\beta D_*^{\,n} \left(ss\theta \, H_{bf}\big|_{s_s} \right)^2 \left(S_f\big|_{s_s} \right)^m} \tag{28}$$

A ghost node, immediately basinward of the delta topset is implemented according to Eq. (29).

$$\frac{\partial \gamma_{ghost}}{\partial \hat{t}} = C_1 \frac{v_{s,fine}}{H_{bf}} \left(\gamma_{max} - \gamma_{ghost} \right) - C_2 \frac{\dot{s}_s}{s_s} \left(\gamma_{ghost} - \gamma_{min} \right) \tag{29}$$

This equation is defined in dimensionless derivative because it always relates to a location immediately basinward from the delta topset after flow becomes completely unconfined. The first term is identical to Eq. (25), and the 2nd term is always negative and relates the value of γ_{ghost} to the progradation rate of the delta. Altogether, the equation is dimensionally homogenous and quantified the tendency toward channel maturation via sediment deposition along the banks and away from channel maturation as the delta progrades, creating new channels. The slope of γ at the topset-foreset break can be approximated with a central difference scheme, with γ_{ghost} immediately basinward from the last node.

The decay rate in bankfull Shields number is related to the lack of flow confinement, so there is a physical trend that relates ε and γ. However, the details of this trend are unknown at this time, and since measured values show similar magnitude, we assume they are equal. Therefore, their derivatives are also set to be equal; as the temporal evolution of γ is modelled, we assume $\gamma = \varepsilon$ is always true.

Uniform flow model

The Kim et al. (2009a) model uses closures for bankfull width B_{bf}, bankfull depth H_{bf}, and reach-averaged bed slope S of an assumed single, lumped channel with constant bankfull Shields Number, normal flow hydraulics, and the Engelund-Hansen (1967) sediment transport equation for unimodal sand bed channels via Parker (2004). These are included in Eqs. (30)-(32) and modified from the original equations by incorporating Eqs. (19) and (20).

$$S = \frac{R}{Cz\alpha_{EH}\varepsilon\gamma\tau_{bf}^*} \frac{Q_t}{Q_{w,tot}} \tag{30}$$

$$\frac{B_{bf}}{D_{50}} = \frac{1}{\alpha_{EH} Cz^2 \left(\gamma\tau_{bf}^* \right)^{2.5}} \frac{Q_t}{\sqrt{RgD_{50}} D_{50}^2} \tag{31}$$

$$\frac{H_{bf}}{D_{50}} = \alpha_{EH} \varepsilon Cz D_{50} \left(\gamma\tau_{bf}^* \right)^2 \frac{Q_{w,tot}}{Q_t} \tag{32}$$

Li et al. (2015, 2016) modify these equations with slope-dependent forms of Bankfull Shields Number and Chezy coefficient. These equations depend on bankfull water discharge Q_w, bankfull sediment discharge Q_t, median bed material grainsize D_{50}, constants for gravitational acceleration g, submerged specific gravity R, and other parameters. We modify the Li et al. (2016) equations here with amendments for juvenile channels according to Eqs. (33)-(36).

$$S = \left[\frac{R}{\alpha_{EH} \alpha_{Cz} \gamma \beta D^{*n}} \right]^{1/(1+m-n_{Cz})} \left(\frac{Q_t}{\varepsilon Q_{w,tot}} \right)^{1/(1+m-n_{Cz})} \tag{33}$$

$$\frac{B_{bf}}{D_{50}} = \frac{1}{\alpha_{EH} \alpha_{Cz}^2 \gamma^{2.5} \beta^{2.5} \sqrt{R} D^{*2.5n} \left[\frac{R}{\alpha_{EH} \alpha_{Cz} \gamma \beta D^{*n}} \right]^{\frac{2.5m-2n_{Cz}}{1+m-n_{Cz}}}} \left(\frac{\varepsilon Q_{w,tot}}{Q_t} \right)^{-\frac{2.5m-2n_{Cz}}{1+m-n_{Cz}}} \frac{Q_t}{\sqrt{g D_{50}}\, D_{50}^{\,2}} \tag{34}$$

$$\frac{H_{bf}}{D} = \alpha_{EH} \alpha_{Cz} \gamma^2 \beta^2 D^{*2n} \left[\frac{R}{\alpha_{EH} \alpha_{Cz} \gamma \beta D^{*n}} \right]^{\frac{2m-n_{Cz}}{1+m-n_{Cz}}} \left(\frac{Q_t}{\varepsilon Q_{w,tot}} \right)^{\frac{2m-n_{Cz}}{1+m-n_{Cz}}-1} \tag{35}$$

$$Cz = \alpha_{Cz} S^{-n_{Cz}} \tag{36}$$

The values of the coefficients in the above equations are: m = 0.365, n_{CZ} = -0.19; α_{Cz} = 2.53. β = 182 and α_{CH} = 0.05 (Czapiga et al, 2018; Li et al., 2015) The other model components, including Exner equation, shoreline migration rate and topset-foreset and foreset-bottomset migration rates are identical to Kim et al. (2009a).

Gradually Varied Flow model with juvenile, leaky channels

Hydraulics are also solved with the shallow water equations assuming either constant τ^*_{bf} and Cz, (as in Parker and Sequieros, 2006), or with slope-dependent forms of each. In all cases, the equations must account for flow leaking from the channels via overbank or tie-channels. Water discharge in leaky channels was defined in Eq. (19) and the spatial derivative of this equation constitutes the conservation of water mass in the 1D shallow water equation corresponding to Eq. (37). The conservation of momentum equation is shown in Eq. (38).

$$\frac{\partial Q_w}{\partial r} = Q_{w,tot} \frac{\partial \varepsilon}{\partial r} = \frac{Q_w}{\varepsilon} \frac{\partial \varepsilon}{\partial r} \tag{37}$$

$$\frac{\partial}{\partial r} \left(\frac{Q_w^{\,2}}{A_{bf}} \right) = -g A_{bf} \frac{\partial H_{bf}}{\partial r} - g A_{bf} \frac{\partial \eta_C}{\partial r} - g A_{bf} S_f \tag{38}$$

Here A_{bf} is the bankfull channel area equivalent to the product of H_{bf}*$\underline{B}_{bf}$. The left side of Eq. (38) is expanded via the chain rule as shown in Eq. (39).

$$\frac{\partial}{\partial r}\left(\frac{Q_w^{\,2}}{A_{bf}}\right)=\frac{2Q_w}{A_{bf}}\frac{\partial Q_w}{\partial r}-\frac{Q_w^{\,2}}{A_{bf}^{\,2}}\frac{\partial A_{bf}}{\partial r} \tag{39}$$

The spatial gradient in water discharge is provided via the equation for mass conservation in Eq. (37). The spatial gradient in area can be rewritten as Eq. (40). Expanding Eq. (39) and recombining into Eq. (38) gives Eq. (41).

$$\frac{\partial A_{bf}}{\partial r}=H_{bf}\frac{\partial B_{bf}}{\partial r}+B_{bf}\frac{\partial H_{bf}}{\partial r} \tag{40}$$

$$\frac{2}{gA_{bf}^{\,2}}\frac{Q_w^2}{\varepsilon}\frac{\partial \varepsilon}{\partial r}-\frac{Q_w^{\,2}}{gA_{bf}^{\,3}}\left(H_{bf}\frac{\partial B_{bf}}{\partial r}+B_{bf}\frac{\partial H_{bf}}{\partial r}\right)=-\frac{\partial H_{bf}}{\partial r}-\frac{\partial \eta_C}{\partial r}-S_f \tag{41}$$

Substituting in definitions for the square of the Froude number Fr^2 into Eq. (42) and bed slope S into Eq. (43) and rearranging allows further simplification to Eq. (44).

$$Fr^2=\Phi=\frac{Q_{bf}^2}{gH_{bf}^3B_{bf}^2} \tag{42}$$

$$S=-\frac{\partial \eta_C}{\partial r} \tag{43}$$

$$\frac{\partial H_{bf}}{\partial r}=\frac{S-S_f+\Phi\frac{H_{bf}}{B_{bf}}\frac{\partial B_{bf}}{\partial r}-\frac{2H_{bf}}{\varepsilon}\Phi\frac{\partial \varepsilon}{\partial r}}{\left(1-\Phi\right)} \tag{44}$$

The resulting equations includes a term for the spatial derivative of channel width B_{bf}. For most real-world rivers, this term could be scaled out by the width to depth ratio, H_{bf}/B_{bf} since width is typically much larger than depth. The leaky channel parameter ε is either known or modelled independently. However, the equations can also be transformed into a more useful form, as shown below.

Friction slope can be recast as a function of the square of Froude number and Chezy friction coefficient in Eq. (45).

$$S_f=\frac{\Phi}{Cz^2} \tag{45}$$

Our past definitions in Eqs. (21) and (36) show slope-dependent forms for *Cz* and τ^*_{bf}. These formulas are based on river channels where the data is assumed to be captured at near-equilibrium conditions and normal-flow conditions are assumed such that water surface slope and bed slope are parallel. We relax this assumption by replacing S with S_f in Eqs.(21) and (36). Combining Eq. (36), modified to use S_f, with Eq. (45) gives the squared-Froude number as a function of friction slope alone.

$$\Phi = \alpha_{Cz}^2 S_f^{1-2n_{Cz}} \tag{46}$$

Combining Eqs. (46) and (47) gives a simplification for the square of the Froude number:

$$\tau^*_{bf} = \frac{H_{bf} S_f}{RD_{50}} = \gamma\beta\left(D^*\right)^n {S_f}^m \tag{47}$$

$$\Phi = \alpha_{Cz}^2 \left(\gamma\beta RD_{50}\right)^{\frac{1-2n_{Cz}}{1-m}} \left(D^*\right)^{\frac{n\left(1-2n_{Cz}\right)}{1-m}} {H_{bf}}^{-\frac{1-2n_{Cz}}{1-m}} \tag{48}$$

The spatial derivatives of Eq. (42) and Eq. (48) are given in Eq. (49) and Eq. (50), respectively. These can be simplified into the form of Eq.(51):

$$\frac{\partial \Phi}{\partial r} = -\frac{3}{H_{bf}} \Phi \frac{dH_{bf}}{dr} - \frac{2}{B_{bf}} \Phi \frac{dB_{bf}}{dr} \tag{49}$$

$$\frac{\partial \Phi}{\partial r} = -\frac{1-2n_{Cz}}{1-m} \frac{\Phi}{H_{bf}} \frac{\partial H_{bf}}{\partial r} \tag{50}$$

$$\frac{H_{bf}}{B_{bf}} \Phi \frac{dB_{bf}}{dr} = \Phi \frac{\partial H_{bf}}{\partial r} \left(\frac{1}{2} \frac{1-2n_{Cz}}{1-m} - \frac{3}{2} \right) \tag{51}$$

The above relations can be combined yield backwater forms:

$$\frac{\partial H_{bf}}{\partial r} = \frac{S - S_f - \frac{2H_{bf}}{\varepsilon} \Phi \frac{\partial \varepsilon}{\partial r}}{\left(1 - \Phi\left(\frac{1}{2} \frac{1-2n_{Cz}}{1-m} - \frac{1}{2}\right)\right)} \tag{52}$$

$$\frac{1}{s_s}\frac{\partial H_{bf}}{\partial \hat{r}} = \frac{S - S_f - \frac{2H_{bf}}{\varepsilon s_s}\Phi\frac{\partial \varepsilon}{\partial \hat{r}}}{\left(1 - \Phi\left(\frac{1}{2}\frac{1-2n_{Cz}}{1-m} - \frac{1}{2}\right)\right)} \tag{53}$$

Shoreline Migration

Shoreline migration is computed similarly to past models. However, these models had only a single elevation drop from foreset to basement, so the foreset extends from the channel elevation down to the basement elevation. The model described herein assumes that the foreset begins at the average delta elevation and follows a constant, assumed foreset slope S_a to the pre-delta basement layer. The basement surface is assumed to have constant slope, and the delta extends radially across this planar surface. Normal flow models use the shoreline migration equations from Kim et al. (2009a) (as shown in more detail with a moving delta apex in Kim et al., 2009b). Shoreline migration for the backwater models uses a modification of Kim et al. (2009b) to relax the assumption of normal flow. The Parker and Sequieros (2006) model assumes a conical frustum shape for the basement slope such that basement slope S_b cannot be considered constant.

The dimensionless speed of migration of the topset-foreset break $\dot{s}_s$ (shoreline migration speed) and the foreset-bottomset break $\dot{s}_b$ are described in Eq. (54) and Eq. (55) respectively. A full derivation of the former is included in the appendix. The latter is identical to the Parker and Sequieros (2006) method.

$$\dot{s}_s = \frac{1}{S_a}\left(\frac{I_f\left(1+\Omega\right)}{\left(1-\lambda_p\right)\left(\frac{\Theta}{2}s_b^{\,2} - \frac{\theta}{2}s_s^{\,2}\right)}Q_{t,bf}\Big|_{\hat{r}=1} - \frac{\partial \bar{\eta}}{\partial \hat{t}}\Big|_{\hat{r}=1}\right) \tag{54}$$

$$\dot{s}_b = \frac{1}{\left(S_a - S_b\right)}\left(\frac{\partial \bar{\eta}}{\partial \hat{t}}\Big|_{s_s} + S_a\dot{s}_s\right) \tag{55}$$

The delta topset progradation speed plays an important role in the dimensionless Exner equation in Eq. (12), but the shoreline migration rate requires the specification of the temporal derivative of the average delta elevation at the last node, i.e. $r = s_s$. We assume this value to be initially zero, and then update the value after change in elevation has been predicted. The shock condition at the topset-foreset transition includes the term Θ related to connection of the radial topset to the flat basement plane it migrates over. This is defined as Eq. (56); further details are given in the appendix.

$$\Theta = \int_{-\theta_0/2}^{\theta_0/2} \left(1 - \frac{S_b}{S_a}\cos\theta\right)^{-2} d\theta \tag{56}$$

Incision into pre-delta substrate

Shaw et al. (2013) elaborate on the importance for understanding pseudo-bedrock dynamics on the morphology of the Wax Lake Delta. The Holocene-aged clay deposits apparently act to inhibit the channel erosion. The authors suggest a methodology from Lamb et al. (2008) that abrades the basement surface causing incision and found similar results to measured erosion rates in the Wax Lake Outlet. This model has several detailed parameters related to the bedrock characteristics that have yet to be fully detailed in the field. We instead use a simpler model and parameterize the coefficients based on measured bedrock changes through time. The basic function for erosion rate is a rate-excess law, as in Eq. (57), where erosion occurs when a critical threshold bed shear stress is met. This is a typical form to estimate erosion rate of cohesive sediments, e.g. (Garcia, 2008, Eq. 4-35) is based on dimensioned bed shear stress and critical shear stress of cohesive sediments. As in the referenced example, we assume $n_{coh} = 1$ and parameterize α_{coh} and $\tau_{b,coh}$ based on modelled morphodynamic changes. The coefficient α_{coh} affects the temporal rate of basement incision and $\tau_{b,coh}$ affects the spatial extent of basement incision. The latter is additionally modulated by the presence of juvenile channels, which relate to a reduction in bed shear stress. The cover effect is introduced in Eq. (58), as the basement layer is only eroded when bedrock is exposed. The tools-effect model developed by Sklar and Dietrich (2004) implies bedrock erosion is maximal when $p_c = 0.5$, but, the implementation present here allows maximum incision as p_c approaches zero. This is because the substrate is treated a consolidated mud rather than bedrock, so that shear stress rather than tools plays the key role in determining the incision rate (e.g. Garcia, 2008). We use Eq. (58) for this purpose; it is translated into dimensionless terms as in Eq. (59). This methodology is only used when backwater hydraulics and the distributed Exner equation are also implemented; models with normal flow closure are not able to predict channel incision.

$$E_{coh} = \alpha_{coh}\left(\tau_b - \tau_{b,c}\right)^{n_{coh}} \tag{57}$$

$$\frac{\partial \eta_{base}}{\partial t} = \left(1 - p_c\right) E_{coh} \tag{58}$$

$$\frac{\partial \eta_{base}}{\partial \hat{t}} = \left(1 - p_c\right) E_{coh} + \frac{\dot{s}_s}{s_s}\hat{r}\frac{\partial \eta_{base}}{\partial \hat{r}} \tag{59}$$

Results

Generalized width and elevation data at Wax Lake Delta

The delta first showed signs of subaerial growth in 1973 (Roberts et al., 1980; Wellner et al., 2006), though subaqueous development certainly preceded this result. Parker and Sequieros (2006) and Kim et al. (2009a) select 1980 as the initial condition for their model runs per results of Majersky et al. (1997) that suggest the start of rapid delta progradation at that time. We use similar initial conditions suggested in Kim et al. (2009a). Data were collected for cumulative channel width, channel bed elevation, and floodplain/island elevation during four years spaced by ~10 years: 1989, 1998, 2006, and 2015. These data are not monotonically spaced per data availability. Data from the two earliest years (1989, 1998) were collected by the United States Army Corps of Engineers (USACE); these data consist of single beam bathymetry and topography surveys. A 2006 DEM with partial coverage of Wax Lake Delta is available via the United States Geological Survey. The 2015 dataset is a coupled multibeam bathymetric survey and aerial LiDAR topographic survey (Shaw et al. 2016b); this data set has considerably finer resolution and data density than the other sources. The models to be tested herein have generic delta architecture and assume a single lumped channel that is intended to be representative of all delta channels combined.

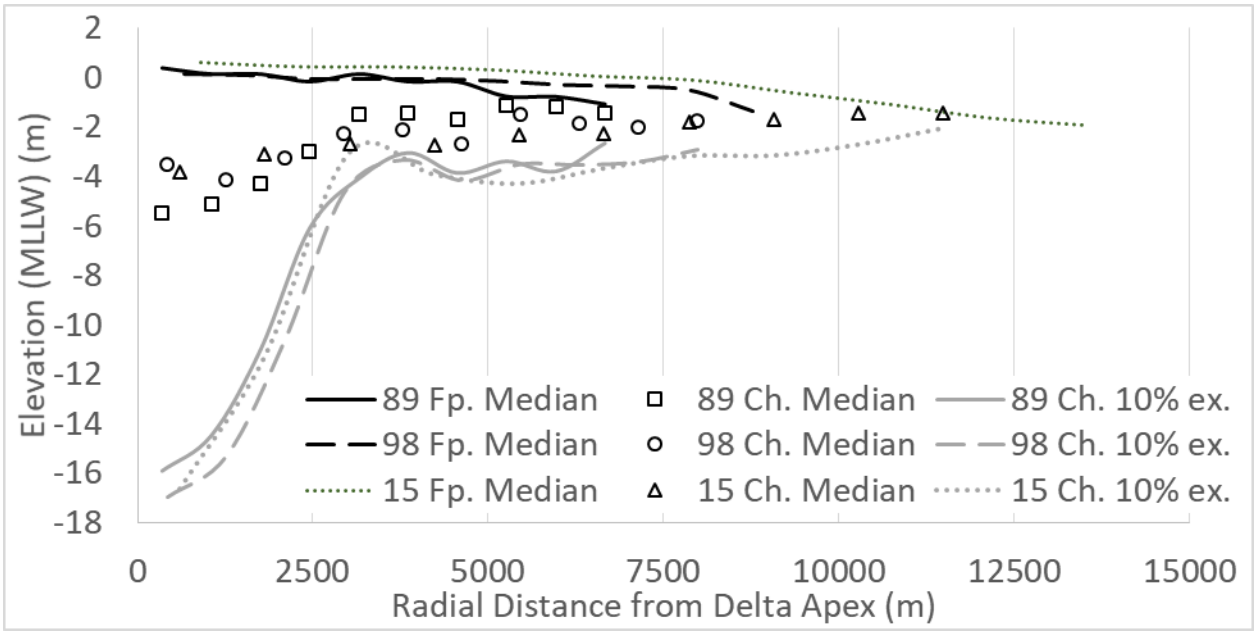

Figure 3-4: Generalized Elevations from Wax Lake Delta in 1989, 1998, and 2015. Here "Fp Median" denotes floodplain median elevation, "Ch Median" denotes channel median elevation, and "Ch 10% ex." denotes thalweg elevation. Data were designated as channel or floodplain areas based on visual inspection of imagery from each year. Data are binned based on radial distance from the delta apex and category, then the median of channel and floodplain areas and the channel elevation that exceeds 10% of all points in the subset are computed.

The complete dataset is generalized by segmenting into discrete bins separated by specified radial distances from the delta apex (Figure 3-4). For each data year, the approximate boundary between channel and inter-channel areas is defined by the measured elevation and through inspection of a LANDSAT Raw Annual satellite image of the delta. The elevation data were separated with these observations to create sample sets for both channel and floodplain elevations. The cumulative distribution function of depth within these regions is computed along with the median value. The channel thalweg is estimated as the elevation that exceeds 10% of the sample set because the minimum measured elevations may be outliers. The model predicts bankfull channel depth, which relates to average channel depth in a cross section. It is not feasible to measure bankfull depths in the 1989 and 1998 datasets due to alignment of the data, nor in 2006 due to insufficient coverage of the DEM. This type of measurement is feasible with the 2015 DEM, and a test at the delta apex shows H_{bf} = 10m, while depths at the thalweg are around 15m (Figure 3-4). Median channel elevation, channel thalweg elevation, and median floodplain/island elevations are plotted in Figure 3-4. In that figure, "Fp Median" denotes floodplain median elevation, "Ch Median" denotes channel median elevation, and "Ch 10% ex." Denotes thalweg elevation.

Cumulative channel width is also collected at selected radial distances away from the delta apex that correspond with the center of each bin and plotted in Figure 3-5. Delta area is measured in 2015 using the DEM based on the subaqueous extent of delta channels. Channel area estimates are computed by creating a mask of channel area based on elevation and through visual inspection of banklines from LANDSAT annually averaged raw imagery. Total channel area only includes main channels, i.e. sub-channels connecting into islands are not included. Only channel area beyond the delta apex is included. In all years, the measured data show rapid spatial width expansion, followed by a decline downstream. Over time, the 2500m wide section seems to extend basinward. The trend for decreased total width beyond this region relates to asymmetry of the delta topset. Average channel width is mostly invariant in space, so the decrease should not be compared to model results that assume axisymmetric growth patterns. See the Appendix for a more detailed explanation.

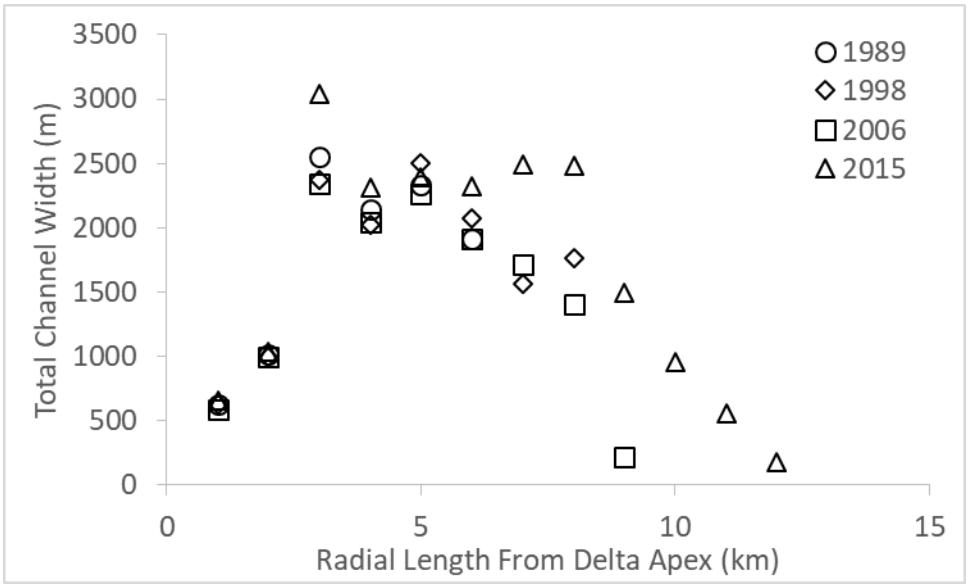

Figure 3-5: Cumulative channel width of all channels at a given radial distance from the delta apex.

The pre-delta substrate elevation is modelled from an initial condition via measurements by Shaw et al. (2013). Substrate elevations within the delta are generalized by radial distance from the delta apex, and the feed channel is assumed to extend past the delta apex per observations of the authors. The Wax Lake Outlet feeder channel depth varies along the channel, but approaches approximately 13m at the delta apex. Values in Shaw et al. (2013) are presented in terms of a mean sea level (year 2000) datum, and translated by assuming constant sea-level rise and subsidence rates, which are identical in all model runs. All elevations were converted to MLLW to match the 2015 DEM via vDatum software (Parker et al., 2003) and relations between mean sea level and MLLW at the Amerada Pass tidal gage in Atchafalaya Delta. Similarly, the modelled water surface elevation is taken as the modern day MSL value adjusted to MLLW reference frame; we subtract the assumed sea level rise rate over 35 years (from 1980 to 2015) so the modelled sea level rise in 2015 matches. The assumed pre-delta surface for modelling delta basement interactions is illustrated in Figure 3-6.

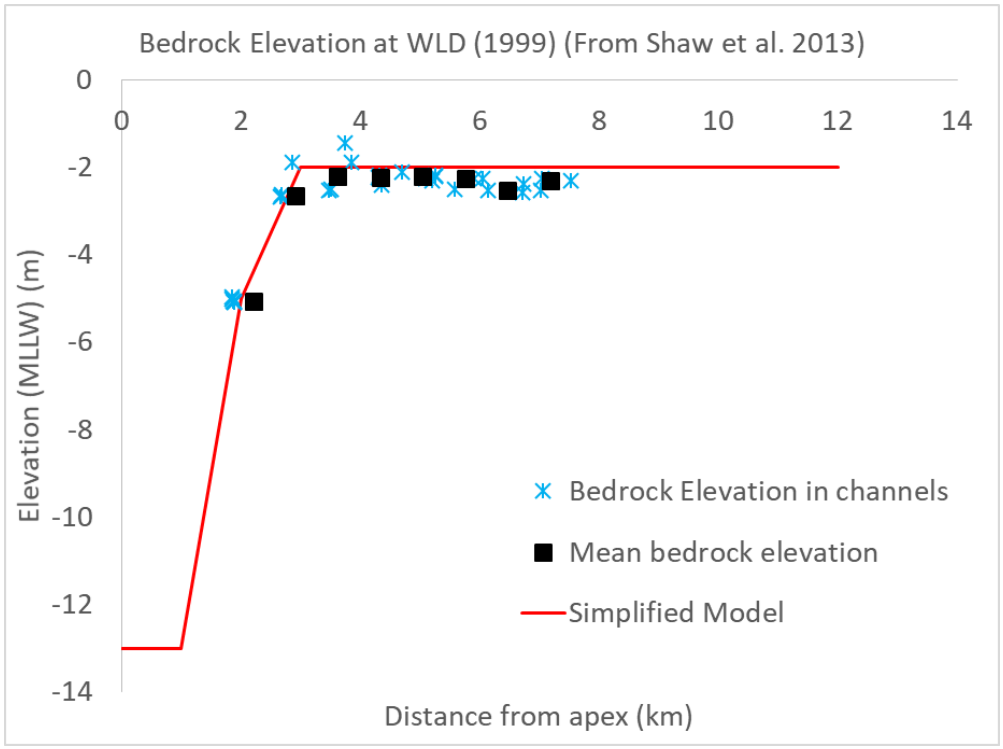

Figure 3-6: The consolidated clay pre-delta/basement elevation is expressed as a function of radial length from the delta apex. The blue asterisks represent basement elevation estimated by Shaw et al. (2013), the black squares are the means of values in discrete bins from the delta apex, and the red line represents a simplified representation of initial condition of the model. The initial basement elevation in the upstream feed channel is approximately -13m (MLLW m) per measurements by Shaw et al. (2013).

The normal flow closures for width, depth and slope require known values for water and sediment discharge, median grain size, and the juvenile channel decay factors ε and γ. By assuming conditions at Wax Lake Delta after Kim et al. (2009a) we compute channel dimensions in the delta, assuming normal flow, by solving a range of decay factors. Water discharge Q_w = 4800 m^3/s, sand discharge Q_t = 0.16 m^3/s, and D_{50} = 0.1 mm. Measurements at Wax Lake Delta suggest ε = 0.6 and γ = 0.6 at the delta periphery, so we can make a first-order assumption that these values are equal. Figure 3-7 shows predicted values for B_{bf}, H_{bf}, and S normalized by the mature conditions when $\varepsilon = \gamma = 1$; these results are shown over a range of ε and γ from 0 to 1, which resemble changes from juvenile to mature channel structure.

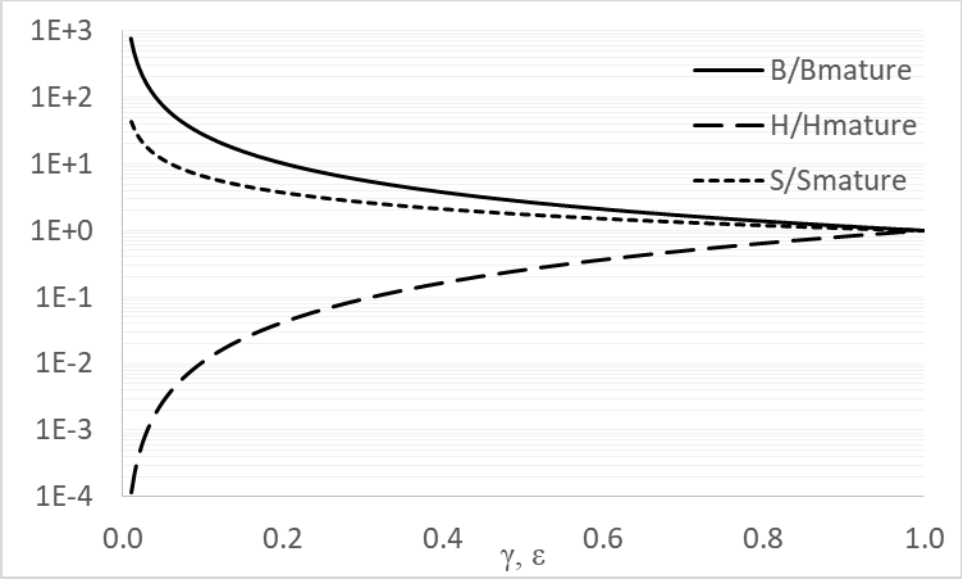

Figure 3-7: A phase diagram of relative relationship between depth, width, and slope as the juvenile channel decay factor γ and flow confinement parameter ε increases from [0,1). These results are derived from the normal flow closures presented here and relate to the Wax Lake Delta values Q_{bf} = 4800 m3/s, Q_t = 0.16 m3/s, and D_{50} = 0.1 mm, as per Kim et al. (2009). All values are normalized by the mature values predicted when γ=1, thus they converge to the point (1,1). The figure shows that, assuming normal flow, as the decay factor γ approaches zero, channels become infinitely wide and infinitesimally deep. Comparing results at γ=0.4, depth decreases by an order of magnitude, width increases by a factor of 5 and slope increases by a factor of one.

Model results

A total of 40 numerical runs were completed to understand how inclusion of different features affect development of typical delta morphodynamics in a geometric style model. The model inputs are shown in Table 3-1. Input conditions for Wax Lake Delta from Kim et al. (2009a) are used, and are consistent for all runs; only various model features are turned on/off. The delta angle is updated from the Kim et al. (2009a) values as elaborated in the Appendix. Each run represents a different binary combination of model features, i.e. with a given feature, such as juvenile channels, turned on and turned off.

Table 3-1: Input Values for model runs.

Term	Symbol	Value	Units
Channel-forming water discharge	Q_w	4800	m3/s
Mean-annual sediment yield	$Q_{t,feed}$	25.6/38.4	Mt/yr
Fraction of sand in sediment yield	f_{sand}	0.183	-
Flood intermittency	I_f	0.35	-
Units washload deposited per unit sand	Ω	0.49	-
Bed material grainsize	D_{50}	0.1	mm
Submerged specific gravity	R	1.65	-
Sediment porosity	λ_p	0.6	-
Chezy coefficient	Cz_{const}	20	-
Coefficient in Cz eqn (Li et al. 2015)	a_{Cz}	2.53	-
Exponent in Cz eqn (Li et al. 2015)	n_{Cz}	-0.19	-
Initial water surface elevation (MLLW)	ξd_0	0.186	m
Initial channel elevation (MLLW) (Normal Flow)	$\eta_{c,0}$	0.186	m
Initial channel elevation (MLLW) (Backwater)	$\eta_{c,0}$	-1.5	-
Initial basement elevation (MLLW)	$\eta_{base,0}$	-2	m
Initial delta length	$s_{s,0}$	4300	m
Initial delta slope	S_0	varies	-
Initial basement slope	S_b	1.80E-04	-
Foreset slope	S_a	0.002	-
Delta topset angle	θ	86	Degrees
Sea-level rise rate	$d\xi/dt$	2	mm/yr
Subsidence rate	σ	5	mm/yr
Initial slope of guide channel (Normal)	S_{guide}	0	-
Initial slope of guide channel (Backwater)	S_{guide}	0	-
Initial width of guide channel	B_g	300	m
Initial Width of guide channel floodplain	$B_{g,f}$	1700	m
Length of guide channel	$L_{g,0}$	25000	m
Model start time	-	1980	-
Model end time	-	2015	-
Channel forming Shields number (constant)	$\tau^*_{bf,const}$	1.86	-
Channel forming Shields number (variable)	β	182	-
Channel forming Shields number (variable)	m	0.365	-
Channel forming Shields number (variable)	n	-0.87	-
Rate coefficient for flow leaking from channels	k_{Qw}	0.5	-
Rate coefficient for decayed Shields stress	k_τ	0.5	-
Macroroughness height/dune height	L_{ac}	0.5	m
Coefficient clay basement incision	α_{coh}	1.00E-08	-
Critical shear stress for cohesive basement	τ^*_c	4	Pa
Coefficient for temporal γ growth	C_1	1.00E-06	-
Coefficient for temporal γ decay	C_2	1.00E+03	-

For normal flow models, 3 binary conditions are tested including: Constant Shields number vs. Variable Shields Number, presence of Juvenile channels vs. only fully mature channels, and Smaller or Larger sediment feed rate ($Q_{t,feed}$); this requires 2^3 (8) model combinations. Models with backwater hydraulics also include additional binary conditions for: assumed fixed-width feed channel versus a self-formed width feed channel and presence of cohesive basement material vs. a fully alluvial basement. The backwater runs include 2^5 (32) combinations, thus reaching 40 total runs. All models include the same initial basement elevation. When the basement is a consolidated clay surface rather than alluvium, the below-capacity transport and basement incision framework are used to model development of this interface. Model runs are compared against measured data presented here along with data from past researchers at Wax Lake Delta. In conditions where present-day data is not available, values are estimated from the 2015 DEM and/or aerial imagery. The figures given below in this section make reference to a full model which includes variable bankfull Shields number, juvenile channels, incision in a pre-delta substrate material and the larger sediment feed rate value. The figures also use models identical to Kim et al. (2009a) and similar to Parker and Sequieros (2006) as base case comparisons for normal flow and backwater hydraulics, respectively.

Delta progradation from 1980 to 2015 is presented in Figure 3-8. Measured delta extent from past years is included for comparison (Roberts et al. 2003, Dumars, 2002, Wellner et al. 2006). The delta extent in 2015 is estimated from the 2015 DEM; the modern delta is elongated along the main axis of the delta, which has shorter radial extents toward the boundary of the accommodation space. The delta angle is selected to minimize total error of the measured arc lengths at discrete radial distances from the delta apex; this process is discussed in more detail in the Appendix. This angle is smaller than values used in Parker and Sequieros (2006) and Kim et al. (2009a), and relates to the mean delta extent. The result of the Kim model is reproduced here for comparison along with a model similar to Parker and Sequieros (2006). The latter is characterized by backwater hydraulics and constant Shields number; it differs from the original model via the distributed Exner framework and the assumption of a flat basement rather than a conical frustum, and updated input conditions. The envelope of all model runs increases in breadth quickly, and then seems to converge to a constant value. The full model, characterized by self-formed feed channel, variable Shields number, juvenile channels, bed rock incision, and the larger $Q_{t,feed}$ rate compares similarly to measured delta progradation rates as the reference models.

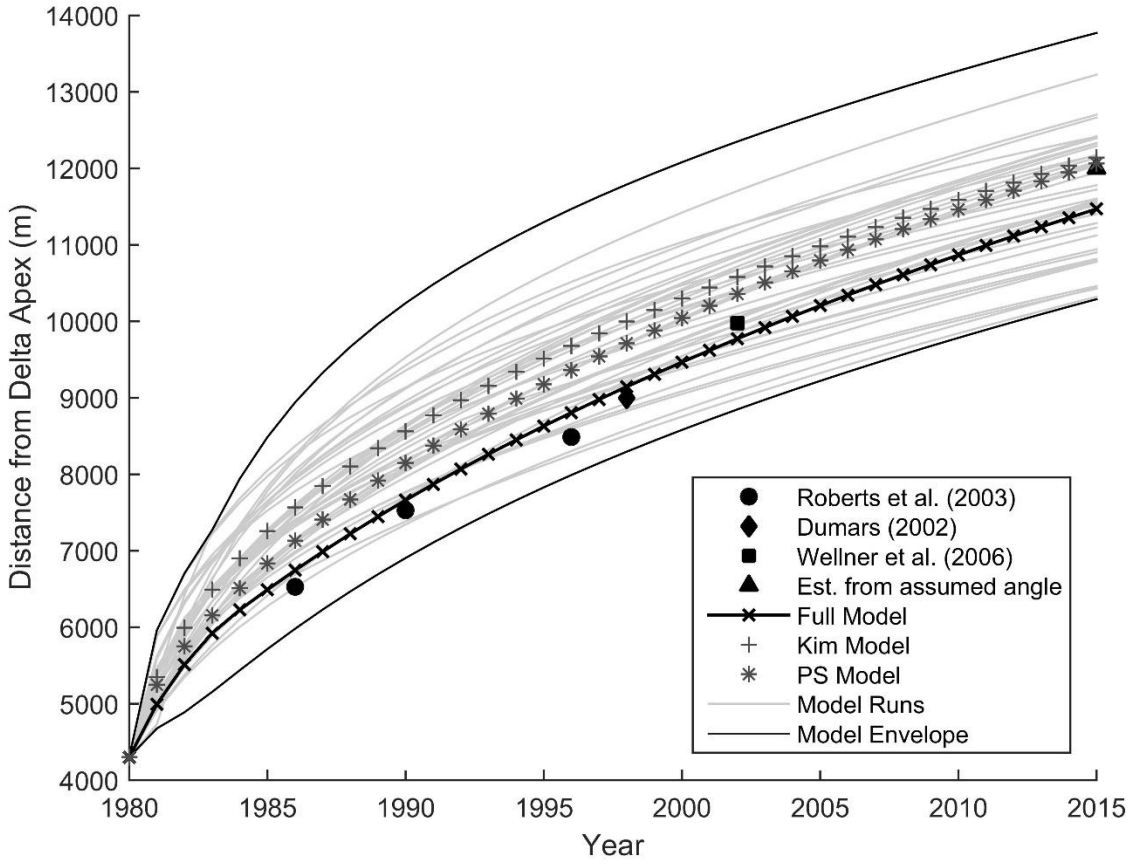

Figure 3-8: Envelope of model results for progradation rate s_s versus time, including all 40 runs. The gray lines represent individual runs and the dark black lines define the envelope of values. Data from past field researcher are shown; an additional point for 2015 is estimated as detailed in Appendix B.

Area of the delta topset is plotted against time in Figure 3-9. Measured data from Majersky et al. (1997) and Roberts et al. (2003) are included with an additional value for 2015. Model results as presented by Parker and Sequieros (2006) and a regression of subaqueous delta area estimated via aerial imagery by Shaw et al., (in preparation) are also included. The two reference models and the full model compare well with measured results. All three models appear to approach parallel to the growth rate estimated by Shaw et al. (in preparation). The uncertainty amongst models appears to plateau at the end of simulation time as the total model run envelope approaches a constant width.

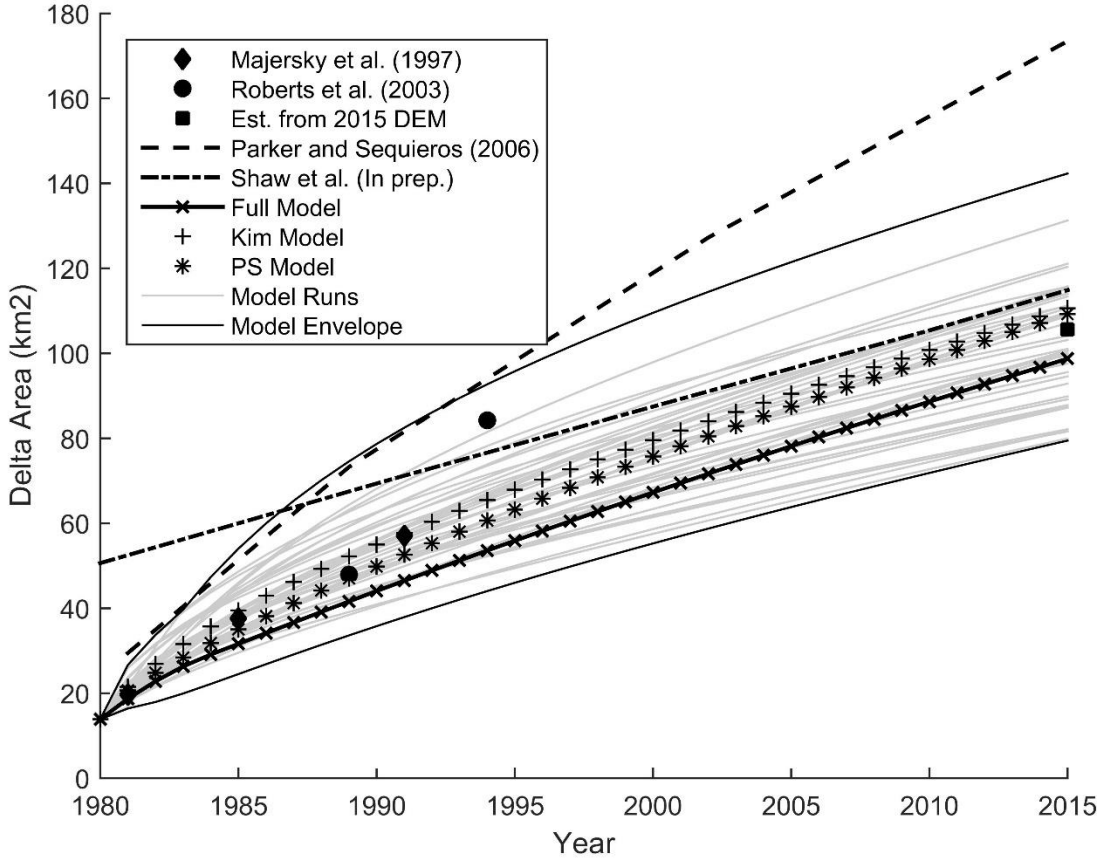

Figure 3-9: Delta area predictions for all 40 model runs. Models with similar features to Parker and Sequieros (2006) and Kim et al. (2009) are presented with the full model with dark markers. Measured data from past researchers are included for comparison; an additional 2015 data point based on the subaqueous channel extent of the 2015 DEM surface is also included. Results from Parker and Sequieros (2006), with their input parameters and conditions, are shown as a heavy dashed line. Also shown is a regression fit on estimated subaqueous channel area from aerial imagery (Shaw, Personal Comm.) is shown with a centerline dash.

Cumulative channel area integrated across the entire delta topset is plotted in Figure 3-10. This figure shows more significant model variation than found in comparison to s_s and A_D. The reference models both under-predict the total channel area in the delta, while the full model follows the observed temporal trend for channel area that increases over time.

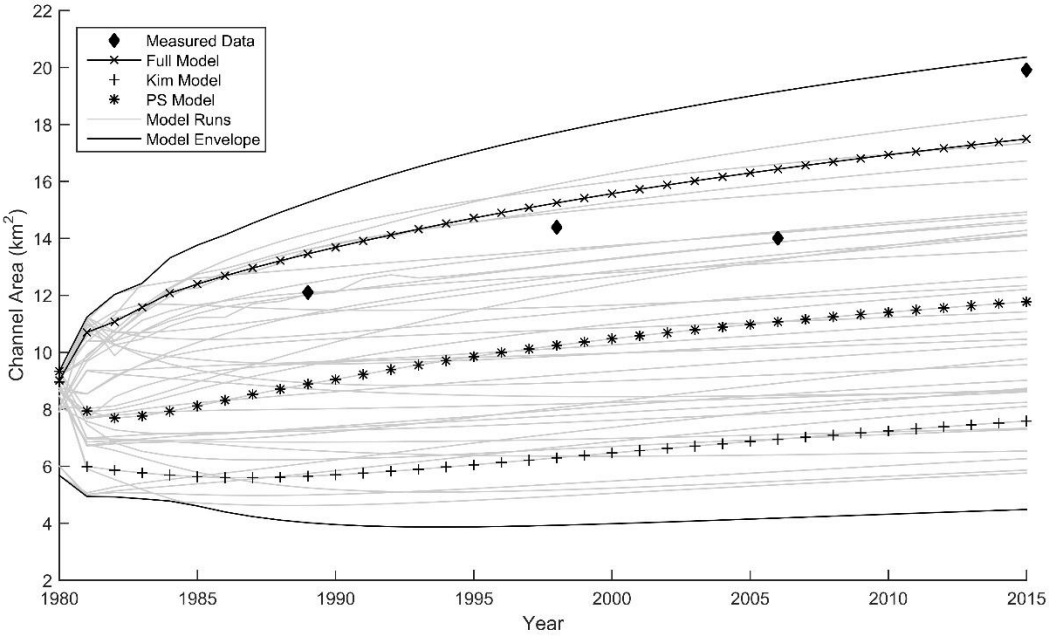

Figure 3-10: Total channel area across the topset over time. Data collected by extracting a channel mask of the subaerial extent of channels from annually averaged imagery. Results from the reference models are shown, along results from all 40 runs with and without backwater.

Models with normal flow conditions are compared using data for delta extent and area in Figure 3-11. The field data presented in each subplot is identical across each row. The lines from the predictions are also identical across each row, but the shading is different so as to emphasize different features.

Figure 3-11-a_1 and Figure 3-11-a_2 compare modeled results for delta extent and delta area, respectively as a function of time, along with observations (circles) and modeling envelopes (thick black lines). In this figure the thin black lines correspond to variable τ^* and the thin gray lines correspond to constant τ^*. Figure 3-11-b_1 and Figure 3-11b_2 contain the same information, except that the thin black lines correspond to the inclusion of juvenile channels and the thin gray lines correspond to mature channels only. Figure 3-11-c_1 and 3-11-c_2 again contain the same information, except that the thin black lines correspond to a larger sediment feed rate, and the thin gray lines correspond to a smaller feed rate. The results are similar among all cases.

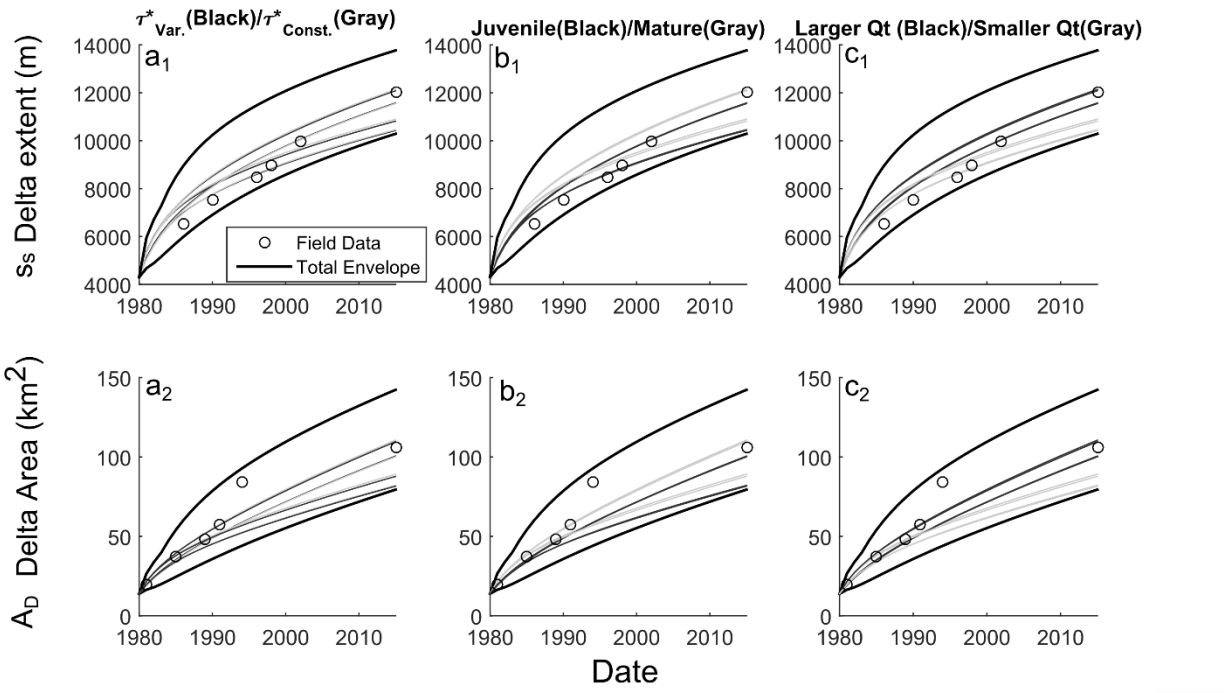

Figure 3-11: Results for all normal flow models are compared against measurements of delta topset extent s_s (top) and delta area A_D (bottom). All plots in the same column show the same data, but with different representation. The black outer lines represent the envelope of all runs, i.e. all cases with backwater and normal flow closures. Each column represents a different pair of conditions;; the first column shows results with variable τ^*_{bf} (dark) and constant τ^*_{bf} (light), the 2nd column shows juvenile channels (dark) and fully-mature channels (light), and the last column shows results with larger $Q_{t,feed}$ (dark) and smaller $Q_{t,feed}$ (light).

Modelled channel width, as represented by a single lumped channel, is compared to cumulative channel widths at specified distances from the delta apex in Figure 3-12. All model runs are shown in gray and the two reference models and full model are highlighted with symbols. No models are capable of accurately capturing the total channel width or its variation at WLD, which includes a rapid width increase from 300 m in the Wax Lake Outlet feeder channel to approximately 2500m over a distance of several kilometers. (The actual length depends on year). The reference models both predict narrow channels with little spatial variation. The full model predicts increased channel width down delta, but under predicts the initial expansion at 5 km from the delta apex. As noted above, the trend for decreasing total channel width beyond the wide section is due to delta asymmetry, so it is not considered in our analysis.

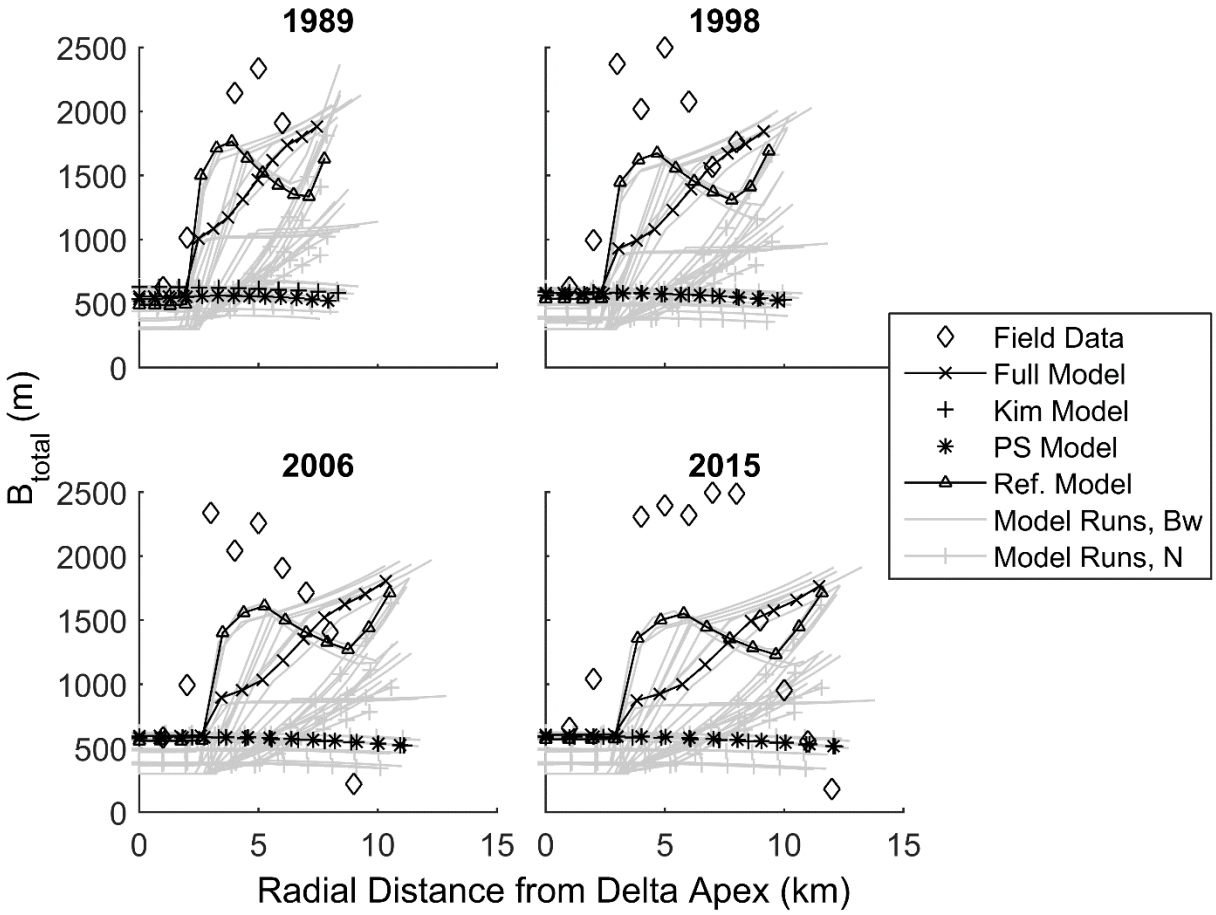

Figure 3-12: Modelled width for all normal flow and backwater hydraulic models with particular focus on a model similar to Parker and Sequieros (2006) (PS), the normal flow model of Kim et al. (2009) and the full model including variable Shields number, basement incision, and juvenile channels. The Ref. Model relates to constant bankfull Shields stress, juvenile channels, and basement incision; the model most closely follows the width trends at WLD. Generalized field data for each of four years are noted in each subplot.

Models that assume a fixed width feed channel develop a narrower and deeper channel than the self-formed model. Models that best represents channel width at WLD (Constant bankfull Shields number, juvenile channels, incision into pre-delta substrate) simply keep the morphology of the initial condition set by Figure 3-6. The constant Shields number model also predicts a constant dimensioned bed shear stress, which is smaller than the specified critical Shields stress for cohesive sediment erosion. This model does indeed predict rapid downstream widening of the channel in the upstream part of the domain, as shown by the triangle markers in the figures, but this is the result of the model's inability to erode basement substrate. The variable Shields number model (full model in the figure) has different results because it is capable of eroding the substrate.

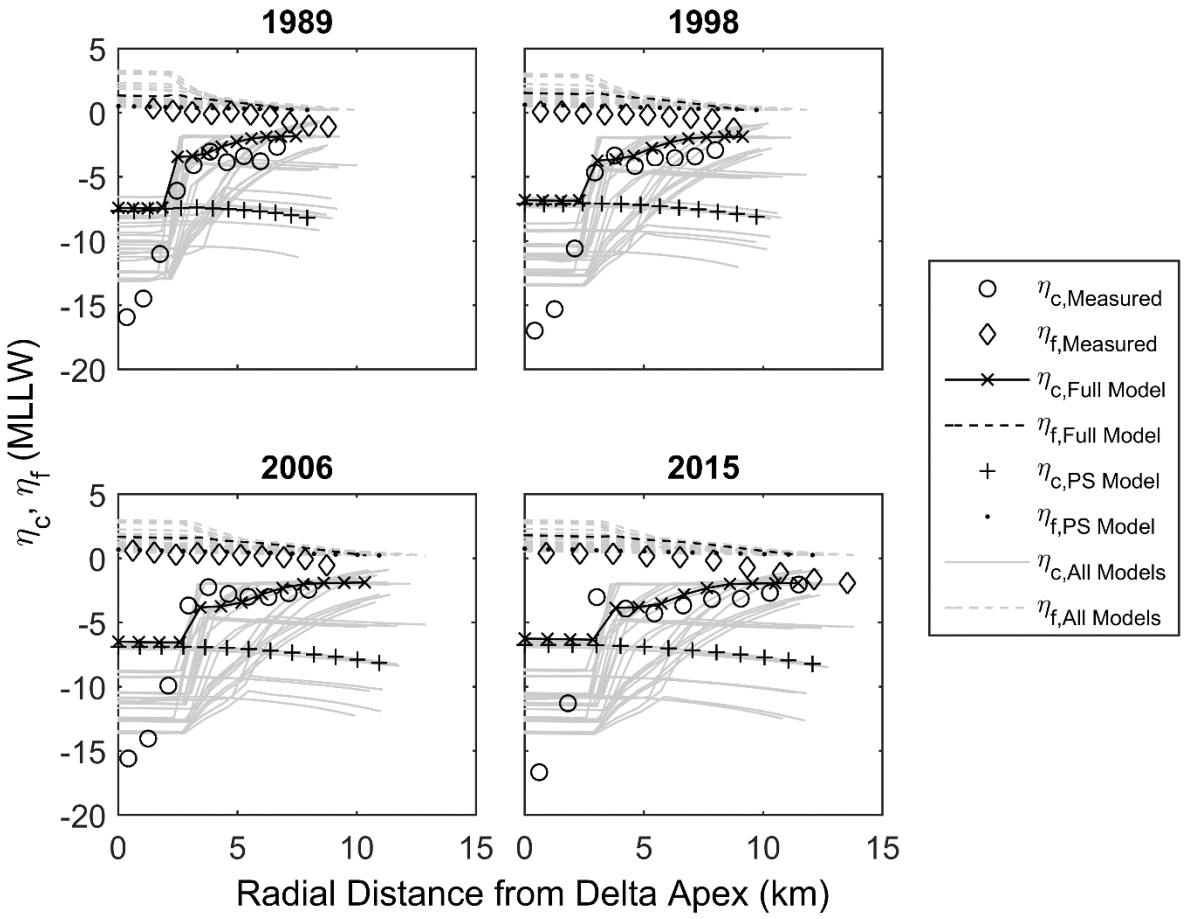

Figure 3-13: Modelled channel and floodplain elevations for all backwater hydraulic models, with particular focus on a model similar to Parker and Sequieros (2006) (PS) and the full model including variable Shields number, basement incision, and juvenile channels. Generalized field data for channel and inter-channel areas for each of four years is noted in each subplot.

Channel and floodplain elevations for all model runs are shown in Figure 3-13. Measured elevations for the channel and floodplain pertain to the generalized measurements discussed above. A reference backwater extension of the Parker and Sequieros (2006) model is highlighted for comparison. Channel and floodplain elevation measurements vary widely depending on model features. The full model presented here assumes a self-formed feed channel that has considerably higher elevation than the measured thalweg elevation.

Models that predict deeper channels either: assume a fixed width in the feed channel, or use a lower $Q_{t,feed}$ with in conjunction with constant bankfull Shields number model. The reference model predicts increasing depth downstream, while the full model better follows basinward trends in measured depth, in that it shows a pattern of shoaling downstream.

It can be useful to assess the effectiveness of model features by performing a leave-one-out analysis, where several model runs with one feature removed from the full model are compared against results of the full model. The effect of different model features on development of total channel width is included in Figure 3-14. This figure includes the full model with a single feature turned off (or turned on for the fixed-width feed channel scenario) along with the base reference models for normal flow and backwater hydraulics.

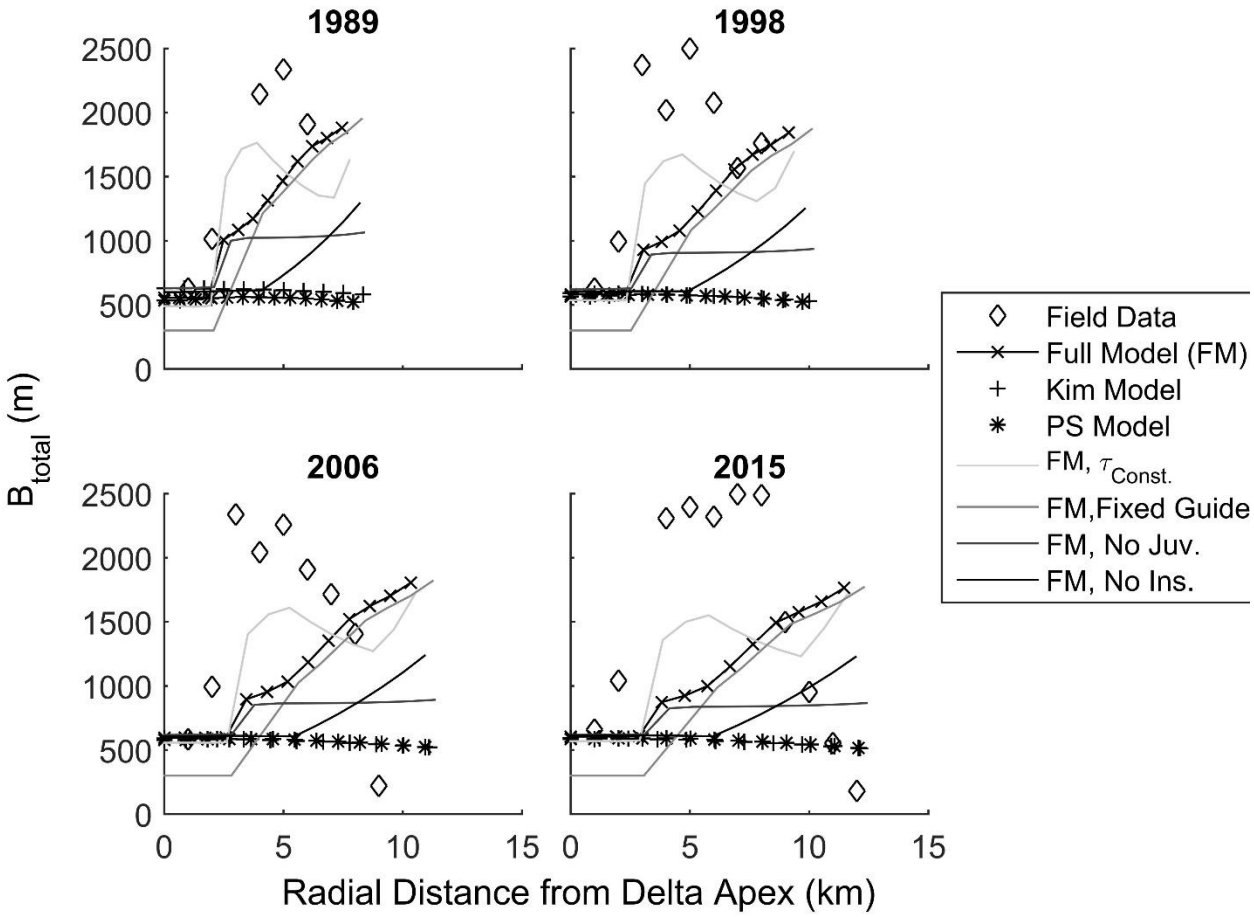

Figure 3-14: Comparison of predicted total channel width between several models that use a backwater hydraulic implementation. The PS Model is a backwater extension of the Parker and Sequieros (2006) model, i.e. constant τ^*_{bf} and Cz, The Kim Model is identical to the model of Kim et al. (2009a), and FM represents the full model presented herein. The full model is compared to similar versions that include one modification per run, e.g. full model with constant rather than variable τ^*_{bf}. Relevant field data are included in the plot.

The full model with constant bankfull Shields stress produces different trends in width when compared to the similar model with bankfull Shields Number, but these are related to the initial conditions as noted above. Including a fixed-width guide channel forces a narrower feed channel, but the downstream trend in width is quite similar to the full model. Assuming a basement composed of alluvium, a channel with little

spatial variation in width extends to r_{flood}, after which the channel width increases linearly. Finally, omitting juvenile channels results in spatially uniform width, as compared to width that increases downstream direction in the full model. When basement substrate is included, the model erodes basement until the shear stress matches the critical shear stress; if, for example, the full model were to predict a higher elevation for the feed channel, it would produce results similar to the base case.

Figure 3-15 shows the same leave-one-out model analysis effect on channel and floodplain elevations. The fixed-width feed channel model most closely resembles measured results at Wax Lake Delta. This model requires a forced width transition zone for model stability, which erases some of the dynamic effects found in the full model.

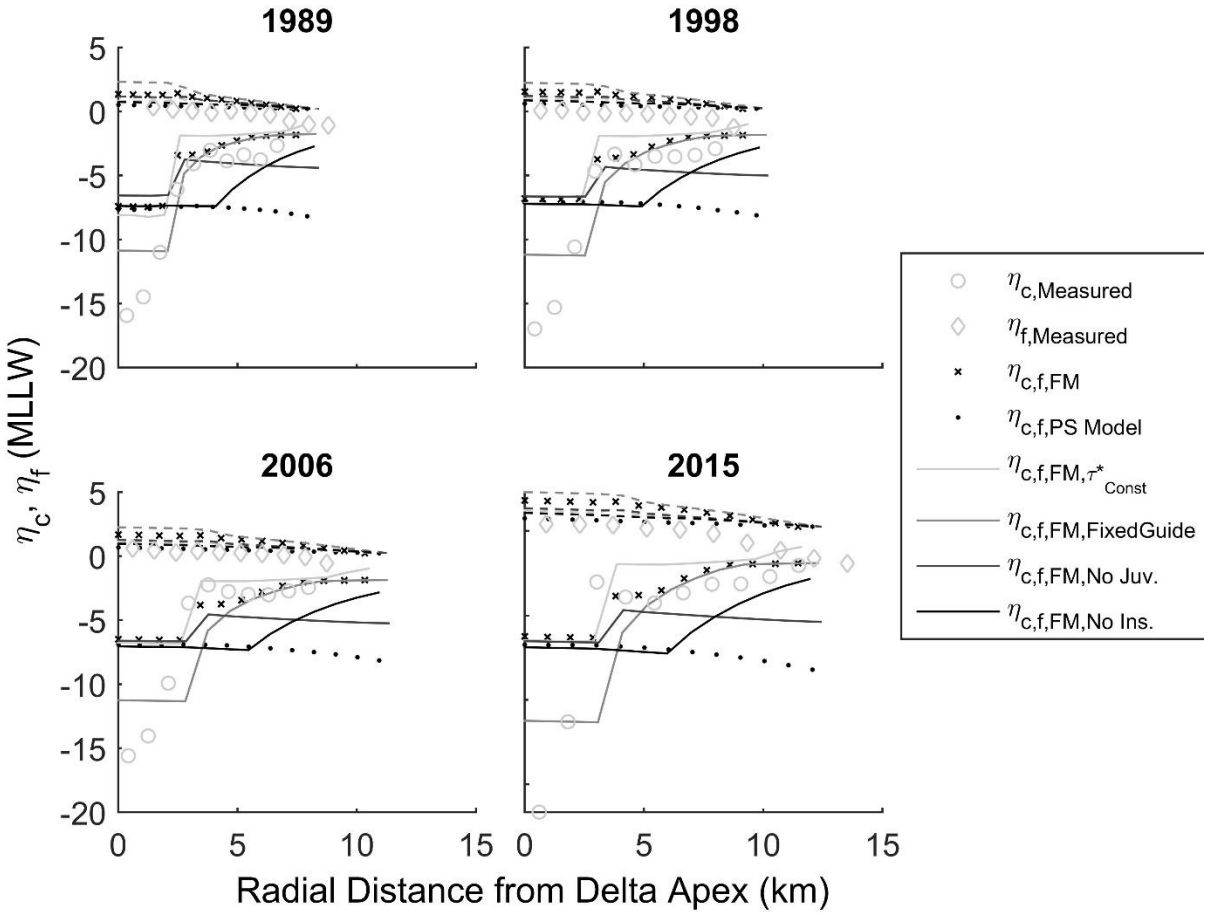

Figure 3-15: Comparison of predicted elevation between several models that use a backwater hydraulic implementation. The PS Model has similar features to the Parker and Sequieros (2006) model, i.e. constant τ^*_{bf} and Cz, and FM represents the full model presented herein. The full model is compared to similar versions that include one modification per run, e.g. full model with constant rather than variable τ^*_{bf}. Relevant field data are included in the figure.

The assumption of self-similar γ and ε is relaxed and applied to the full model to investigate how temporal evolution of these parameters may affect delta morphodynamics. Figure 3-16 illustrates the temporal and spatial evolution of γ and ε given the assumption of self-similarity (left side of figure) and temporal evolution via Eq. (26) (right side of figure). For the condition of self-similarity, slope decreases as the physical domain expands. In both models, the transition between mature and juvenile channels migrates downstream over time. The temporal evolution model involves rapid decrease in γ, ε, followed by steady increase over time. Differences between predicted channel and floodplain elevations from each model are included in Figure 3-17.

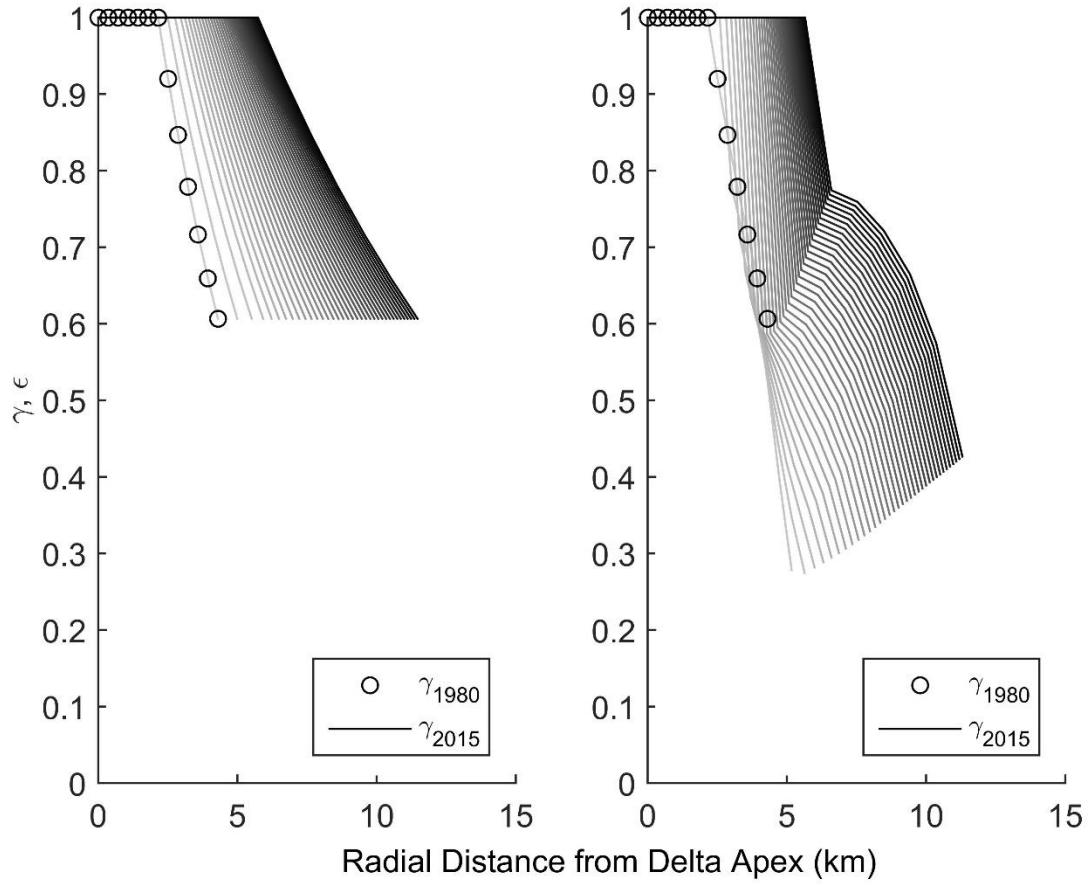

Figure 3-16: (left) Spatial variation in γ and ε for typical model conditions, i.e. assumption of self-similarity in dimensionless space. When γ= ε=1, the channels have a mature structure and maintain their discharge; the slope of γ and ε flattens over time. (right) Temporally evolving γ and ε; both conditions have identical initial conditions, but the temporally evolving model develops a different decay pattern in space.

Model results are generally similar and both tend to create an eroded bench just beyond the initial transition between deep feed channel and the shallow delta channel. This eroded region propagates downstream with delta progradation. The model with temporal evolution in γ and ε predicts a sharp transition between the eroded region and non-eroded region immediately basinward, while the self-similar version is more gradual.

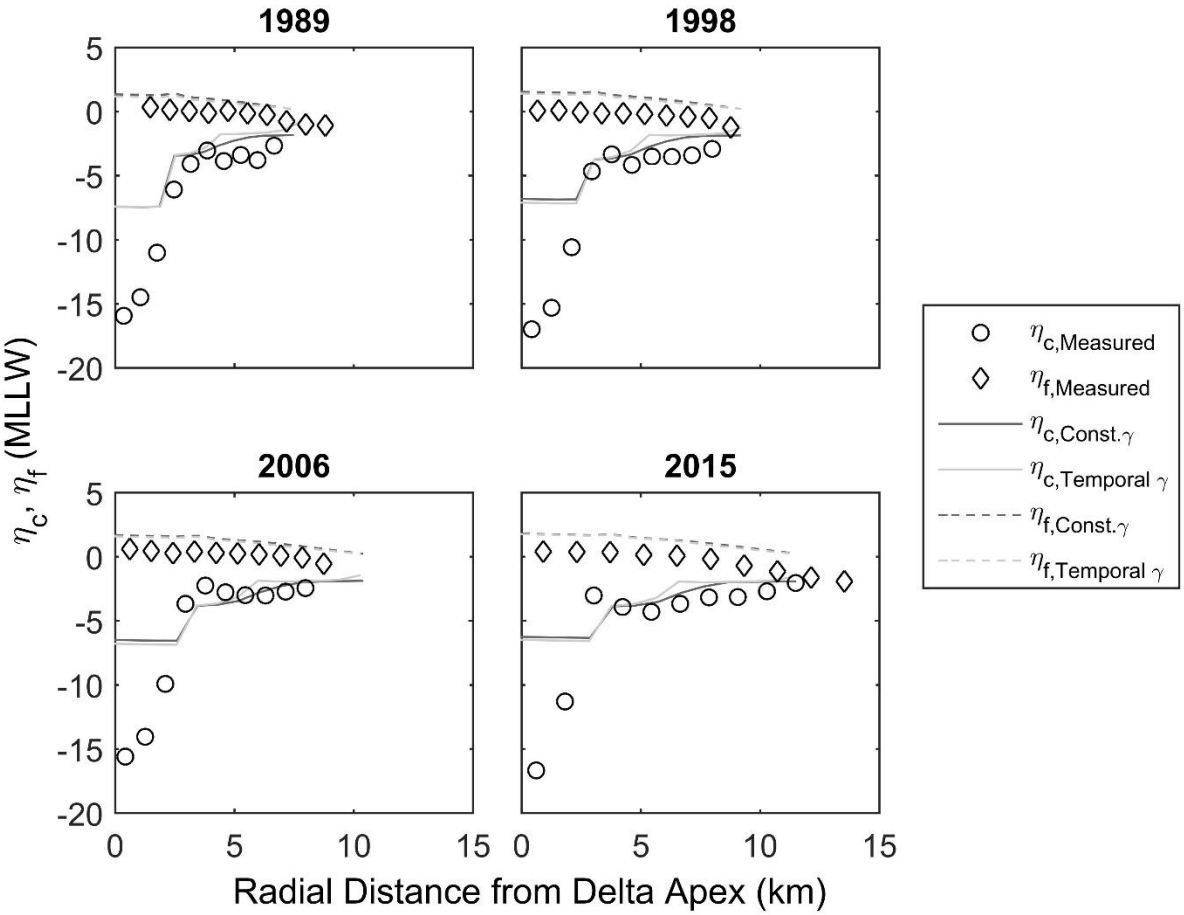

Figure 3-17: Modeled evolution of channel and floodplain elevations through time for the full model with the self- similar formulation for γ and ε versus the full model with temporally evolving γ and ε. Generalized field results from channel and inter-channel areas are included for comparison.

Discussion

Performance of normal flow models

The phase diagram in Figure 3-7 isolates the variation in behavior of the parameters H_{bf}, B_{bf}, and S when the effect of juvenile channels are included. More specifically, it studies how the ratio of each parameter to its mature value changes as the parameter γ or ε increases, so reducing the channel-forming Shields number. The case considered is normal flow. A realistic parameter range for γ and ε is not known, but

measurements at WLD show that both values have minimum value around 0.6. While we plot this phase space with γ or ε in the range (0,1), $\gamma = \varepsilon = 0$ does not necessarily relate to the incipient channel form; this value likely relates more to a no-flow condition, while the incipient channel can be generalized as axisymmetric flow over an unchannelized deltaic surface. The trend in Figure 3-7 is clearly non-linear, as the values deviate rapidly from their mature values as γ, ε approach zero. Depth is the most dependent on the decay factor, a result that is common to both normal flow and backwater models. This closure requires slope to increase as the channel approaches an incipient juvenile state.

Manipulation of Eq. (47) at the delta periphery (where depth is an assumed, known value) leads to the result $S = f(\gamma, H_{bf})$. Here Fr^2 can be calculated through Eq. (46) as a function only of S_f. Finally, channel width can be computed through Eq. (42), such that $Q_w = \varepsilon Q_{w,tot}$ via Eq. (19). Altogether, this yields the result that ε affects only channel width. Therefore, the condition $\varepsilon < \gamma$ could possibly relate to a scenario with both declining width and declining depth. The relationship between ε and γ should be evaluated in future work.

The Kim et al. (2009a) model has been augmented here to include a variable Shields number model and to account for underdeveloped juvenile channels at the delta periphery. Results in Figure 3-11 suggest that predictions for the delta progradation rate and the expansion of delta area not significantly affected by the closure for bankfull Shields number. Channel width is narrower with models that use constant Shields number with fully mature channels, and are wider when juvenile channels are added. The variable Shields number models show similar trends, i.e. nearly spatially invariant width with fully-mature channels and basinward width increase when accounting for juvenile channels, but the pattern of variation is not as strong in comparison to constant Shields number models. Channel width is under-predicted in all model runs. Shaw et al. (2013) discuss the incisional regime of channels in WLD. The measured basement elevation (Figure 3-6) and channel elevation (Figure 3-4) show a rapid streamwise change in depth, which occurs simultaneously with a rapid streamwise change in width (Figure 3-5). The normal flow model framework cannot account for the physics associated with this condition. These results suggest that the additional features of variable Shields number and juvenile channels do not improve normal flow models, because 1) the present models adequately predict progradation, and the predicted delta geometry well-represents reality, and 2) the added features are insufficient to capture the physics that control channel width selection, at least considering the pre-delta substrate effects at Wax Lake Delta.

Performance of backwater models

Model runs that use a backwater hydraulics framework create a wide array of model predictions. The modelled delta extent in 2015 varied from 10 km to 13.5 km, while delta area in 2015 range from 80 km^2 to 140 km^2. The base models predict these quantities as well as the full model, which includes all the

added features including juvenile channels, bedrock incision and variable bankfull Shields number. None of the models are capable of predicting the rapid transitions in channel width observed at Wax Lake Delta, but the full model is able to improve on predictions for the increase in channel area over time. Basement dynamics at Wax Lake Delta play a major role in setting the morphodynamics, as noted by Shaw et al. (2013). Channel elevation is modelled well when both basement interactions and juvenile channels are included. The model framework allows for basinward propagation of channel maturation. As the channels mature, they are capable of eroding into the delta substrate, which causes a basinward incisional wave as a direct result of channel maturation. Wagner et al. (2017) have shown that the basinward edge of WLD shows the most aggradation in recent years. This results in an overall flattening of the delta topset slope, and ostensibly further confinement of the delta channel. The mechanism discussed here could cause further downstream incision into the pre-delta substrate in the future.

Predictions of channel width are not sufficiently accurate when compared to data; some aspect of the physics is thus not properly accounted for with the set of models described here. The model runs that most closely resemble the spatial width variation are unable to erode the basement material and select a self-formed width. Both the constant and the variable Shields number closures relate to general trends in rivers with much scatter in the data used to determine them. Li et al. (2015) model the Fly River with their slope-dependent closure, but only after adjustment by referencing a parameter to an upstream scale. A similar procedure may be necessary to generate the proper width predictions at WLD.

Temporal evolution of γ does not dramatically change results when included into the full model, but the implementation merits further study in a more advanced form. The framework presented here accounts for dynamic channel development such that channel maturation process can be modulated by the relative timescales of sediment emplacement on the channel banks versus channel extension through delta progradation. As the delta expands and the progradation rate decreases, we should expect more mature channels to develop at the delta periphery. This compares with results of Muto et al. (2016) that relate the progradation rate of deltas to the basin characteristics.

Recommendations for future modelling

Our results show how inclusion of a range of model features, including variable bankfull Shields number, juvenile channels, bedrock incision and backwater affects predictions of delta morphodynamics. The results indicate that progradation rate and delta area are well computed with simple normal flow closures. Predicting channel depth requires the inclusion of both juvenile channels and bedrock morphodynamics. Edmonds et al. (2011) describe a paradigm for topset-dominated deltas to characterize stratigraphic changes. The authors note that when basins are shallow, channel networks often incise into pre-delta material. In such cases, the alluvial-bedrock framework presented here would be a necessary component

to properly estimate channel elevations. A downstream shoaling pattern has been noted by many researchers, e.g. Shaw et al. (2016a). The juvenile channel framework allows for shoaling along with simultaneous channel widening. The inability of the model to predict total channel depth may be due to site-specific considerations such as basement dynamics. Perhaps this shortcoming could be overcome by including an explicit channel network. This topic should be investigated in the future.

Conclusions

A 1D self-formed channel river delta model was developed to build upon past models by including several new features, including: a distributed Exner equation that accounts for channel, floodplain and average delta elevations simultaneously; a slope-dependent variable bankfull channel Shields number model, framework for incision into pre-delta substrate, and a framework to account for leaky, physically under-developed juvenile channels at the delta periphery. Forty model runs, including 8 with uniform normal flow hydraulics, and 32 with steady, shallow water equation hydraulics are carried out to model the evolution of Wax Lake Delta in Louisiana, USA. The model runs each correspond to a different combination of model features. Differences in model results are analyzed to determine the necessary model features to predict typical delta morphologies such as delta progradation rate, delta areal growth rate, channel width, and channel depth. Normal flow hydraulic models seemed to predict progradation rate and delta areal growth well regardless of the bankfull Shields number closure; however, adding juvenile channels does slightly decrease the growth rates. Models that use the steady shallow water hydraulics have wider variance in all predicted quantities. Channel elevation dynamics were predicted well when basement incision and juvenile channels were included in the model run, but no models were able to accurately predict channel width. Juvenile channels are modelled through a linear decay factor of the bankfull Shields number closure, which relates to a mature river architecture. Leaky channels are accounted for with a similar linear decay factor; both parameters are estimated with field data at Wax Lake Delta. This implementation is tested first assuming self-similarity, such that the initial values for each factor are constant, but stretch with progradation of the delta topset. An alternative method involves temporal and spatial evolution of these decay parameters subject to the growth rate of the delta

Notation List

α_{EH} = Coefficient in Engelund-Hansen equation [-]

α_{Cz} = Coefficient in Cz equation (Li et al. 2015) [-]

β = Coefficient in τ_{bf}^{*} equation (Czapiga et al. 2018) [-]

γ = Juvenile channel decay function [-]

ε = Proportion of flow retained in the channel [-]

ν = Kinematic viscosity [m^2s^{-1}]

Ω = Proportion of mud deposited per unit sand [-]

σ = Global subsidence rate [mm/yr]

$\dot{\xi}$ = Sea-level rise [mm/yr]

τ_{bf} = Bankfull bed shear stress [Pa]

τ_{bf}^{*} = Bankfull Shields Number [-]

$\tau_{bf,mature}^{*}$ = Mature value of Bankfull Shields Number [-]

η_c = Channel elevation [m]

η_f = Channel elevation [m]

η_{base} = Basement elevation [m]

$\overline{\eta}$ = Average delta elevation [m]

B_{bf} = Bankfull width [m]

B_f = Floodplain width [m]

B_{total} = Total Width [m]

Cz = Dimensionless Bankfull Chezy Roughness coefficient [-]

D_{50} = Median grainsize [m]

D_* = Dimensionless grainsize [-]

g = Gravitational acceleration [m^3s^{-1}]

k_τ = Rate coefficient for spatial decay in γ

k_Q = Rate coefficient for spatial decay in ε

p_c = Areal cover factor on the bed [-]

H_{bf} = Bankfull depth [m]

I_f = Intermittency Factor [-]

L_{ac} = Representative Dune Height [m]

m = Slope exponent in τ_{bf}^* equation (Czapiga et al. 2018) [-]

n = Dimensionless grainsize exponent in τ_{bf}^* equation (Czapiga et al. 2018) [-]

n_{Cz} = Exponent in Cz equation (Li et al. 2015) [-]

r = radial extent from the delta apex [m]

R = Submerged specific gravity [-]

S = Average bed slope [-]

s_s = Radial extent of the delta apex [m]

$\dot{s}_s$ = Shoreline shock-condition

s_b = Radial extent of the foreset-bottomset transition [m]

$\dot{s}_b$ = Shoreline shock-condition

Q_w = Bankfull water discharge [m^3s^{-1}]

$Q_{w,tot}$ = Total Bankfull water discharge [m^3s^{-1}]

Q_t = Bankfull sediment discharge [m^3s^{-1}]

$Q_{t.c}$ = Capacity bankfull sediment discharge [m^3s^{-1}]

References

1. Burpee, A. P., Slingerland, R. L., Edmonds, D. A., Parsons, D., Best, J., Cederberg, J., ... & Royce, J. (2015). Grain-size controls on the morphology and internal geometry of river-dominated deltas. *Journal of Sedimentary Research*, *85*(6), 699-714.
2. Caldwell, R. L., & Edmonds, D. A. (2014). The effects of sediment properties on deltaic processes and morphologies: A numerical modeling study. *Journal of Geophysical Research: Earth Surface*, *119*(5), 961-982.
3. Carle, M. M. (2013). *Spatial Structure and Dynamics of the Plant Communities in a Pro-grading River Delta: Wax Lake Delta, Atchafalaya Bay, Louisiana*. Retrieved from http://etd.lsu.edu/docs/available/etd-11152013-110148/\nhttp://etd.lsu.edu/docs/available/etd-11152013-110148/unrestricted/Carle_Dissertation.pdf
4. Chatanantavet, P., & Lamb, M. P. (2014). Sediment transport and topographic evolution of a coupled river and river plume system: An experimental and numerical study. *Journal of Geophysical Research: Earth Surface*, *119*(6), 1263-1282.
5. Czapiga, M.J., McElroy, B.M., Parker, G. (2018) Depth versus Grainsize and Slope. Submitted to Journal of Hydraulic Research. In Review.
6. DuMars, A.J. 2002. *Distributary mouth bar formation andchannel bifurcation in the Wax Lake Delta, Atchafalaya Bay, Louisiana*. M.S. thesis, Louisiana State University, 88 p.
7. Edmonds, D.A. and R.L. Slingerland, 2010, Significant effect of sediment cohesion on delta morphology: Nature Geoscience, v. 3/2, p. 105- 109.
8. Edmonds, D. A., Shaw, J. B., & Mohrig, D. (2011). Topset-dominated deltas: A new model for river delta stratigraphy. *Geology*, *39*(12), 1175-1178.
9. Engelund, F., and Hansen, E. (1967). "A Monograph on Sediment Transport in Alluvial Streams." Teknisk Vorlag, Copenhagen, Denmark, 1967.
10. Garcia, M. H. (2006). ASCE Manual of Practice 110—Sedimentation Engineering: Processes, Measurements, Modeling and Practice. In World Environmental and Water Resource Congress 2006: Examining the Confluence of Environmental and Water Concerns (pp. 1-4).
11. Geleynse, N., Hiatt, M., Sangireddy, H., & Passalacqua, P. (2015). Identifying environmental controls on the shoreline. *Journal of Geophysical Research: Earth Surface*, *120*, 877–893. http://doi.org/10.1002/2014JF003408
12. Hiatt, M., & Passalacqua, P. (2015). Hydrological connectivity in river deltas: The first-order importance of channel-island exchange. *Water Resources Research*, *51*(4), 2264-2282.

13. Hiatt, M., & Passalacqua, P. (2017). *What controls the transition from confined to unconfined flow? Analysis of hydraulics in a coastal river delta* (Doctoral dissertation, American Society of Civil Engineers).
14. Horowitz, A. J. (2006), The effect of the "Great Flood of 1993" on subsequent suspended sediment concentrations and fluxes in the Mississippi River Basin, USA, *IAHS-AISH Publ.*(306), 110–119.
15. Hoyal, D. C. J. D., & Sheets, B. a. (2009). Morphodynamic evolution of experimental cohesive deltas. *Journal of Geophysical Research*, *114*(F2), F02009. http://doi.org/10.1029/2007JF000882
16. Ke, W.-T., and H. Capart (2015), Theory for the curvature dependence of delta front progradation, Geophys. Res. Lett., 42, 10,680–10,688, doi:10.1002/2015GL066455.
17. Kim, W., Mohrig, D., Twilley, R., Paola, C., Parker, G. (2009). Is It Feasible to Build New Land in the Mississippi River Delta ? *EOS*, *90*(42), 373–384. http://doi.org/10.1029/2009EO420001
18. Kim, W., Dai, A., Muto, T., & Parker, G. (2009). Delta progradation driven by an advancing sediment source: Coupled theory and experiment describing the evolution of elongated deltas. *Water Resources Research*, *45*(6).
19. Lamb, M. P., W. E. Dietrich, and L. S. Sklar (2008), A model for fluvial bedrock incision by impacting suspended and bed load sediment, Journal of Geophysical Research F, 113(F3), F03025.
20. Li, C., Czapiga, M. J., Eke, E. C., Viparelli, E., & Parker, G. (2015). Variable Shields number model for river bankfull geometry: bankfull shear velocity is viscosity-dependent but grain size-independent. *Journal of Hydraulic Research*, *1686*(January), 1–13. http://doi.org/10.1080/00221686.2014.939113
21. Li, C., Czapiga, M. J., Eke, E. C., Viparelli, E., & Parker, G. (2016). Closure to "Variable Shields number model for river bankfull geometry: Bankfull shear velocity is viscosity-dependent but grain size-independent" by Li, C., Czapiga, M. J., Eke, E. C., Viparelli, E., & Parker, G, J. Hydraulic Res. 53(1), 2. Journal of Hydraulic Research, 54(2). http://doi.org/10.1080/00221686.2015.1137088
22. Liang, M., Voller, V. R., & Paola, C. (2015). A reduced-complexity model for river delta formation – Part 1: Modeling deltas with channel dynamics. Earth Surf. Dynam, 3, 67–86. http://doi.org/10.5194/esurf-3-67-2015
23. Lorenzo-Trueba, J., Voller, V. R., Muto, T., Kim, W., Paola, C., & Swenson, J. B. (2009). A similarity solution for a dual moving boundary problem associated with a coastal-plain depositional system. *Journal of Fluid Mechanics*, *628*, 427-443.

24. Lorenzo-Trueba, J., & Voller, V. R. (2010). Analytical and numerical solution of a generalized Stefan problem exhibiting two moving boundaries with application to ocean delta formation. *Journal of Mathematical Analysis and Applications*, *366*(2), 538-549.
25. Majersky, S., Roberts, H. H., Cunningham, R., Kemp, G. P., & John, C. J. (1997). Facies development in the Wax Lake Outlet delta: Present and future trends: Basin Research Institute Bulletin 7. *Louisiana State University*.
26. Muto, T., Furubayashi, R., Tomer, A., Sato, T., Kim, W., Naruse, H., & Parker, G. (2016). Planform evolution of deltas with graded alluvial topsets: Insights from three-dimensional tank experiments, geometric considerations and field applications. Sedimentology, 63(7), 2158-2189.
27. Nardin, W., Edmonds, D. A., & Fagherazzi, S. (2016). Influence of vegetation on spatial patterns of sediment deposition in deltaic islands during flood. *Advances in Water Resources*, *93*, 236-248.
28. Paola, C., Heller, P. L. and Angevine, C. L., 1992, The large-scale dynamics of grain-size variation in alluvial basins. I: Theory, Basin Research, 4, 73-90.
29. Parker, G. (1978a). Self-formed straight rivers with equilibrium banks and mobile bed. Part 1. The sand-silt river. *Journal of Fluid Mechanics*, *89*(1), 109-125.
30. Parker, G. (1978b). Self-formed straight rivers with equilibrium banks and mobile bed. Part 2. The gravel river. *Journal of Fluid mechanics*, *89*(1), 127-146.
31. Parker, G., Paola, C., Whipple, K. X. and Mohrig, D., 1998, Alluvial fans formed by channelized fluvial and sheet flow. I: Theory, Journal of Hydraulic Engineering, 124(10), 985-995.
32. Parker, B., D. Milbert, K. Hess, and S. Gill (2003), National VDatum–The implementation of a national vertical datum transformation database, in Proceeding from the US Hydro'2003 Conference, pp. 24–27.
33. Parker, G. (2004), 1D sediment transport morphodynamics with applications to rivers and turbidity currents. E-book located at: http://cee.uiuc.edu/people/parkerg/morphodynamics_ebook.htm
34. Parker, G., & Sequeiros, O. (2006, September). Large scale river morphodynamics: Application to the Mississippi Delta. In *River Flow 2006: Proceedings of the International Conference on Fluvial Hydraulics* (pp. 3-11).
35. Parker, G., Wilcock, P. R., Paola, C., Dietrich, W. E., & Pitlick, J. (2007). Physical basis for quasi-universal relations describing bankfull hydraulic geometry of single-thread gravel bed rivers. *Journal of Geophysical Research: Earth Surface*, *112*(F4).

36. Parker, G., Muto, T., Akamatsu, Y., Dietrich, W. E., & Lauer, J. W. (2008). Unravelling the conundrum of river response to rising sea-level from laboratory to field. Part I: Laboratory experiments. Sedimentology, 55(6), 1643–1655.
37. Reuss, M. 2004. Designing the Bayous: The Control of water in the Atchafalaya Basin 1800 – 1995. College Station: Texas A&M University Press. 496 p.
38. Roberts, H. H., Walker, N., Cunningham, R., Kemp, G. P., & Majersky, S. (1997). Evolution of sedimentary architecture and surface morphology: Atchafalaya and Wax Lake Deltas, Louisiana (1973-1994). Gulf Coast Association of Geological Societies Transactions, 47, 477–484.
39. Roberts, H. H., Coleman, J. M., Bentley, S. J., & Walker, N. (2003). An embryonic major delta lobe: A new generation of delta studies in the Atchafalaya-Wax Lake Delta system.
40. Shaw, J. B., Mohrig, D., & Whitman, S. K. (2013). The morphology and evolution of channels on the Wax Lake Delta, Louisiana, USA. Journal of Geophysical Research: Earth Surface, 118(3), 1562–1584. http://doi.org/10.1002/jgrf.20123
41. Shaw, J. B., & Mohrig, D. (2014). The importance of erosion in distributary channel network growth, Wax Lake Delta, Louisiana, USA. *Geology*, *42*(1), 31–34. http://doi.org/10.1130/G34751.1
42. Shaw, J. B., Mohrig, D., & Wagner, R. W. (2016a). Flow patterns and morphology of a prograding river delta. *Journal of Geophysical Research: Earth Surface*, *121*(2), 372-391.
43. Shaw, J. B., Ayoub, F., Jones, C. E., Lamb, M. P., Holt, B., Wagner, R. W., ... & Mohrig, D. (2016b). Airborne radar imaging of subaqueous channel evolution in Wax Lake Delta, Louisiana, USA. *Geophysical Research Letters*, *43*(10), 5035-5042.
44. Sklar, L. S., and W. E. Dietrich (2004), A mechanistic model for river incision into bedrock by saltating bed load, Water Resources Research, 40(6), W06301.
45. Sun, T., Paola, C., Parker, G., & Meakin, P. (2002). Fluvial fan deltas: Linking channel processes with large-scale morphodynamics. *Water Resources Research*, *38*(8).
46. Swenson, J. B., Voller, V. R., Paola, C., Parker, G., & Marr, J. G. (2000). Fluvio-deltaic sedimentation: A generalized Stefan problem. European Journal of Applied Mathematics, 11(5), 433–452.
47. Trampush, S. M., Huzurbazar, S., & McElroy, B. (2014). Empirical assessment of theory for bankfull characteristics of alluvial channels. *Water Resources Research*, *50*(12), 9211-9220.
48. Van Rijn, L. C. (1984). "Sediment transport, part I: bed load transport." Journal of Hydraulic Engineering, ASCE, 110(10),1431–1456.
49. Viparelli, E., Shaw, J., Bevington, A., Meselhe, E., Holm, G. O., Mohrig, D., Parker, G. (2011). Inundation model as an aid for predicting ecological succession on newly-created deltaic land

associated with Mississippi River diversions: Application to the Wax Lake delta. In World Environmental and Water Resources Congress (pp. 2340–2349).

50. Viparelli, E., Nittrouer, J.A.; Parker, G. (2015). Modeling flow and sediment transport dynamics in the lowermost Mississippi River, Louisiana, USA, with an upstream alluvial-bedrock transition and a downstream bedrock-alluvial transition: Implications for land building using engineered. *Journal of Geophysical Research: Earth Surface*, *120*, 534–563. http://doi.org/10.1002/2014JF003270.Received
51. Wagner, W., Lague, D., Mohrig, D., Passalacqua, P., Shaw, J., & Moffett, K. (2017). Elevation change and stability on a prograding delta. *Geophysical Research Letters*, *44*(4), 1786-1794.
52. Wilkerson, G. V., & Parker, G. (2010). Physical basis for quasi-universal relationships describing bankfull hydraulic geometry of sand-bed rivers. *Journal of Hydraulic Engineering*, *137*(7), 739-753.
53. Zhang, L., G. Parker, C. S. Stark, T. Inoue, E. Viparelli, X. D. Fu, and N. Izumi (2014), Macro-roughness model of bedrock-alluvial river morphodynamics, Earth Surf. Dyn., 2(1), 297–355, doi:10.5194/esurfd-2-297-2014.

CHAPTER 4 : A TWO-PARAMETER MODEL FOR SEDIMENT TRAPPING EFFICIENCY IN JUVENILE RIVER DELTAS

Abstract

River deltas consist of a network of channels that move water and sediment from an upstream river channel and deposit into a basin. Bifurcation, which causes declining water discharge and bed shear stress in channels towards the basin, and sediment transport dynamics suggest a non-linear decrease in sediment transport capacity. Here these concepts are combined to develop a simple quantitative measure of the sediment trapping efficiency of a delta topset that depends only on a) a characteristic length scale taken as the distance to first bifurcation, and b) two rate coefficients governing the spatial rate of channel bifurcation and spatial rate of channel maturation, i.e. juvenile vs. mature channel structure. The former parameter can be estimated from aerial imagery, and the latter is estimated using volumetric changes in the prodelta and delta topset at Wax Lake Delta, Louisiana, USA, segmented into two periods over 26 years. The model reasonably estimates spatial variation of normalized width and depth parameters, indicating that basic morphodynamics are sufficiently captured. This formulation is autogenic and does not require changes to hydrology, sediment supply, or basin conditions to drive evolving delta topset processes. A generalized version of the model is discussed showing combinations of the two-parameters that cause topset deposition or delta progradation. A cyclical paradigm is described, based on limited data at Wax Lake Delta, which suggests juvenile deltas may require alternating phases of high capture efficiency followed by low capture efficiency. Our model suggests this feature is modulated by maturity of delta channels at the periphery.

Introduction

River deltas lie at the boundary between fluvial and basin environments and form as discharge from the upstream river expands, causing sediment deposition. However, of 6,050 active river mouths with widths exceeding 30 meters worldwide, only 25% develop deltaic landforms (Baumgardner, 2016). Deltas are self-constructed via deposition of sediments carried by the upstream river, and sometimes shaped or reworked by winds, tides, or human activity. If an insufficient quantity of sediment is delivered to the basin, a delta may never develop; similarly, existing deltas may drown or deconstruct via basin forces or allogenic changes such as base level rise. We seek to identify the conditions required to trap enough sediment to retain a deltaic landform considering autogenic conditions, i.e. with no changes to the water discharge, sediment discharge, or basin fluctuations related to either sea level rise or fall.

Past experiments (Muto et al. 2016, Pilourais, 2016, Kim et al. 2009b) and numerical results (Kim et al. 2009a, Kim et al. 2009b) describe autogenic delta growth rates over time. Kim et al. (2009a) numerically model deltaic growth as a single lumped channel, sans network, that sweeps across the delta topset. This type of model carries the assumptions that 100% of bed material load is captured in the delta or prodelta, and washload is passively deposited at a specified rate. Under autogenic conditions, nearly all sediment leaving the upstream river boundary exits for progradation. The delta channel tends to a quasi-equilibrium slope with uniform normal flow, so the only sediment trapped in the delta relates to aggradation required to maintain this equilibrium slope as the delta progrades into the basin. Kim et al. (2009b) develop a similar model, but assume the delta apex propagates forward as the delta topset expands; the authors compare experiment and model results assuming different slopes of the pre-delta basement surface. Muto et al. (2016) perform experiments with constant base level as well as falling base level to reach a graded state. The experiments without sea level rise require the delta to prograde out to a steeper basin slope, which the authors compare to a continental shelf edge delta. The rapid offshore increase in accommodation space in the experiments results in stagnated delta progradation, and generates a graded topset that delivers nearly all input sediments to the deep basin. Piliouras et al. (2017) add vegetation to enhance channel stabilization and sediment trapping efficiency. The authors found that including a low-discharge inter-flood condition allowed for more persistent channels capable of transporting sediment to the shoreline, leading to a condition where progradation and topset aggradation are both significant. Nardin and Edwards (2014) show the type and density of vegetation differently affects sand or mud deposition. They found that sand trapping is inefficient when tall or dense vegetation lines the channel banks, limiting transport into the island areas, and mud trapping is inefficient if no vegetation exists to increase flow roughness on submerged islands. Similarly, Hiatt and Passalacqua (2017) show that

hydraulic roughness of subaqueous banks adjacent to a channel, which can be controlled by vegetation density, affect the flow patterns, which has direct impact on sedimentation processes.

The examples presented herein are autogenic river dominated deltas with no or negligible forces from winds, tides, or storms. Some of these experiments are either avulsion dominated or channel migration dominated, processes that deposit sediment locally then shift across the delta topset over time. These mechanisms result in spatially non-uniform deposition on short timescales, but equal spatial deposition rates over longer timescales. Several other models include dynamic channel networks that distribute sediment across the topset, or at least across a sub-lobe of the topset, e.g. Liang et al. 2015. We simplify our scope further to focus on the effect of channel network distribution of sediments in a river-dominated delta. This scope is narrow, but applicable to juvenile deltas in sheltered basins not subject to sea level rise, an idealized condition that is convenient for studying engineered land building via river diversion, e.g. West Bay diversion (Kolker et al., 2012).

Analogue to engineering land diversions

Laboratory experiments and field-scale experiments at juvenile deltas can provide appropriate platforms for the design of engineered water and sediment diversions meant to construct new land. Cubits Gap, in the Mississippi Delta, is a deltaic deposit that has been a growing since 1862, when a channel was dug through the current Mississippi River bank to form a faster path of transit to the Gulf of Mexico (Campbell, 1988). Wax Lake Delta extends from a flood relief channel dug in 1941 to limit flooding in Morgan City, LA (Wellner et al. 2005). More recently, several field scale experiments have been planned to divert water and sediment at various points in the lower Mississippi River. Of particular interest is the West Bay diversion, which emanates from a narrow cut into the upper portion of a Mississippi River levee just upstream of the head of passes. Kolker et al. (2012) note that most deposition occurs at the basinward end of the Bay, and estimates that ~70% of sediment is retained. Yuill et al. (2016) show an initial erosional phase proximal to the channel cut, followed by a transition to a more depositional regime throughout. Nittrouer et al. (2011) determined that 40% of sand flux from the Mississippi River is transported and completely deposited within the Bonnet Carré Spillway despite that face that the spillway pulled flow from the top of the water column. Paola et al. (2011) suggest that the area of the delta plain depends on the volumetric sediment input, basin characteristics, and a specified sediment trapping efficiency. We seek to understand the sediment transport dynamics in these growing juvenile deltas as a means to evaluate sediment trapping efficiencies, which can be applied to temporal development of engineering water and sediment diversions.

Here we consider the sediment transport characteristics of a delta with bifurcating channels. Although we apply the normal flow condition everywhere, the presence of bifurcating channels, which become ever

more poorly defined (ever more juvenile) downstream leads in most cases to a downstream decline in sediment transport capacity. This allows us to characterize the tendency for sediment retention in the delta relative to delivery to the shoreline. The model does not include sediment morphodynamics, but could easily be extended to do so.

The crux of our argument relates to three basic conditions inherent to river deltas and sediment transport dynamics. Together, they are as follows.

1) As channels bifurcate throughout deltas, the input discharge is split across many channels.
2) As discharge in each channel declines, dimensionless bed shear stress declines.
3) As dimensionless shear stress declines, sediment transport declines even faster.

The first statement is verified through simple mass balance along with assumption that the delta network is fed solely from a single river channel. Tejedor et al. (2017) use channel width as a proxy for channel water and sediment discharge to suggest that delta networks organize themselves so that a given water or sediment particle has equal probability of reaching the delta/basin boundary via each of the network distributaries. However, the partitioning of water and sediment is not necessarily equal, as shown by e.g. Wang et al. (1995). The model presented here is focused on the effective sediment transport to the delta periphery, rather than the specifics of channel bifurcation. We assume water and sediment is split evenly as a means to ensure similar deposition rates across the topset. This assumption can be relaxed in future implementations. The second condition is not immediately obvious, but past bathymetric studies in deltas have shown systematic shallowing down delta, e.g. Shaw et al. [2013], Shaw et al. [2014]. The bed shear stress τ_b in a channel can be estimated as in eq. (1), where ρ is density of water, assumed to be 1000 [kg/m^3], g is gravitational acceleration, H is channel depth, and S is slope. Bed slope in a delta can be adverse, coincident with decreasing channel depth basinward, so the slope here is friction slope S_f, which quantifies the driving force. The dimensionless bed shear stress, or Shields' stress τ^* is shown in eq. (2), where R is submerged specific gravity, assumed to be 1.65 for quartz, and D_{50} is median bed material grain size.

$$\tau_b = \rho g H S_f \tag{1}$$

$$\tau^* = \frac{HS_f}{RD_{50}} \tag{2}$$

If D_{50} is constant in the delta, then Shields stress changes are driven solely by the depth-slope product. The final of the three conditions be demonstrated using a variety of sediment transport equations, which hold the general form for the Einstein number q_t^* as in eq. (3).

$$q_t^* = C_1\left(\tau^* - \tau_c^*\right)^{n_t} \quad (3)$$

where

$$q_t^* = \frac{q_t}{\sqrt{RgD_{50}}\,D_{50}}$$

and q_t denotes the volume bed material transport rate per unit width.

Here τ_c^* is the critical Shields number for incipient motion, and n_t is an exponent typically larger than one (Garcia, 2008). The nonlinearity in this relation indicated that it is plausible that a unit relative decrease in discharge, e.g. 10% decrease, may result in a larger relative decrease in the sediment transport rate. A negative divergence of sediment transport rate implies deposition, and persistent deposition implies sediment trapping.

We define a model framework to quantify the sediment trapping efficiency in a delta resulting from decline in sediment transport capacity according to the nonlinearity inherent in eq (2). These results can be summarized through the trapping ratio ψ, which is the ratio of the total sediment load exiting the delta against the supply rate. If ψ is small, the delta channels cannot convey much of the supplied sediment to the shoreline, thus forcing sediment retention on the topset; as ψ approaches unity the delta approximates a graded state where the transport exiting the delta and driving progradation equals the supply rate. Finally, when ψ exceeds one, the topset is mined and the delta progrades faster than during the graded state.

The condition $\psi \leq 1$ can capture tendencies toward purely autogenic evolution (but not the evolution itself. The condition $\psi > 1$ necessarily implies allogenic forcing, which complicates the framework. Even though allogenic forces are not considered here, when $\psi > 1$, our model predicts that the main channel bifurcates into several channels that each have similar capacity to transport sediment, resulting in a net downstream increase in cumulative sediment flux. The condition where the topset is mined, causing faster progradation, can be related to a reduction in sediment supply or base level fall, such that the channels erode sediments from the topset with insufficient replenishment from the input flux.

Methodology

Model Assumptions

We assume a model domain consisting of a radially symmetric fan delta with channel and inter-channel areas, the planform of which is described in Figure 4-1. Here *r* denotes the radial distance *r* from delta apex, θ denotes the planform topset angle and *B* denotes the width of any given channel in the network.

The channel network structure is implicit, i.e. the details of individual migrating or avulsing channels are not modeled, and while the number of channels λ depends on r, it is invariant in θ. The delta is axisymmetric, such that all channels at common radial lengths from the delta apex are identical. Channel properties include median grain size D_{50}, width B, depth H, slope S, discharge Q, and bed material load sediment transport rate Q_t. While the model does not compute morphodynamic change, the framework includes inter-channel areas where sediment deposition can occur by over-spilling.

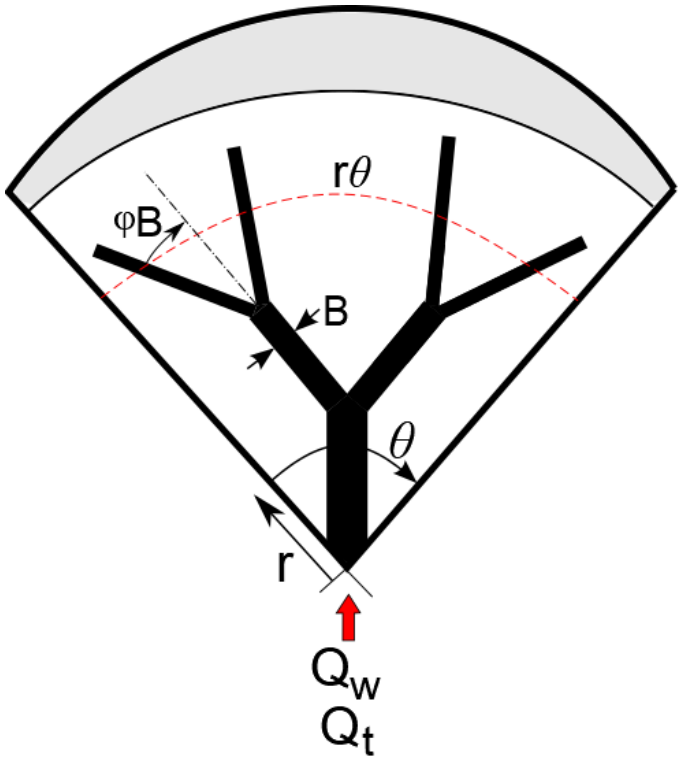

Figure 4-1: The model domain is drawn with an arbitrary network. The topset is defined by the radial distance from the delta apex, r, and topset angle θ. *The arc length at any location is defined by rθ,* and this width is composed of channel B and inter-channel areas φB. *A constant flux of water and sediment discharge enter the delta as noted by Qw and Qt, respectively.*

The model includes several equations to govern flow, sediment transport, spatial bifurcation rate, bankfull Shields number, and physical aspects of the domain. Each variable in the system is normalized by its respective input value, denoted as the "upstream" value with subscript u as shown for the generic variable x in eq. (4).

$$x = \tilde{x}x_u \tag{4}$$

Here $\tilde{x}$ denotes the dimensionless version of the dimensioned variable x. For example, the physical domain variables for the radial distance from the delta apex r and delta topset angle θ (Figure 1), are normalized as $r = \tilde{r}r_u$ and $\theta = \tilde{\theta}\theta_u$, respectively. Upstream values for width B_u, depth H_u, slope S_u,

discharge Q_u, and sediment transport rate $Q_{t,u}$ relate to conditions in the feed channel. The model delta emanates from a single channel, so the upstream channel number λ_u equals one there. Thus, the number of channels λ is equal to its normalized value $\tilde{\lambda}$. The upstream delta angle θ_u is a prescribed value relative to the initial basin space.

Model Framework

We begin with an assumption for uniform normal flow via the Chezy equation as shown in eq. (5), along with the normalized form in eq. (6).

$$Q = CzBH^{3/2}S^{1/2} \tag{5}$$

$$\tilde{Q} = \tilde{B}\tilde{H}^{3/2}\tilde{S}^{1/2} \tag{6}$$

In deriving eq. (6) from eq, (5), it is assumed that the Chezy coefficient Cz is constant in time and space, which implies that $Cz = Cz_u$. Discharge in eqs. (7) and (8) relates to discharge in each channel, which is equal to the inflow discharge divided by the number of channels. This means that no flow is specifically allocated to the inter-channel areas. This is not the case for the Wax Lake Delta; Hiatt and Passalacqua [2015] and Shaw et al. [2016a] illustrate the presence of inter-channel flow Instead of modeling this feature explicitly, we account for the net effect of flow lost from the channels via the modification to a variable Shields number equation.

$$Q = \lambda^{-1}Q_u \tag{7}$$

$$\tilde{Q} = \tilde{\lambda}^{-1} \tag{8}$$

Rivers show scaling laws suggesting that channel width scales with bankfull discharge to approximately the ½ power (Leopold and Maddock, 1957). Edmonds and Slingerland (2007) compare hydraulic geometry from 11 deltas that show good agreement with the hydraulic geometry equations measured from deltas by Mikhailov [1970] and Andren [1994]. These equations use exponents equal to 0.5 and 0.39, respectively, suggesting that the assumption that channel width scales with discharge to ½ power is acceptable for delta channels. Channel width B is thus parameterized in eqs. (9) and (10).

$$B = C_0 Q^{1/2} \tag{9}$$

$$\tilde{B} = \tilde{Q}^{1/2} = \tilde{\lambda}^{-1/2} \tag{10}$$

The bankfull Shields stress given in eq. (2) is normalized into eq. (11).

$$\tilde{\tau}_* = \tilde{H}\tilde{S} \tag{11}$$

Li et al. [2015,2016], Trampush et al. [2014] and Czapiga et al. [2018] relate the bankfull Shields number to a dimensionless grainsize and bed slope from bankfull river channels. This equation can be useful in

numerical modelling of river morphodynamics when channels have well-constructed banks and floodplains. Delta channels develop from an incipient state with unconfined flow due to the construction of subaqueous channel banks adjacent to the channel bed. Delta channels adjacent to the distal end, i.e. near the receiving basin, are in this juvenile state, as discussed in Chapter 2, but can approach a mature river structure in older up-delta channels. In this model, it is assumed that channels at the distal end of the delta are in a juvenile, or incompletely formed state. We assume that the Shields number relation of Czapiga et al. [2018] describing mature channels can be modified to include a power-law decay factor relating to the spatial (down-delta) transition from a mature channel structure in the upstream portion of the delta to juvenile, non-confined channels basinward as in eqs. (12), (13), and (14). The exponent m = 0.365, per Czapiga et al. [2018].

$$\tau_{bf}^{*} = \gamma\beta S^{m} D_{*}^{n} \tag{12}$$

$$\gamma = \tilde{r}^{-k_{\tau}} \tag{13}$$

$$\tilde{\tau}_{bf}^{*} = \tilde{r}^{-k_{\tau}} \tilde{S}^{m} \tag{14}$$

The parameter γ satisfying the condition $0 < \gamma \leq 1$ specifies the degree of juvenility of the channel, such that $\gamma = 1$ corresponds to a fully developed channel, and $\gamma < 1$ described an incompletely developed channel. In eq. (13), we choose $k_{\tau} > 0$, so that channels become increasingly more juvenile downstream. Other parameters in the above equations are β = 182 and n = - 0.87, but these scale out upon non-dimensionalization according to Eq. (4).

Sediment transport is modeled with the Engelund-Hansen equation and sediment size is restricted to sand, i.e. 0.065 mm $\leq D_{50} \leq$ 2 mm. Again, the Chezy roughness coefficient scales out of the equation, as it is constant in space. Where Q_t = the total volume sand transport rate in a given channel,

$$Q_t = 0.05 C z^{2} \tau_{bf}^{*\,5/2} B \sqrt{RgD_{50}} D_{50} \tag{15}$$

$$\tilde{Q}_t = \tilde{B}\left(\tilde{r}^{-k_{\tau}} \tilde{H} \tilde{S}\right)^{5/2} \tag{16}$$

The delta network is assumed to be constructed through a series of bifurcations, and we assume this follows eq. (17), where α is a scaling coefficient that is not a function of r. This equation integrates to eq. (18), which is in turn normalized in eq. (19) so that the dimensionless channel number is a power-law function of dimensionless radial length and parameter α.

$$\frac{d\lambda}{dr} = \alpha \frac{\lambda}{r} \tag{17}$$

$$\lambda = C_1 r^{\alpha} \tag{18}$$

$$\tilde{\lambda} = \tilde{r}^{\alpha} \tag{19}$$

The preceding methodology relates to in-channel characteristics for hydraulics and sediment transport mechanisms. We construct inter-channel areas through assumptions for the transverse depositional length scale from a channel. This implies builds a delta islands adjacent to channels. We assume that these implicit islands linearly scale to adjacent channel width as a first-order assumption. That is,

$$\lambda = \frac{r\theta}{(2\phi + 1)B} \tag{20}$$

$$\tilde{\lambda} = \frac{\tilde{r}\tilde{\theta}}{\tilde{B}} \tag{21}$$

where the island width on either side of a channel is ϕB.

The normalized governing equations can be manipulated to solve for morphodynamic variables. All variables can be recast in terms the normalized radial length $\tilde{r}$; the normalized channel number $\tilde{\lambda}$ is already defined in this form as in eq. (19). Normalized discharge and width are both functions of channel number alone and are easily manipulated to the forms of eqs. (22) and (23).

$$\tilde{Q} = \tilde{r}^{-\alpha} \tag{22}$$

$$\tilde{B} = \tilde{r}^{-\alpha/2} \tag{23}$$

The normalized flow equation, eq. (5), and normalized bankfull Shields number eqs. (11) and (14) can be combined with eqs. (22) and (23) to obtain equations for $\tilde{H}$ and $\tilde{S}$, i.e. eqs. (24) and (25), respectively.

$$\tilde{H} = \tilde{r}^{\frac{k_r - \alpha(m-1)}{3m-2}} \tag{24}$$

$$\tilde{S} = \tilde{r}^{\frac{3k_r - \alpha}{3m-2}} \tag{25}$$

The normalized delta topset angle is solved by combining eqs. (19), (21), and (23), resulting in eq. (26).

$$\tilde{\theta} = \tilde{r}^{\alpha/2-1} \tag{26}$$

Finally, the normalized sediment transport rate per channel $\tilde{Q}_t$ is redefined by combining eqs. (16), (23), (24), and (25), as in eq. (27) below. We use a simplifying assumption of no active sediment transport outside the channels; these areas, which we refer to as islands, are implicit deposition zones. Shaw et al. (2013) show that the Wax Lake Delta channel are incised into antecedent consolidated shelf mud, while islands have significant deposition. We explicitly treat neither feature here, an instead consider the sediment transport efficiency of the bifurcating delta itself. The cumulative sediment transport at any

radial distance along the delta $Q_{t,total}$ in the delta is the product of sediment transport rate and number of channels, as in eq. (28).

$$\tilde{Q}_t = \tilde{r}^{\frac{5}{2}\left(-\frac{\alpha}{5}-k_\tau+\frac{4k_\tau-\alpha m}{3m-2}\right)} \tag{27}$$

$$\tilde{Q}_{t,total} = \tilde{\lambda}\tilde{Q}_t = \tilde{r}^{\frac{5}{2}\left(\frac{\alpha}{5}-k_\tau+\frac{4k_\tau-\alpha m}{3m-2}\right)} \tag{28}$$

The trapping efficiency ratio ψ based on channel transport capacity is mathematically defined as in eq. (29); the upstream value of $\tilde{Q}_{t,total}$ equals one, so ψ is obtained from eq. (28), evaluated at the dimensionless distance to shoreline $\tilde{r}_{\max}$. When $\psi = 1$, all input sediment is retained in the delta; when $\psi = 0$, all input sediment is exported from the delta; and when $\psi < 0$, the output sediment flux is greater than input, signifying sediment removal from the topset. A negative value of ψ can be explained in terms of allogenic changes such as increase in inflow water discharge, decrease in input sediment flux, or decrease in basin water surface elevation, none of which is explicitly captured in this model framework. The only autogenic process available to mine sediments from the delta topset relates to channel maturity, such that the channels at the delta periphery are rendered more capable of moving sediment. However, this alone is not capable of causing a net erosional condition, whereby more sediment leaves the delta than enters.

$$\psi = 1 - \frac{Q_{t,total}\big|_{\tilde{r}_{\max}}}{Q_{t,total}\big|_{feed}} = 1 - \tilde{Q}_{t,total}\big|_{\tilde{r}_{\max}} \tag{29}$$

Evaluating r_u, α, and k_τ

We evaluate the exponent m in eq. (28) from Czapiga et al. (2018); their value is 0.365. The final model equations leave three as-yet unspecified parameters; the upstream length scale r_u, the power-law rate coefficient of channel bifurcation α, and the power-law rate coefficient for decay in the bankfull Shields number k_τ accounting for increasingly more juvenile channels downstream. Unlike the other upstream values related to feed channel characteristics, the upstream length r_u is ambiguous. A delta network is commonly related to a more simplistic fractal tree configuration, where an input "trunk" length is split into two bifurcates with lengths relative to the upstream channel; this methodology is systematically repeated to create a dendritic distribution network. We assume a similar structural similarity by defining r_u as the distance from delta apex to the first bifurcation. This first-order assumption implies that this length scale is representative of the overall delta scale. However, our model framework does not force a systematic spatial bifurcation rate such in a fractal network, but rather scales a bifurcation rate to the rate coefficient α in eq. (19). This parameter and the upstream length scale r_u are easily extracted from aerial

imagery. The number of channels at the delta periphery and the radial length of the delta r_{max} divided by r_u are entered into eq. (19); as shown in eq. (30); after manipulation, α is computed via eq. (31).

$$\tilde{\lambda}\Big|_{\tilde{r}_{\max}} = \lambda\Big|_{\tilde{r}_{\max}} = \tilde{r}_{\max}{}^{\alpha} \tag{30}$$

$$\alpha = \frac{\log\left(\tilde{\lambda}\Big|_{\tilde{r}_{\max}}\right)}{\log\left(\tilde{r}_{\max}\right)} \tag{31}$$

Here we determine α from field data. We could, on the other hand, evaluate it from model results, e.g. using the jet model of Edmonds and Slingerland (2007) and Canestrelli and Slingerland (2014). As this model is being compared to a real world example where α can be measured directly, we obtain it from planform images.

Finally, the decay rate for Shields number related to increasingly juvenile channels downstream depends on the rate coefficient k_τ. This value has not previously been directly measured in the field. In Chapter 3 it is shown that bankfull Shields number closures for mature river channels can be modified with such a decay factor to match the morphodynamics of Wax Lake Delta. We do not offer a closure for this variable, but rather back-calculate it using volumetric changes in the field. This merits a mechanistic explanation, which should be pursued in the future.

Application to Wax Lake Delta

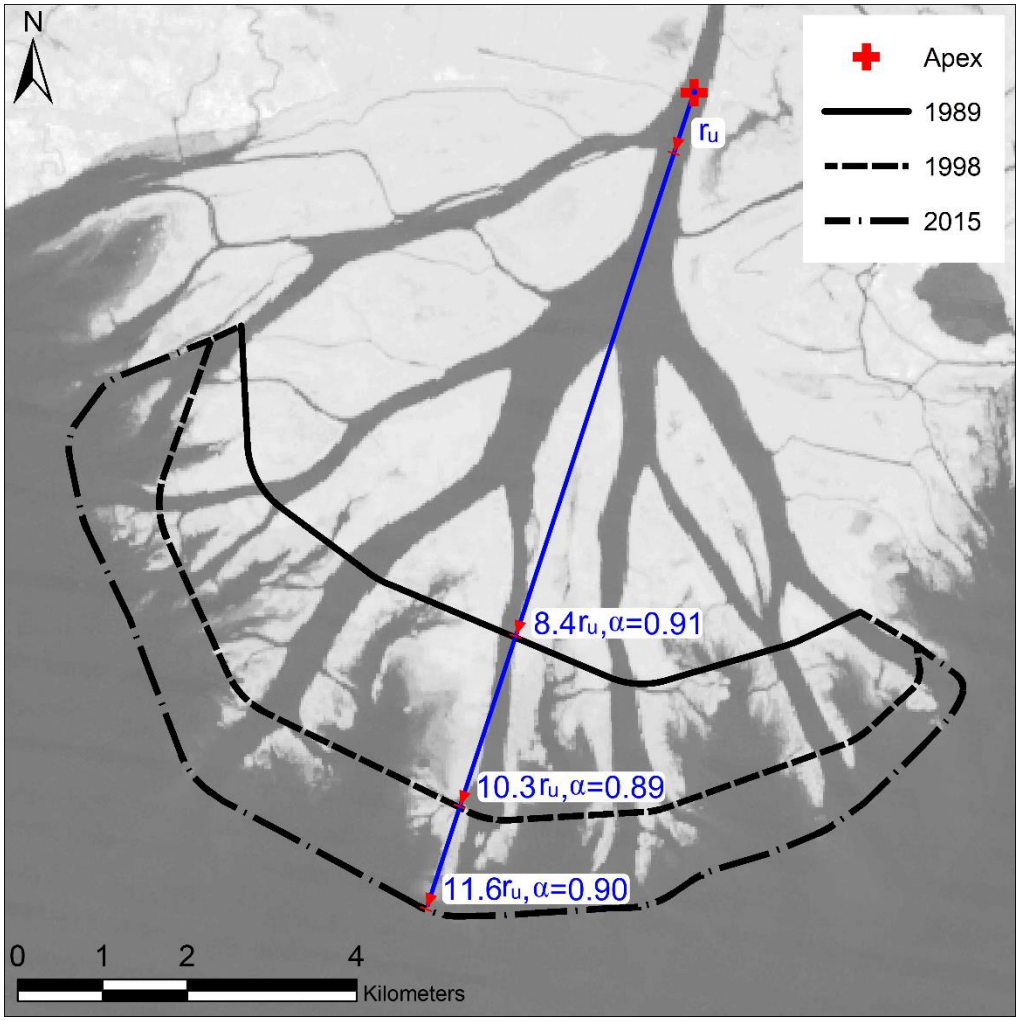

Figure 4-2: Approximate subaerial extent of Wax Lake Delta (image shown is an annual average image from 2015). Delta topset area, extent, and the number of channels are estimated visually from annually averaged images in years 1989, 1998, and 2015. Given the measured normalized length scale, α is computed via eq. (31).

We use Wax Lake Delta (WLD), a delta dominated by juvenile channels in coastal Louisiana, USA, as a test site for model application. Bathymetry and satellite imagery are available for WLD over the last 20 years. The United States Army Corps of Engineers (USACE) collected subaerial and subaqueous data from the delta in 1989 and 1998. A stitched Digital Elevation Model (DEM) of airborne LiDAR and subaqueous bathymetry was also collected in 2015 (Shaw et al. 2016b). In Chapter 3, we generalize the data by characterizing channel or inter-channel areas and determining the mean and median of morphodynamic values at discrete radial distance from the delta apex. Data so obtained include channel

width, channel depth, channel elevation, inter-channel elevation, and number of channels. The subaerial extent of the delta is estimated from annual raw LANDSAT images from years 1989, 1998, and 2015 (

Figure 4-2); each image is composed of the cloud-adjusted median annual average per pixel (Bryk et al. 2014).

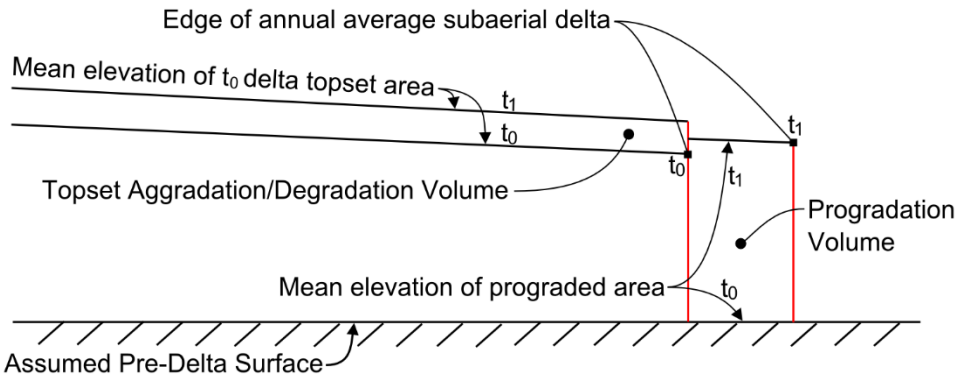

Figure 4-3: Schematic explaining the methodology for defining the volumetric changes associated with delta topset deposition and progradation. The pre-delta substrate elevation was assumed to be spatially constant for simplicity.

Volumetric changes to the delta topset and volume of delta progradation were computed between 1989-1998 and 1998-2015; a schematic of the methodology is outlined in Figure 4-3. Volumetric change in the topset between times t_1 and t_2, i.e. 1989 to 1998 or 1998 to 2015, is estimated via the product of the average topset elevation $\Delta\bar{\eta}_{topset}$ (eq. (32)) and the topset area (eq. (33)). The USACE surveys do not sufficiently measure bathymetry in the prodelta, so we assume the pre-delta elevation of the basin is -2 m Mean Lower Low Water Elevation (MLLW) via Shaw et al. (2013). The progradation volume is estimated as the product of change in delta area from t_1 to t_2 and the difference between average elevation of this area and the pre-delta surface, as in eq. (34). Sediment porosity is assumed to be constant in time and space, such that it cancels from any computation. The measured sediment trapping efficiency $\psi_{measured}$ is computed from the ratio of progradation volume divided by the volumetric change in the delta topset. The parameter k_τ cannot be calculated directly, so it must be estimated by matching ψ between the model and measured values in WLD.

$$\Delta\bar{\eta}_{topset} = \bar{\eta}_{topset,t_2} - \bar{\eta}_{topset,t_1} \tag{32}$$

$$\Delta V_{topset} = \Delta\bar{\eta}_{topset} A_{topset} \tag{33}$$

$$\Delta V_{foreset} = \left(A_{topset,t_2} - A_{topset,t_1}\right)\left(\bar{\eta}_{foreset,t_2} - \bar{\eta}_{basin}\right) \tag{34}$$

Results and Discussion

Results for Wax Lake Delta

The length from delta apex to first bifurcation ru is approximately 0.8 km, as labeled in Figure 4-2. The rate coefficient of channel growth α is estimated from images in 1989, 1998, and 2015 via eq. (31). These values range from 0.89 to 0.9; here we use the mean value of 0.9. Volumetric changes between two periods: 1989-1998 and 1998-2015 are estimated from bathymetric survey measurements. The measured sediment transport efficiency is inferred from volumetric changes; the computed values are shown in Table 4-1. As α and $\psi_{measured}$ are known values, k_τ is computed in terms of the model input value required to predict $\psi_{measured}$. This parameter was found to take the value $k_\tau = 0.096$ from 1989-1998 and the value $k_\tau = 0.128$ from 1998-2015.

Table 4-1: Volumetric change in Wax Lake Delta in two periods.

	Volumetric change (km^2)			Measured	Measured juvenile
Years	Aggradation/ Degradation	Progradation	Total	Sediment Trapping Efficiency $\psi_{measured}$	channel decay coefficient k_τ
1989 to 1998	-7.12	22.01	14.89	-0.48	0.096
1998 to 2015	7.04	5.61	12.65	0.56	0.128

The volumetric change in the WLD shows dramatically different trends between the two periods tested. The first period, from 1989-1998, shows a decrease in average elevation of the topset area defined by subaerial delta extent in 1989. This relates to apparent erosion of the channels as discussed in Shaw et al. (2013) and Shaw et al. (2014); this extra sediment, plus assumed bypass of the feed sediment flux through the delta created rapid delta progradation. The following period brought net aggradation to the topset, while still advancing the subaerial delta front. Wagner et al. (2017) corroborate this trend and find most of the inter-channel deposition from 2009 to 2013 occur near the delta periphery. Our delta model is configured to match the number of channels and cumulative sediment flux at the delta periphery; the variation in normalized channel depth, width, and slope are predicted by the model equations (24), (23), and (25) . We compare the model output for these morphodynamic variables to measured data from WLD [Czapiga and Parker, 2018]. Figure 4-4 shows model results for both periods. Modelled $\tilde{H}$ fits the WLD data well. Model results for $\tilde{B}$ represent an under-prediction, but the trend for mild decrease downstream is similar. WLD has a very wide section downstream from the apex, which means the model is not be able to fit the data for width for any set of parameters.

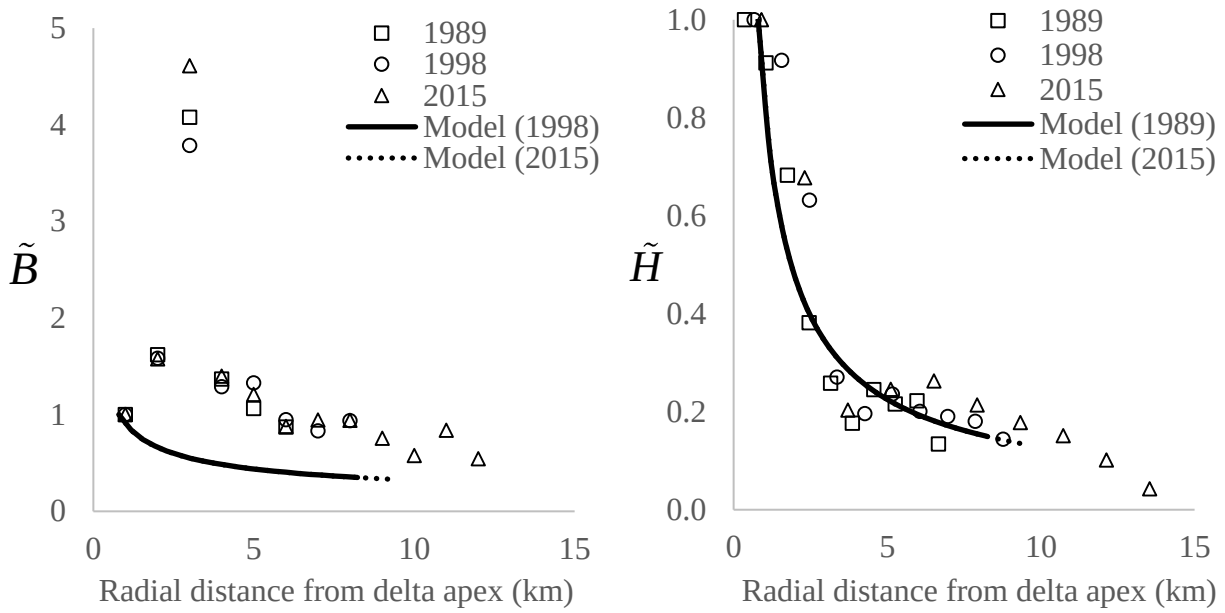

Figure 4-4: Model results for $\tilde{B}$ (left) and $\tilde{H}$ (right) along with generalized results of Wax Lake Delta from 1989, 1998, and 2015. The extent of the model domain relates to the measured average radial extent of the subaerial delta in 1998 and 2015. The 2015 data could be extended seaward because additional subaqueous measurements were available. Model results corresponding to each period have equivalent $\tilde{B}$, as this parameter only depends on α, which is constant. There are only modest changes for $\tilde{H}$.

As is clear in eq (23), $\tilde{B}$ is invariant to k_τ, so model results do not vary between the two periods. There is, however, a very slight deviation in modelled $\tilde{H}$ between these periods. The spatial trends for these variables do not vary temporally at Wax Lake Delta, suggesting that α, parameterizing the channel bifurcation rate, is the most influential parameter to understand channel depth and width in a delta. The normal flow closure used in this model is not physically accurate at the periphery, and the model predicts increased slope downdelta for most conditions. Measured bed slope at WLD (e.g. Chapter 2) shows the opposite trend. It is difficult to assess small scale slope changes in the delta topset, so a comparison for this term is not provided here. The rate coefficient for juvenile channels k_τ has minimal impact on $\tilde{H}$, $\tilde{S}$ is sensitive to its variation, and the per-channel and cumulative sediment flux rates are extremely sensitive to it (Figure 4-5).

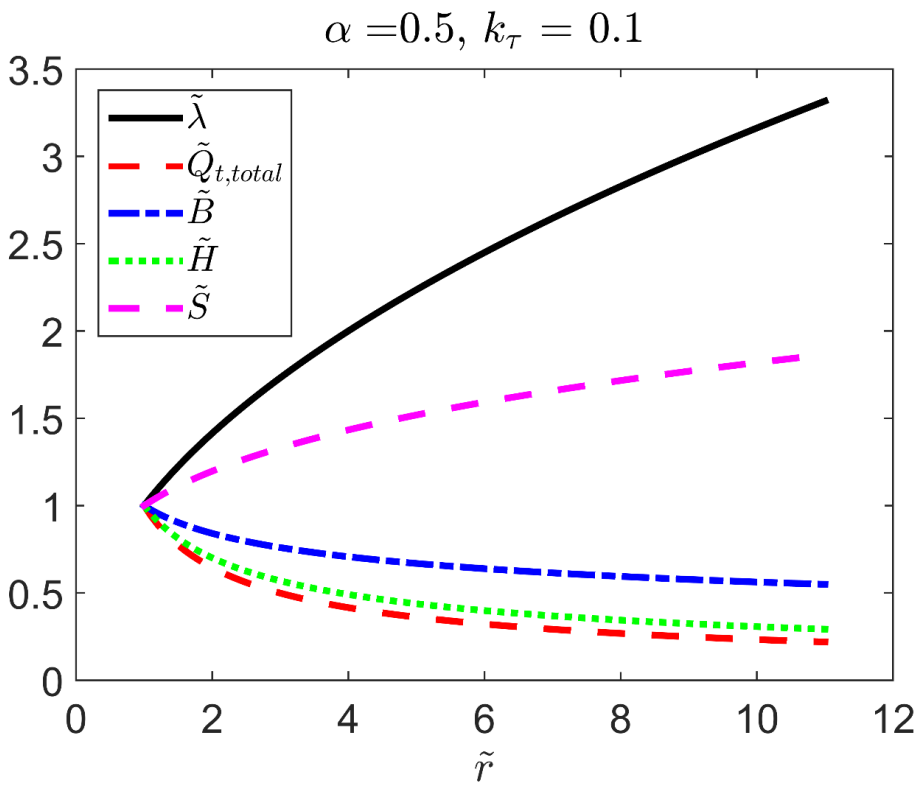

Figure 4-5: Sample output from the model for several morphodynamic variables when α = 0.5 and k_τ = 0.1.

Results of the model are compared to volumetric changes in the topset, but variation in input sediment is not directly accounted for. The model assumes a constant feed rate of water and sediment. In the period between 1989 and 1998, the topset elevation decreased, forcing the model to assume a value for k_τ that relates to over-mature channels with cumulative capacity to transport more sediment than the input rate. However, a rock weir was constructed upstream of WLD during this period (Reuss, 2004; pg. 342). This feature may have affected the delta development by cutting off much of the sediment supply. Relationship between α, k_τ, and receiving basin geometry

Muto et al. (2016) discuss the relationship between equilibrium delta slope and the receiving basin geometry. Edmonds et al. (2011) separate deltas by the ratio of topset/channel depth to the basin depth and describe physical differences between the two paradigms. When the receiving basin is deep, delta progradation is slowed or arrested and a quasi-equilibrium slope can be constructed in the topset. It might be intuitive to think of α and k_τ as topset-controlled parameters, but they are intrinsically tied to accommodation space of the basin geometry similarly to the result of Muto et al. Delta channels at a fixed position evolve over time as sediment is deposited on channel banks, increasing the transport capacity. When the delta is prograding, new channels are also formed at the delta periphery. If the delta were to

stop prograding, the channels could develop without extending and the system would approach a graded state. The spatial bifurcation rate is not governed by accommodation space alone. The results at WLD also vary from model results for sediment retention trends in time. The measured α did not change significantly from 1989 to 2015, so a possible explanation for deviation from idealized models and real WLD results may involve a cyclical variation for the ratio k_τ/α. This could be characterized as a "slinky" effect, with periodic variation between high sediment retention, topset steepening and maturation of distal channels, followed by increased sediment export from the delta due to channel maturity at the periphery, causing rapid growth of many highly juvenile channels. Similar observations have been noted at WLD by Wagner et al. (2017) suggesting that the WLD topset slope is decreasing as the basinward half of WLD aggrades. Floodplain aggradation next to the juvenile channels could imply channel maturation through better channel confinement, which would allow more sediment to exit the delta and contribute to progradation.

Generic model results

The model uses $\tilde{r}$, α, and the juvenile channel rate coefficient k_τ to predict the sediment trapping efficiency ψ. By definition, $\tilde{r} \geq 1$ and both α and k_τ must be non-negative. When $\alpha = 0$, the delta has a single channel that never bifurcates; the uniform normal flow closure forces channel properties including width, depth, slope, discharge, and sediment flux to remain constant in space. When $k_\tau = 0$, all the channels are fully mature, even at the delta periphery. Considering the likely case of $\alpha > 0$ (bifurcating channels), the number of channels $\tilde{\lambda}$ increases and $\tilde{B}$, $\tilde{Q}$, and $\tilde{H}$ all decrease downdelta, regardless of the value of k_τ. The normalized delta angle $\tilde{\theta}$ is constant in space when $\alpha = 2$ (resembling a pie-shaped delta), concave inward when $\alpha < 2$, and convex outward when $\alpha > 2$, as shown in Figure 4-6.

Other morphodynamic terms such as $\tilde{S}$, $\tilde{Q}_t$, $\tilde{Q}_{t,total}$ depend on the ratio of α to k_τ. Each of these variables decreases downdelta for the following conditions: $\tilde{S}$ decreases when $k_\tau > (1/3)\alpha$, $\tilde{Q}_t$ decreases when $k_\tau > \frac{2(4m-1)}{15(2-m)}\alpha$, and $\tilde{Q}_{t,total}$ decreases when $k_\tau > \frac{2(m+1)}{15(2-m)}\alpha$. A sample result for these trends with selected values of α and k_τ is included as Figure 4-5.

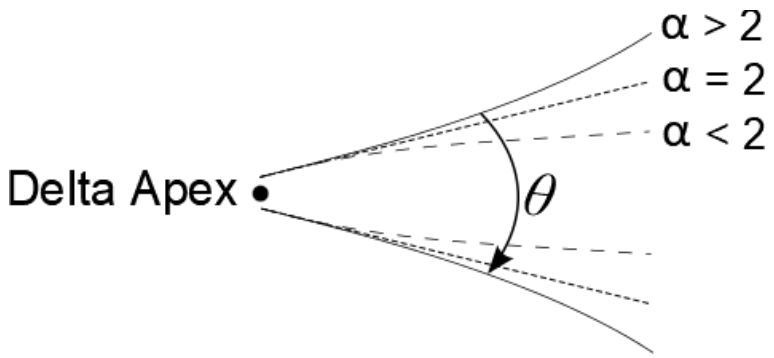

Figure 4-6: Example of delta area shape depending on the rate coefficient for channel growth α. When α=2, the delta takes a pie-shaped domain as drawn in Figure 4-1, but values less than 2 develop a concave inward domain and α > 2 generates a convex delta shape.

We consider a sample parameter envelope to show the dependence of sediment trapping efficiency α and k_τ. When $\alpha = 0$, the delta has a single channel that never bifurcates, and when $k_\tau = 0$ all the channels are fully mature, even at the delta periphery. Although it is not clear what the maximum value of α should be, it should have a physical limit that can be inferred by studying the range of values for many real-world deltas. The trends detailed above suggest the ratio of k_τ/α may be used in place of just k_τ, and it is intuitive that the spatial rate of channel bifurcation should be correlated to the development of juvenile channels. We measured α in the Mossy Delta, another juvenile delta in Saskatchewan, Canada, and found a value of 0.75. Based on data for WLD and Mossy Delta, we suggest an upper limit for α of 1, which equates to an additional channel forming every r_u distance from the delta apex. Recalling the general equation results, the condition for topset sediment retention is satisfied when $k_\tau/\alpha = 0.111$, if $m = 0.365$, so we suggest $k_\tau/\alpha = 1/2$ should be sufficiently large to give the full range of model results for ψ. Therefore, we assume α ranges within (0,1) and k_τ/α ranges within (0, 0.5).

A general form of model results over this range of values is shown in Figure 4-7, with the specific results from WLD noted as well. This figure only shows the range of ψ for a specific normalized length scale $\tilde{r}_{\max} = 11$, which represents the median of length scales at WLD for 1989-1998 and 1998-2015 conditions; this allows a general comparison as to how these two data points sit within the parameter space of Figure 4-7.

Comparison to geometric models

Recent numerical and physical models examine delta evolution through topset adjustment and progradation via a geometrically defined closure. The Kim et al. (2009a) model uses a framework similar to this manuscript, without including bifurcation and a channel network. Their normal flow closure enforces a condition such that once the delta topset aggrades to an equilibrium slope, nearly all the input

flux is transported to the delta edge. Even when the delta is at this equilibrium slope, delta progradation will force sedimentation to maintain it; therefore a delta can never be completely at grade unless progradation is arrested. The relatively short topset transition time predicted by Kim et al. (2009a) relates to the fact that it satisfied on the range $0 < \psi < 1$, Once a near-equilibrium slope is achieved, ψ becomes slightly above zero, increasing with progradation. Muto et al. (2016) develop a geometrical explanation for deltas at grade, a similar condition prevails for the Kim et al. (2009a) result as well. The Muto et al. experiments under purely autogenic conditions, a near-grade delta forms with no sea level rise after advancing to a continental shelf, and then experiences rapid change when the delta reaches the deep basin. Similarly to the scenario suggested herein, this result of Muto et al. (2016) also mirrors a condition where ψ is slightly above zero. These results generally follow the intuitive idea that deltas evolve through cycles of sediment retention and sediment expulsion regimes defined, by topset steepening (retention) and delta progradation (expulsion) respectively.

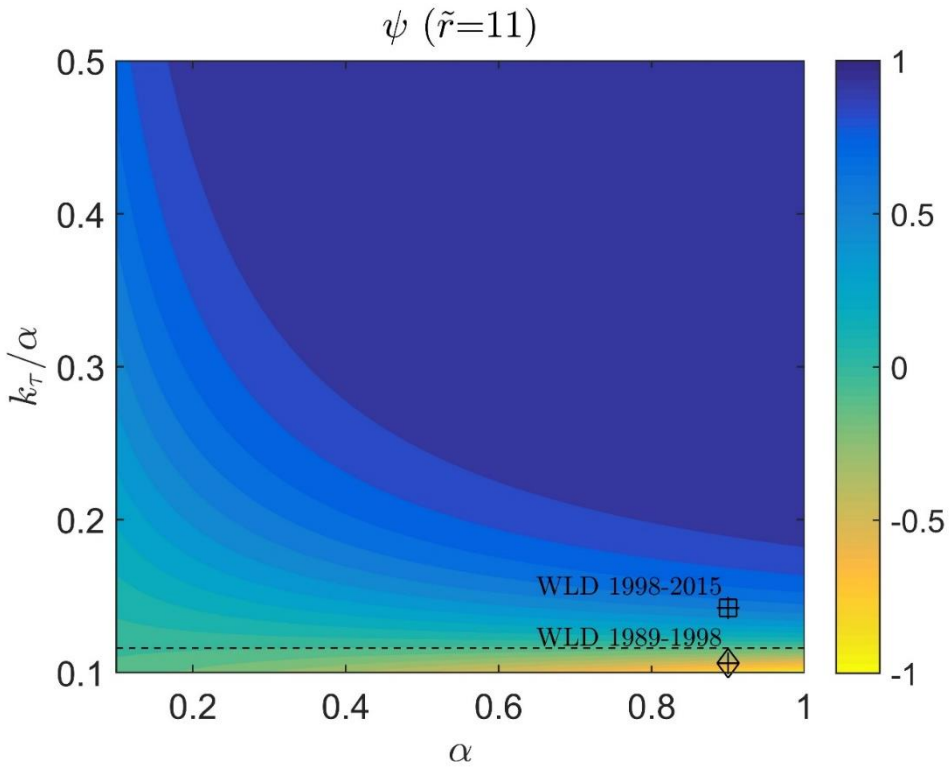

Figure 4-7: The sediment trapping efficiency ψ as a function of α and the ratio k_τ/α for normalized length $\tilde{r}_{max} = 11$ from the delta apex. This length scale is the average of subaerial normalized delta extent between the two tested periods at Wax Lake Delta. Results are shown over a selected range of α and k_τ/α values that represent conditions that range from pure retention and pure export of all the feed sediment. The sediment trapping efficiency ψ thus ranges from -1 to 1. This includes conditions where; all feed sediment is deposited in the topset (ψ=1); sediment is trapped in the topset and exported to the prodelta ($0<\psi<1$); all feed sediment is exported (ψ=1; identified by the dashed line in plot); and the topset is eroded and all feed sediment is exported to the prodelta ($\psi<0$).

Assumption of axisymmetric distribution and fully channelized flow

The model requires many assumptions to simplify the physics to a few important variables. The framework does not configure complexity in natural delta networks that includes e.g. unequal water and sediment distributions between channels of a given bifurcation order or redundant path connections. The model output rather represents an overall estimate for channel characteristics throughout the delta. Furthermore, a key question in regard to the model relates to cumulative sediment transport to the delta periphery. In our model, sediment is distributed evenly across the delta/basin boundary, which agrees with findings of Tejedor (2017) that suggest real delta networks evolve such that all areas in the delta have equal probability to receive water and sediment flux. A delta dominated by avulsion, a factor that is not included here, would likely show different characteristics from our model.

The model framework additionally enforces the condition that flow is confined to the channels. Hiatt and Passalacqua (2015) show this is far from reality at Wax Lake Delta, yet we capture the resulting down-delta decline in sediment transport via the decay rate of bankfull Shields number. As noted above, our model indirectly accounts for lost flow, so a direct accounting may not be necessary.

Implications of scaling parameters to an upstream value

The model framework enforces that all variables are scaled relative to the upstream value. As previously mentioned, this is only acceptable for a river dominated delta system where the forces at the delta periphery are negligible. Model results are independent of the input variables, but the feed channel must be in equilibrium and the actual sediment transport rate must be equal to capacity, i.e. nothing limits sediment supply or transport such as bedrock. As all variables are scaled by the upstream quantity, the derivation of the upstream length scale r_u requires significant accuracy. The model is scale invariant within the constraints of its application. Therefore, the results indicate general trends in sediment transport dynamics within a distribution network dominated by a fluvial input.

Implications for land building via engineered diversions

The presented model simplifies a system of complex processes that govern sediment transport and deposition in a young river delta. The model is able to reasonably reproduce morphodynamic quantities for spatial variation in channel width and channel depth when k_τ is scaled from volumetric changes at Wax Lake Delta. These positive results help identify the necessary variables to simplify a complex system of processes that govern land growth in young deltas, as well as the relative importance of those variables. The result that the model is strongly sensitive to variation in k_τ is an important outcome and, and provides a challenge for future applications. Measurements of the spatial change in Shields' stress are presently insufficient to allow direct evaluation of k_τ, but our result highlights the importance of collecting such data in the future. Additionally, measurements at WLD suggest a natural cyclical prototype, i.e topset

retention followed by expulsion, to mimic in future engineering diversion applications. Our model requires two parameters, i.e. rate parameter for transition to juvenile channels k_τ and spatial bifurcation coefficient α; the latter was found to be nearly constant over the tested period. Therefore, the pattern of sediment retention of the delta can be exclusively linked to the degree of channel maturity. A basinward decline in bed shear stress, as illustrated in Figure 4-8, relates to a progressive lack of channel confinement downstream (Hiatt and Passalacqua, 2015 and Hiatt and Passalacqua, 2017).

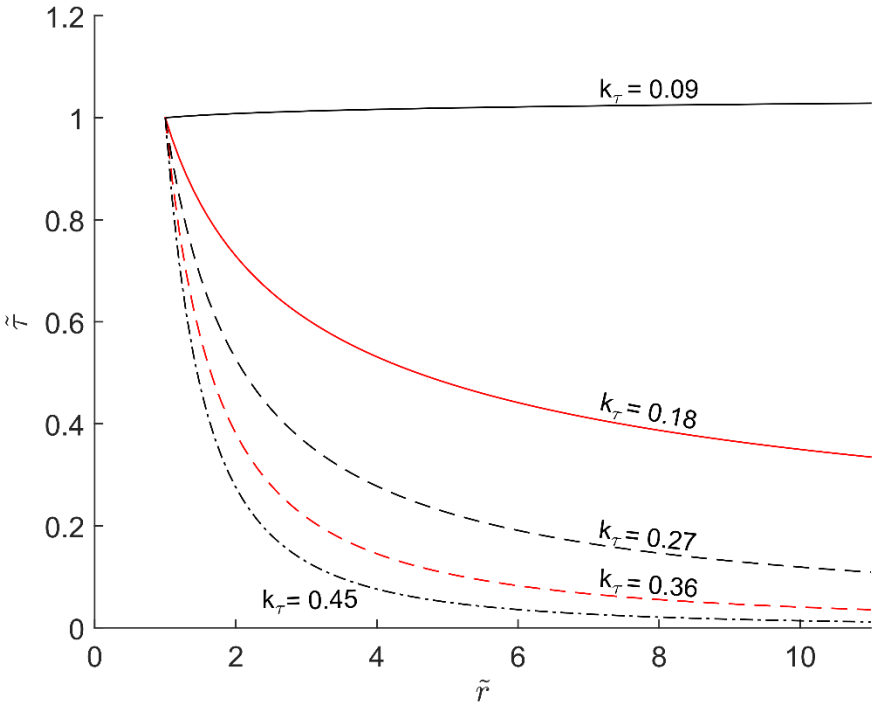

Figure 4-8: Effect of variation of k_τ on dimensionless bed shear stress $\tilde{\tau} = \tilde{H}\tilde{S}$ in space. Values are plotted for α = 0.9 as per Wax Lake Delta measurements. There is a significant change in predictions for $\tilde{\tau}$ between the cases k_τ = 0.09 and k_τ = 0.18; these conditions result in sediment trapping efficiencies at $\tilde{r}$ =11 of ψ = -0.81 and ψ = 0.93, respectively. The area bounded by these two curves therefore represents the range of realistic conditions.

A long-term engineering plan may include alterations of the channels at the delta periphery so as to selectively increase or decrease inter-channel flow, thus modulating the effectiveness of channels to export sediments to the adjacent prodelta. The results of this paper motivate future numerical and experimental modeling to assess the degree of downstream decrease of shear stress and sediment transport in the channels caused by loss of water discharge to the inter-channel zones.

Conclusions

A modeling framework is derived that relates sediment trapping efficiency in deltas to a combination of channel bifurcation, declining bed shear stress, and the non-linear relationship between bed shear stress and sediment transport rate. The governing equations are simplified to relate a normalized channel length scale to two input parameters: the power-law rate coefficient of channel growth, and the power-law rate coefficient of channel maturity describing spatial transition from juvenile channels to mature channels within the delta topset. These two parameters characterize the delta topset, but covary and are tied to receiving basin depth, as deeper basins slow delta progradation and allow more time for channels to develop. Despite the simplistic framework, the model is capable of matching morphodynamic parameters for channel depth and channel width evolution at Wax Lake Delta. The trends at Wax Lake Delta suggest a plausible cyclical relationship between delta aggradation and progradation. The two paradigms are highlighted by the presence or absence of juvenile channels at the delta periphery. When juvenile channels are dominant at the distal end, sediment is trapped within the delta topset. Upon channel maturation, the delta is able to export sediment to the prodelta. Model results are compared to numerical and experimental geometrically-defined models that can produce the same range of sediment trapping efficiency ratios, but only in the transition from their initial state to an equilibrium state. The model was evaluated within a sample parameter space allowing inference of the ratio of inflow sediment trapped within the delta at a relative distance from the delta apex. The parameter k_τ characterizing the spatial rate of transition toward juvenile channels requires more investigation, as the measurements to extract its value are not currently available. A more precise functional relation for this parameter would allow for direct modelling of sediment trapping efficiency. Our model can be applied to understand and potentially engineer manmade deltas created by diversions of water and sediment. The key parameters relate to the ability of channels at the delta periphery to export sediment. Engineers may use in sight from this type of model to develop procedures that mimic the hypothesized slinky effect between periods of progradation and periods of aggradation.

Acknowledgements

The authors thank Alex Bryk for assistance in developing annually averaged images of Wax Lake Delta and Hajime Naruse and Wonsuck Kim for their helpful comments.

Funding

This research was partially supported by the United States National Science Foundation, through Award Numbers 1209427 (WSC-Category 2) 1135427 (FESD Type I).

Notation List

B_{bf} = Bankfull Width [m]

Cz = Chezy Roughness Coefficient [-]

D_{50} = Median grain size [m]

D^* = van Rijn's dimensionless grain size [-]

g = Gravitational acceleration, 9.81 [ms^{-2}]

H_{bf} = Bankfull depth [m]

k_τ = Rate of decay in τ^*_{bf} , γ

r = Radial length [m]

R = Submerged specific gravity, 1.65 [-]

S = Reach-averaged bed slope [-]

S_f = Friction Slope [-]

Q_w = Bankfull Discharge [m^3s^{-1}]

Q_t = Bankfull Sediment Flux in a given channel [m^3s^{-1}]

$Q_{t,total}$ = Bankfull Sediment Flux summed over all channels [m^3s^{-1}]

v = Kinematic viscosity, 1e-6 [m^2s^{-1}]

ρ = Density of water, 1000 [kg/m^3]

τ_b = Bed shear stress [Pa]

τ^*_{bf} = Bankfull Shields number, [-]

α = Rate Coefficient of channel bifurcation [-]

γ = Decay factor in for juvenile channels [-]

λ = Number of channels [-]

λQ_t = Cumulative Sediment Flux in the delta [$m^3 s^{-1}$]

φ = Factor for levee width adjacent to channels [-]

θ = Angle of delta topset [rad]

ψ = Sediment Transport Efficiency Ratio [-]

References

1. Baumgardner, Sarah. (2016). Quantifying Galloway: Fluvial, Tidal, and Wave Influence on Experimental and Field Deltas. University of Minnesota, 2016.
2. Bryk, A.B., Dietrich, W.E., Gorelick, N., Sargent, R., Braudrick, C.A. (2014) Global Analysis of River Planform Change using the Google Earth Engine. American Geophysical Union Fall Meeting 2014, San Francisco, CA.
3. Canestrelli, A., Nardin, W., Edmonds, D., Fagherazzi, S., & Slingerland, R. (2014). Importance of frictional effects and jet instability on the morphodynamics of river mouth bars and levees. Journal of Geophysical Research: Oceans, 119(1), 509-522.
4. Coleman, J. M. (1988). Dynamic changes and processes in the Mississippi River delta. Geological Society of America Bulletin, 100(7), 999-1015.
5. Czapiga, M.J., McElroy, B.M., & Parker, G. (2018) Bankfull Shields Number versus Grain Size and Slope. Journal of Hydraulic Research. In Review.
6. Czapiga, M.J. (2018). Identifying the Minimum Factors to Predict Delta Morphology. Water Resources Research. Chapter 2
7. Edmonds, D. A., & Slingerland, R. L. (2007). Mechanics of river mouth bar formation: Implications for the morphodynamics of delta distributary networks. Journal of Geophysical Research: Earth Surface, 112(F2).
8. Edmonds, D. A., Shaw, J. B., & Mohrig, D. (2011). Topset-dominated deltas: A new model for river delta stratigraphy. Geology, 39(12), 1175-1178.
9. Garcia, M. H. (2006). ASCE Manual of Practice 110—Sedimentation Engineering: Processes, Measurements, Modeling and Practice. In World Environmental and Water Resource Congress 2006: Examining the Confluence of Environmental and Water Concerns (pp. 1-4).
10. Hiatt, M., & Passalacqua, P. (2017). What controls the transition from confined to unconfined flow?: Analysis of hydraulics in a river delta. Journal of Hydraulic Engineering, 143(6).
11. Hiatt, M., & Passalacqua, P. (2015). Hydrological connectivity in river deltas: The first-order importance of channel-island exchange. Water Resources Research, 51(4), 2264-2282.
12. Kim, W., Paola, C., Swenson, J. B., & Voller, V. R. (2006). Shoreline response to autogenic processes of sediment storage and release in the fluvial system. Journal of Geophysical Research: Earth Surface, 111(F4).
13. Kim, W., Mohrig, D., Twilley, R., Paola, C. & Parker, G. (2009). Land building in the delta of the Mississippi River: is it feasible? Eos, 90(42).

14. Kolker, A. S., Miner, M. D., & Weathers, H. D. (2012). Depositional dynamics in a river diversion receiving basin: The case of the West Bay Mississippi River Diversion. Estuarine, Coastal and Shelf Science, 106, 1-12.
15. Li, C., Czapiga, M. J., Eke, E. C., Viparelli, E., & Parker, G. (2015). Variable Shields number model for river bankfull geometry: bankfull shear velocity is viscosity-dependent but grain size-independent. Journal of Hydraulic Research, 1686(January), 1–13. http://doi.org/10.1080/00221686.2014.939113
16. Li, C., Czapiga, M. J., Eke, E. C., Viparelli, E., & Parker, G. (2016). Closure to "Variable Shields number model for river bankfull geometry: Bankfull shear velocity is viscosity-dependent but grain size-independent" by Li, C., Czapiga, M. J., Eke, E. C., Viparelli, E., & Parker, G, J. Hydraulic Res. 53(1), 2. Journal of Hydraulic Research, 54(2). http://doi.org/10.1080/00221686.2015.1137088
17. Liang, M., Voller, V. R., & Paola, C. (2015). A reduced-complexity model for river delta formation – Part 1: Modeling deltas with channel dynamics. Earth Surf. Dynam, 3, 67–86. http://doi.org/10.5194/esurf-3-67-2015
18.
19. Muto, T. & Steel, R.J. (1997) Principles of Regression and Transgression: The Nature of the Interplay between Accommodation and Sediment Supply. Journal of Sedimentary Research. Vol 67. No. 6, pgs. 994-1000.
20. Nardin, W., D. A. Edmonds, and S. Fagherazzi. Influence of vegetation on spatial patterns of sediment deposition in deltaic islands during flood. Advances in Water Resources 93 (2016): 236-248.
21. Nittrouer, J. A., Best, J. L., Brantley, C., Cash, R. W., Czapiga, M., Kumar, P., & Parker, G. (2012). Mitigating land loss in coastal Louisiana by controlled diversion of Mississippi River sand. Nature Geoscience, 5(8), 534.
22. Paola, C., Twilley, R. R., Edmonds, D. A., Kim, W., Mohrig, D., Parker, G., & Voller, V. R. (2011). Natural processes in delta restoration: Application to the Mississippi Delta. Annual Review of Marine Science, 3, 67-91.
23. Piliouras, A., Kim, W., & Carlson, B. (2017). Balancing aggradation and progradation on a vegetated delta: The importance of fluctuating discharge in depositional systems. Journal of Geophysical Research: Earth Surface, 122(10), 1882-1900.
24. Reuss, M. (2004). Designing the Bayous: The Control of Water in the Atchafalaya Basin, 1800-1995. Corpus Christi, TX. Texas A&M University Press.

25. Shaw, J. B., Mohrig, D., & Whitman, S. K. (2013). The morphology and evolution of channels on the Wax Lake Delta, Louisiana, USA. Journal of Geophysical Research: Earth Surface, 118(3), 1562-1584.
26. Shaw, J. B., & Mohrig, D. (2014). The importance of erosion in distributary channel network growth, Wax Lake Delta, Louisiana, USA. Geology, 42(1), 31-34.
27. Shaw, J. B., Mohrig, D., & Wagner, R. W. (2016a). Flow patterns and morphology of a prograding river delta. Journal of Geophysical Research: Earth Surface, 121(2), 372-391.
28. Shaw, J. B., Ayoub, F., Jones, C. E., Lamb, M. P., Holt, B., Wagner, R. W., & Mohrig, D. (2016b). Airborne radar imaging of subaqueous channel evolution in Wax Lake Delta, Louisiana, USA. Geophysical Research Letters, 43(10), 5035-5042.
29. Wagner, W., Lague, D., Mohrig, D., Passalacqua, P., Shaw, J., & Moffett, K. (2017). Elevation change and stability on a prograding delta. Geophysical Research Letters, 44(4), 1786-1794.
30. Wang, Z., R. Fokkink, M. D. Vries, and A. Langerak (1995). Stability of river bifurcations in 1d morphodynamic models. J. of Hydraulic Research 33(6), 739–750.
31. Wellner, R., Beaubouef, R., Van Wagoner, J., Roberts, H., & Sun, T. (2005). Jet-plume depositional bodies—the primary building blocks of Wax Lake Delta.
32. Yuill, B. T., Khadka, A. K., Pereira, J., Allison, M. A., & Meselhe, E. A. (2016). Morphodynamics of the erosional phase of crevasse-splay evolution and implications for river sediment diversion function. Geomorphology, 259, 12-29.

CHAPTER 5 : CONCLUSIONS

A multiple linear regression of bankfull channel depth, reach-averaged bed slope, and median bed material grainsize is carried out to improve a predictive closure for the bankfull Shields number. We use major axis regression, a symmetric scheme that assumes error in the dependent variable and the independent variables, to reduce bias. Past researchers have paired a closure for the bankfull Shields number with equations for water and sediment conservation to model evolution of channel bed elevation with self-formed channel width. With our new closure, we develop two numerical models of fluvially-dominant river deltas.

A morphodynamic river delta model with a single, lumped channel is developed beyond efforts of past researchers. The improved bankfull Shields Number closure is used to model self-formed channel width. A modified, distributed Exner equation is adopted to simultaneously model channel and floodplain elevations. This allows the delta to develop incisional channels within a net-depositional delta. A below-capacity sediment transport framework is borrowed from bedrock river modelling literature and a rate-law incision equation is included for erosion into a pre-delta cohesive sediment basement layer. Our closure for bankfull Shields number relates to mature river channels, so we include a linear function that accounts for juvenile, underdeveloped channels at the delta periphery.

Hindcast modelling of Wax Lake Delta was carried out by including various combinations of model features to identify those necessary to replicate historic morphodynamic changes. Past models have accurately predicted evolution of delta area and progradation rate and our results show these new features do not offer improvement in prediction of these features. However, the key finding of this model is significant improvement in predictions for width and depth. In particular, inclusion of basement dynamics is vital for predictions of channel depth and accounting for juvenile channels is necessary to model spatially varying width in Wax Lake Delta, Louisiana, USA. The framework shows promise for application to deltas in low-slope basins with a cohesive pre-delta surface.

An analytical delta model is developed to understand trends of sediment trapping efficiency in a bifurcating delta. The equations are assembled such that all variables are normalized by their upstream quantities, and morphodynamic variables, such as channel width or depth, are evaluated with only two rate coefficient parameters. These parameters represent the rate of channel bifurcation and the spatial rate of juvenile channel development. Within this framework, we see that discharge, depth, and width always decrease basinward and the number of channels always increases basinward. Other key variables are conditional to the relationship between the two parameters.

Of particular interest is the spatial variation in cumulative sediment transport rate amongst all channels. Sediment trapping efficiency is defined by the ratio of cumulative sediment transport capacity at the delta periphery against the upstream transport rate. Therefore, if transport capacity reduces along the delta, this implies deposition within the delta. A field comparison to Wax Lake Delta uses measured volumetric changes in two periods; a first period includes topset incision and rapid progradation followed by a period of topset aggradation and moderate progradation. We back calculate the juvenile channel decay rate by forcing the model to predict measured volumetric changes in Wax Lake Delta. Modelled channel width and depth reasonably match the trends at Wax Lake Delta during the tested periods, which suggests the model captures the basic physics of the system with only two parameters.

The model is solved in a parameter space to investigate the effect of both parameters on the trapping efficiency of the delta. The decay rate related to juvenile channels cannot be measured presently, so future work is necessary to estimate this term. The model can be useful for informing predictive capability of delta channels to export sediment; this is particularly important for engineered diversions to mitigate land loss in coastal areas.

APPENDIX A: CHAPTER 2

The analysis in the main body of the paper involves implementing linear regression in logarithmic space for the variables H_{bf}, S, D_{50}. A commonly used basic assumption is independence between the 'independent' variables. If we are regressing $Y = f(X_1, X_2)$, then it can be problematic for regression if X_1 and X_2 are highly correlated, as both variables would then contribute to the same variance in the response variable Y. In order to study this, we here include interaction terms that are the products of the two independent variables in any given regression. Now, returning to the variables regressed in the main body of the paper, we can develop two new models with these interaction variables. These are given as in Eqs. (A.1) and (A.2) below, which correspond to Eqs. (12) and (7), respectively, in the main text. For the sake of comparison, Eq. (A.2) is algebraically adjusted to solve for $\log(H_{bf})$ according to Eq. (A.3). The coefficients $\delta_0 - \delta_3$ in Eq. (A3) are then manipulated to the simpler form of Eq. (A.4) where $\Phi_0 = -\delta_0/\delta_1$, $\Phi_1 = 1/\delta_1$, $\Phi_2 = -\delta_2/\delta_1$, and $\Phi_3 = -\delta_3/\delta_1$.

$$\log H_{bf} = \chi_0 + \chi_1 \log S + \chi_2 \log D_{50} + \chi_3 \log SD_{50} \tag{A.1}$$

$$\log S = \delta_0 + \delta_1 \log H_{bf} + \delta_2 \log D_{50} + \delta_3 \log H_{bf} D_{50} \tag{A.2}$$

$$\log H_{bf} = -\frac{\delta_0}{\delta_1} + \frac{1}{\delta_1} \log S - \frac{\delta_2}{\delta_1} \log D_{50} - \frac{\delta_3}{\delta_1} \log H_{bf} D_{50} \tag{A.3}$$

$$\log H_{bf} = \phi_0 + \phi_1 \log S + \phi_2 \log D_{50} + \phi_3 \log H_{bf} D_{50} \tag{A.4}$$

Tables A-1 and A-2 show regression results for Eq. (A.1) for $H_{bf} = f(S, D_{50})$ regressions, and Eq. (A.4) for $S = f(H_{bf}, D_{50})$ regressions. Each table shows regression results with ordinary least squares (OLS) and major axis (MA) regressions. The columns denoted "basic form" relate to models in the main body of the paper, and other columns include interaction terms via Eqs. (A.1) and (A.4). The tables differ through treatment of the variables; Table A-1 uses mean-centering and Table A-2 uses z-scores, where variables are normalized by the standard deviation of the variable in question after mean-centering. Eqs. (A.5) and (A.6) show how any arbitrary variable X is standardized via mean-centering or z-scores, where X_{avg} is the average of variable X and σ_X is the standard deviation of X.

$$X_{mc} = X - X_{avg} \tag{A.5}$$

$$X_{z-score} = \frac{X - X_{avg}}{\sigma_X} \tag{A.6}$$

Both standardization methods reduce multicollinearity in results, but using z-scores additionally converts variables so as to use a relative variance. Variance is now relative to the number of standard deviations from the mean rather than a length scale relative to the variable itself. After regression, the coefficients are translated to represent the original variable values (rather than standardized forms).

Regardless of the data set, Table A.1, which uses a mean-centering treatment of variables as in (A.5), shows similar behavior when comparing the results of the basic forms to regressions with interaction variables. The interaction variables in the OLS regressions are small, but can be of the same order of magnitude as χ_2 in (A.1) or Φ_2 in (A.4). While regression values for Φ_0, Φ_1, and Φ_2 are consistent in MA regressions, the magnitude of χ_3 in both data sets is sufficiently large to be of concern.

Table A.2 uses z-score treatment of the variables as in (A.6). For OLS regressions, analysis with interaction variables show identical results when compared to the basic forms of the model relations given in the main text. The MA basic form regression with standardized z-score variables is somewhat different to the MA basic form model with mean-centered variables (Table A.1, column 6), but gives results similar to the basic forms when interaction terms are included. The magnitudes of the interaction terms in Table A.2 are not as large as those found when variables are mean-centered. The result with MA regression when variables are standardized with the z-score method more closely mimics the initial regression result found by Trampush et al. (2014). Since variance is scaled by standard deviation and S has a much larger standard deviation that H_{bf}, the regression gives a result closer to the geometric mean of the OLS regressions. The MA regression with mean-centered variable treatment tends toward the OLS regression with the form $H_{bf} = f(S,D_{50})$, i.e. Eq. (12) in Chapter 2.

Table A-1: Regression coefficients including interaction terms; variables have been mean-centered before regression.

Regression type	**OLS, H_{bf} = f(S,D_{50})**		**OLS, S = f(H_{bf},D_{50})†**		**MA**		
Coefficient	Basic form	with SD_{50}	Basic form	with HD_{50}	Basic form	with SD_{50}	with HD_{50}
Φ_0, χ_0	-1.203	-1.056	-1.899	-2.158	-1.381	-1.229	-1.055
Φ_1, χ_1	-0.530	-0.484	-0.918	-0.849	-0.635	-0.583	-0.494
Φ_2, χ_2	0.073	0.086	0.241	0.224	0.124	0.130	0.099
χ_3 (SD_{50})	-	0.110	-	-	-	0.097	-
Φ_3 ($H_{bf}D_{50}$)	-	-	-	-0.101	-	-	-0.296

† Regressed as S =f(H_{bf},D_{50}) and re-arranged to solve for H_{bf}

Table A-2: Regression coefficients including interaction terms; variables have been standardized with z-scores before regression.

Regression type	**OLS, H_{bf} = f(S,D_{50})**		**OLS, S = f(H_{bf},D_{50})†**		**MA**		
Coefficient	Basic form	with SD_{50}	Basic form	with HD_{50}	Basic form	with SD_{50}	with HD_{50}
Φ_0, χ_0	-1.203	-1.0555	-1.8986	-1.7495	-1.5911	-1.4501	-1.2867
Φ_1, χ_1	-0.5295	-0.4843	-0.9183	-2.4591	-0.7845	-0.7322	-0.6363
Φ_2, χ_2	0.0727	0.0864	0.2411	0.3815	0.2171	0.218	0.1726
χ_3 (SD_{50})	-	0.0831	-	-	-	0.0366	-
Φ_3 ($H_{bf}D_{50}$)	-	-	-	-0.0459	-	-	-0.0606

APPENDIX B: CHAPTER 3

Shoreline migration (topset-foreset) (backwater version)

We apply a modification of the shock condition from Kim et al. (2009b) to treat shoreline migration. That model assumes an advancing sediment source and an accommodation space with 180-degree angle, i.e. a half circle delta planform. The models presented herein assume a fixed delta apex and a user-specified delta topset angle.

There are slight differences between the implementation of the shock condition between normal flow and backwater flow models. The normal flow models assume a single delta elevation that is fixed to the water surface at the last delta node and the foreset emanates from this point. The foreset in backwater models extends from the average delta elevation $\overline{\eta}$ to the delta basement; $\overline{\eta}$ is necessarily lower than the water surface elevation by definition.

The elevation of the delta foreset and material derivative for normal flow models are:

$$\eta_{fs} = \eta_c - S_a\left(r - s_s\right) \quad , \quad s_s \le r \le s_b$$

$$\frac{\partial \eta_{fs}}{\partial t} = \left.\frac{\partial \eta_c}{\partial t}\right|_{s_s} + \left.\frac{\partial \eta_c}{\partial r}\right|_{s_s} \dot{s}_s + S_a \dot{s}_s$$

Since the delta elevation at the foreset is tied to the water surface, the temporal derivative of delta elevation at the topset-foreset transition is equal to the rate of sea level rise.

$$\frac{\partial \eta}{\partial t} = \dot{\xi} + \left.\frac{\partial \eta_c}{\partial r}\right|_{s_s} \dot{s}_s + S_a \dot{s}_s$$

Similarly, the same equations for the backwater models are:

$$\eta_{fs} = \overline{\eta} - S_a\left(r - s_s\right) \quad , \quad s_s \le r \le s_b$$

$$\frac{\partial \eta_{fs}}{\partial t} = \left.\frac{\partial \overline{\eta}}{\partial t}\right|_{s_s} + \left.\frac{\partial \overline{\eta}}{\partial r}\right|_{s_s} \dot{s}_s + S_a \dot{s}_s$$

We begin with the Exner equation in polar coordinates:

$$\left(1-\lambda_p\right)\left(\frac{\partial \eta_{fs}}{\partial t} + \sigma\right) = \frac{-I_f\left(1+\Omega\right)}{r}\left(\frac{\partial r q_{t,r}}{\partial r} + \frac{\partial r q_{t,\theta}}{\partial r}\right)$$

where λ_p denotes sediment porosity, σ denotes a basement subsidence rate, and $q_{t,r}$ and $q_{t,\theta}$ denote volume sediment transport rates per unit width in the r and θ directions. If sediment transport is limited to the radial direction, this can be simplified to:

$$\left(1-\lambda_p\right)\left(\frac{\partial \eta_{fs}}{\partial t}+\sigma\right)=\frac{-I_f\left(1+\Omega\right)}{r}\frac{\partial r q_{t,r}}{\partial r}$$

Integrating from s_s to s_b, i.e. over the foreset, gives:

$$(1-\lambda_p)\int_{-\theta_0/2}^{\theta_0/2}\int_{s_s}^{s_b} r\frac{\partial \eta_{fs}}{\partial t}drd\theta=-I_f\left(1+\Omega\right)\int_{-\theta_0/2}^{\theta_0/2}\int_{s_s}^{s_b}\frac{\partial q_{t,r}}{\partial \hat{r}}drd\theta$$

where θ_0 is the delta topset angle. As Kim et al. (2009) show, the right hand side can be simplified assuming the sediment flux is radially symmetric and no bed material load passes the foreset-bottomset break.

$$-I_f\left(1+\Omega\right)\int_{-\theta_0/2}^{\theta_0/2}\int_{s_s}^{s_b}\frac{\partial q_{t,r}}{\partial \hat{r}}drd\theta=I_f\left(1+\Omega\right)Q_t\Big|_{s_s}$$

Integrating the Exner equation over r and simplifying the right hand side gives:

$$(1-\lambda_p)\frac{\partial \eta_{fs}}{\partial t}\int_{-\theta_0/2}^{\theta_0/2}\left(s_b{}^2-s_s{}^2\right)d\theta=I_f\left(1+\Omega\right)Q_t\Big|_{s_s}$$

Considering a radial fan delta advancing onto a flat basement plane with constant slope S_b aligned with the angle $\theta = 0$, the location where the delta intersects the bed will vary depending on the angle. Kim et al. (2009) show this distance is, upon modification for a stationary delta apex given as:

$$s_b=\left(1-\frac{S_b}{S_a}\cos\theta\right)^{-1}\left(s_s+\frac{\eta_{fs}\Big|_{s_s}-\eta_{base,o}}{S_a}\right)$$

Here, $\bar{\eta}_{base,o}$ is the basement elevation beneath the delta apex. Some backwater models presented here include bedrock incision that may erode channels below $\bar{\eta}_{base,o}$. This term is taken to be unaffected by channel incision, and therefore has elevation that only changes due to subsidence:

$$\eta_{base,o}\left(t\right)=\eta_{base,sb,0}+S_b s_{b,0}-\sigma t$$

The initial basement elevation at the delta foreset-bottomset transition $\eta_{base,s_b,0}$ and basement slope S_b are specified by the user.

As detailed in the appendix to Kim et al. (2009b), this equation can be integrated to:

$$\left(\frac{\Theta}{2}\left(s_s+\frac{\bar{\eta}\big|_{s_s}-\eta_{base,0}}{S_a}\right)^2-\frac{\theta_0}{2}s_s{}^2\right)\left[\frac{\partial_{fs}}{\partial t}+\sigma\right]=\frac{I_f\left(1+\Omega\right)}{\left(1-\lambda_p\right)}Q_t\big|_{s_s}$$

where Θ is defined by the parameter:

$$\Theta=\int_{-\theta_0/2}^{\theta_0/2}\left(1-\frac{S_b}{S_a}\cos\theta\right)^{-2}d\theta$$

Therefore, the dimensioned shoreline migration rate $\dot{s}_s$ in normal flow models is specified by the relation:

$$\left(\frac{\Theta}{2}\left(s_s+\frac{\bar{\eta}\big|_{s_s}-\eta_{base,0}}{S_a}\right)^2-\frac{\theta_0}{2}s_s{}^2\right)\left[\dot{\xi}+\left(S_a+\frac{\partial\eta}{\partial r}\bigg|_{s_s}\right)\dot{s}_s+\sigma\right]=\frac{I_f\left(1+\Omega\right)}{\left(1-\lambda_p\right)}Q_t\big|_{s_s}$$

Finally, rearranged for $\dot{s}_s$:

$$\dot{s}_s=\frac{1}{S_a+\frac{\partial\eta}{\partial r}\Big|_{s_s}}\left[\frac{I_f\left(1+\Omega\right)}{\left(1-\lambda_p\right)}Q_t\big|_{s_s}\left(\frac{\Theta}{2}\left(s_s+\frac{\bar{\eta}\big|_{s_s}-\eta_{base,0}}{S_a}\right)^2-\frac{\theta_0}{2}s_s{}^2\right)^{-1}-\dot{\xi}-\sigma\right]$$

Forms expressed moving boundary radial coordinate $\hat{r}$ and time $\hat{t}$

After some work, the following relations are obtained.

$$\frac{\partial\eta}{\partial t}=\frac{\partial\bar{\eta}}{\partial\hat{t}}\bigg|_{\hat{r}=1}-\frac{\dot{s}_s}{s_s}\hat{r}\frac{\partial\bar{\eta}}{\partial\hat{r}}\bigg|_{\hat{r}=1}+\frac{1}{s_s}\frac{\partial\bar{\eta}}{\partial\hat{r}}\bigg|_{\hat{r}=1}\dot{s}_s+S_a\dot{s}_s=\frac{\partial\bar{\eta}}{\partial\hat{t}}\bigg|_{\hat{r}=1}+S_a\dot{s}_s$$

$$(1-\lambda_p)\int_{-\theta_0/2}^{\theta_0/2}\int_{s_s}^{s_b}\hat{r}\left(\frac{\partial\bar{\eta}}{\partial\hat{t}}\bigg|_{s_s}+S_a\dot{s}_s\right)d\hat{r}d\theta=-I_f\left(1+\Omega\right)Q_t\big|_{\hat{r}=1}$$

$$\left(\frac{\Theta}{2}\left(s_s+\frac{\bar{\eta}\big|_{s_s}-\eta_{base,0}}{S_a}\right)^2-\frac{\theta_0}{2}{s_s}^2\right)\left[\left.\frac{\partial\bar{\eta}}{\partial\hat{t}}\right|_{\hat{r}=1}+\left(S_a\right)\dot{s}_s+\sigma\right]=\frac{I_f\left(1+\Omega\right)}{\left(1-\lambda_p\right)}Q_t\big|_{\hat{r}=1}$$

$$\dot{s}_s=\frac{1}{S_a}\left[\frac{I_f\left(1+\Omega\right)}{\left(1-\lambda_p\right)}\left(\frac{\Theta}{2}\left(s_s+\frac{\bar{\eta}\big|_{s_s}-\eta_{b,0}}{S_a}\right)^2-\frac{\theta_0}{2}{s_s}^2\right)^{-1}Q_t\big|_{\hat{r}=1}-\left.\frac{\partial\bar{\eta}}{\partial\hat{t}}\right|_{\hat{r}=1}+\sigma\right]$$

Shoreline migration (foreset-bottomset)

$$\bar{\eta}[s_s(t),t]-S_a\left(s_b(t)-s_s(t)\right)=\eta_b[s_b(t),t]$$

$$\left.\frac{\partial\bar{\eta}}{\partial t}\right|_{s_s}+\left.\frac{\partial\bar{\eta}}{\partial r}\right|_{s_s}\dot{s}_s-S_a(\dot{s}_b-\dot{s}_s)=\left.\frac{\partial\eta_b}{\partial r}\right|_{s_b}\dot{s}_b$$

$$\left.\frac{\partial\bar{\eta}}{\partial\hat{t}}\right|_{s_s}-\frac{\dot{s}_s}{s_s}\hat{r}\left.\frac{\partial\bar{\eta}}{\partial\hat{r}}\right|_{s_s}+\left.\frac{\partial\bar{\eta}}{\partial\hat{r}}\right|_{s_s}\frac{\dot{s}_s}{s_s}-S_a(\dot{s}_b-\dot{s}_s)=\left.\frac{\partial\eta_b}{\partial r}\right|_{s_b}\dot{s}_b$$

$$\left.\frac{\partial\bar{\eta}}{\partial\hat{t}}\right|_{s_s}-S_a(\dot{s}_b-\dot{s}_s)=S_b\dot{s}_b$$

$$\dot{s}_b=\frac{1}{\left(S_a-S_b\right)}\left(\left.\frac{\partial\bar{\eta}}{\partial\hat{t}}\right|_{s_s}+S_a\dot{s}_s\right)$$

Estimation of the leaky channel coefficient k_{Qw}

The approach presented herein includes two provisions for underdeveloped juvenile channels; these account for a decrease in the bankfull Shields stress and for flow lost from the channels to the inter-channel area. Concerning the latter, we extract data collected by Hiatt and Passalacqua (2015) across two channels in Wax Lake Delta. The channels Gadwall Pass and Main Pass run along the Western boundary and Eastern Boundary of Main Island, respectively. As shown in Figure A.1, both channels exist beyond the approximate boundary for typical flood inundation as estimated through inundation lengths during flood events (Gelensye et al. 2015).

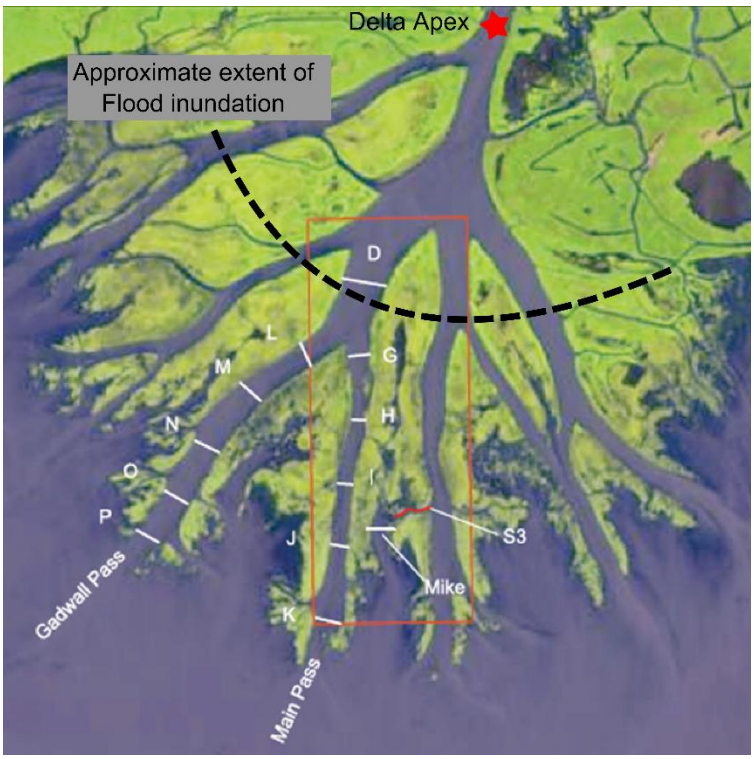

Figure B-1: Figure modified from Hiatt and Passalacqua (2015). An approximation of the typical flooding length scale r_{flood} from results of Gelensye et al (2015) can be estimated from the distance to the shoreline during floods. The lettered cross sections represent locations where discharge was measured in Gadwall Pass and Main Pass.

Measurements by Hiatt and Passalacqua (2015) were not done at flood discharge, but these represent the only such measurements available at this time, so they can act as a baseline representation of how much flow is leaving the delta. Discharge along each channel was measured twice during various times of a tidal cycle. We generalize data from all the discharge measurements of both channels and normalize the discharge relative to the value just downstream of the bifurcation. This allows an estimate of the fraction of flow incoming at the apex that remains in the channel of $\varepsilon_{measured}$, as defined in the main text. Figure

A.2 shows that approximately 60% of the flow at an island apex remains in the channel at the downstream end of the island. Shaw et al. (2016a) suggest 40% based on mass conservation.

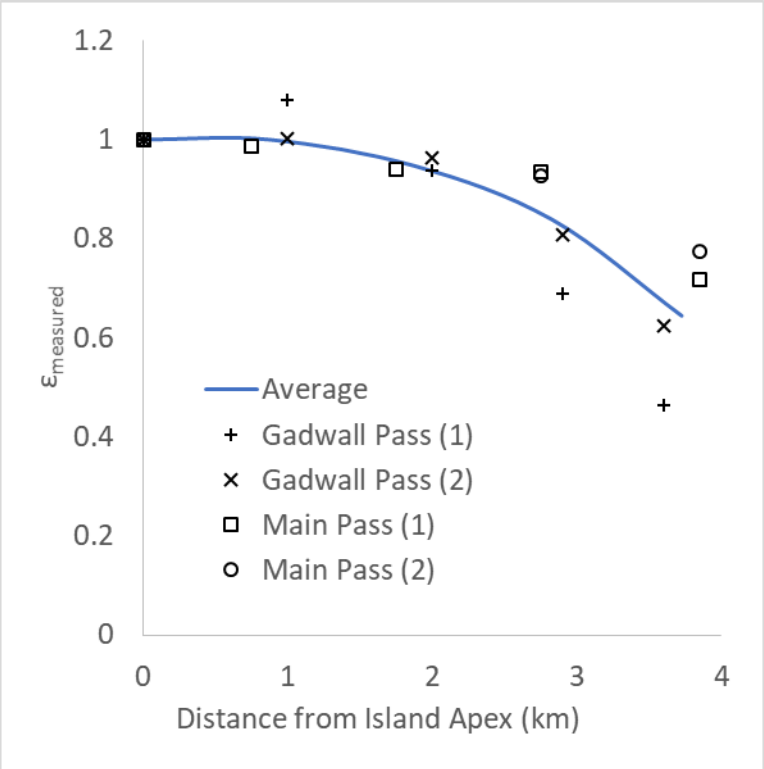

Figure B-2: Measurements by Hiatt and Passalacqua (2015) are collected and generalized to approximate the spatial change in ε from island apex to the periphery of the sub-aerial delta (as shown in Figure A.1). Here ε denotes the fraction of incoming flow at the upstream end of an island that remains farther downstream along the island.

The parameter k_Q, as in Eq. *(23)* in Chapter 3, is chosen so as to yield $\varepsilon = 0.6$ at the delta periphery As shown below.

$$k_{Q_w} = -ln(\varepsilon) = -ln(0.6)$$

Estimation of bankfull Shields decay coefficient k_τ

The decay rate of bankfull Shields stress γ is estimated from field bathymetry data according to several assumptions. Following Eq. (22) in Chapter 3, we can rearrange to solve for γ.

$$\gamma = \frac{HS^{1-m}}{RD\beta D_*^{n}}$$

We can assume grain size is constant throughout Wax Lake Delta as in Kim et al. (2009a). Additionally, since they are naturally low-slope environments, the delta slope cannot vary significantly. We therefore,

make a simplifying assumption that slope is spatially constant. Under these assumptions, γ only varies spatially with depth, so we can estimate $\gamma_{measured}$ as:

$$\gamma_{measured} \approx \frac{H_{bf}\left(r\right)}{H_{bf}\left(r_{flood}\right)}$$

We use mean channel elevations in discrete bins from the generalized 2015 DEM dataset to define this value per the eq. above. The results suggest that γ at the delta periphery is approximately equal to 0.6.

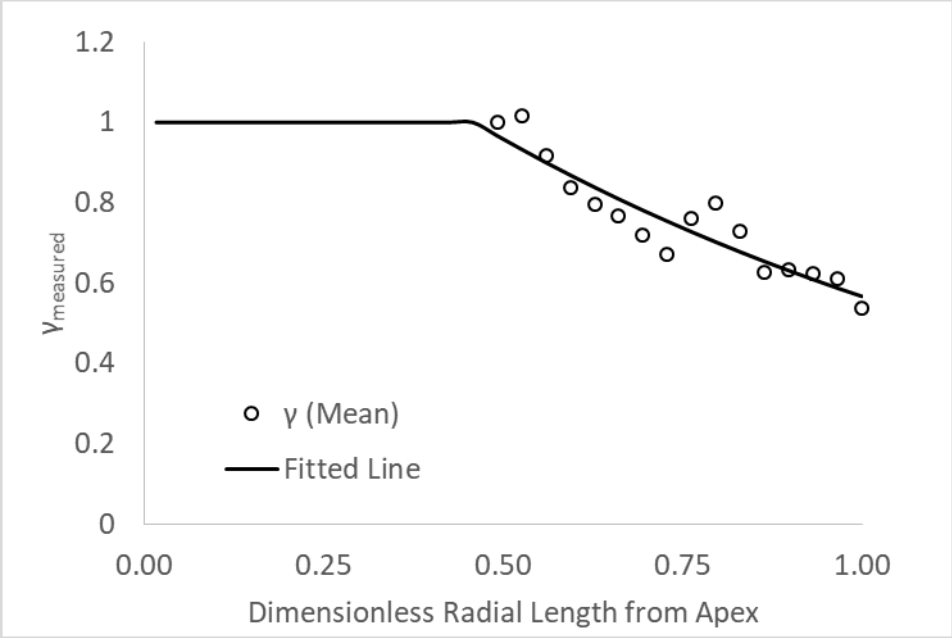

Figure B-3: Estimated values for $\gamma_{measured}$ from 2015 DEM of Wax Lake Delta. These values assume grainsize and slope are constant over the domain of measurement. A fitted line corresponds to Eq. (22) *in Chapter 3 and is used within the numerical model.*

The rate coefficient k_τ can therefore be defined as:

$$k_\tau = -ln\left(0.6\right)$$

Proportion of water and sediment discharge in Wax Lake Delta

Kim et al. 2009 suggest two sediment transport rates that relate to either 30% or 45% of the total flow distributed from the Atchafalaya River. A total sediment budget for the Atchafalaya River was conducted by Horowitz et al. (2001) and adopted by Kim et al. (2009a). The authors assume that sediment and water flux partitioning are equivalent; so 30% of water flux should relate to 30% of the annual sediment budget. Data were collected from Wax Lake Outlet and Atchafalaya river gages (both downstream of their point of bifurcation). There are no other major tributaries or distributaries to this channel, so we assume that the summation of the two gages represents the total water flux in the upstream Atchafalaya and therefore the proportion of flow can be directly calculated from the instantaneous measurements of these flows. We consider data collected on the same day from 1972 to 2015, which accounts for all the data availability. Figure A.4 below outlines the trends in flow partitioning between the two distributaries. From the starting date, Wax Lake Delta appeared to take approximately 30% of the total flow; this value started to rise, and a rock weir was installed in 1987 and maintained until 1995, which brought values down over this period (Reuss, 2004; pg. 342). Following removal, Wax Lake Delta has steadily pulled more water to the latest measurement, suggests a 55/45 split in favor of the Atchafalaya Delta as shown in Figure A.4. In the future, we can explore a parameterization that models an increasing water discharge and sediment transport rate into the delta, with a 7-year removal of sediment supply (Roberts et al., 1997). For now, given the high variability of sediment transport rates in general, modelling with a constant supply rate of water and sediment is sufficient. The results presented in this chapter show that the development of the delta is strongly dependent on the sediment feed rate, but it is unclear whether the trends in this figure will affect morphodynamics.

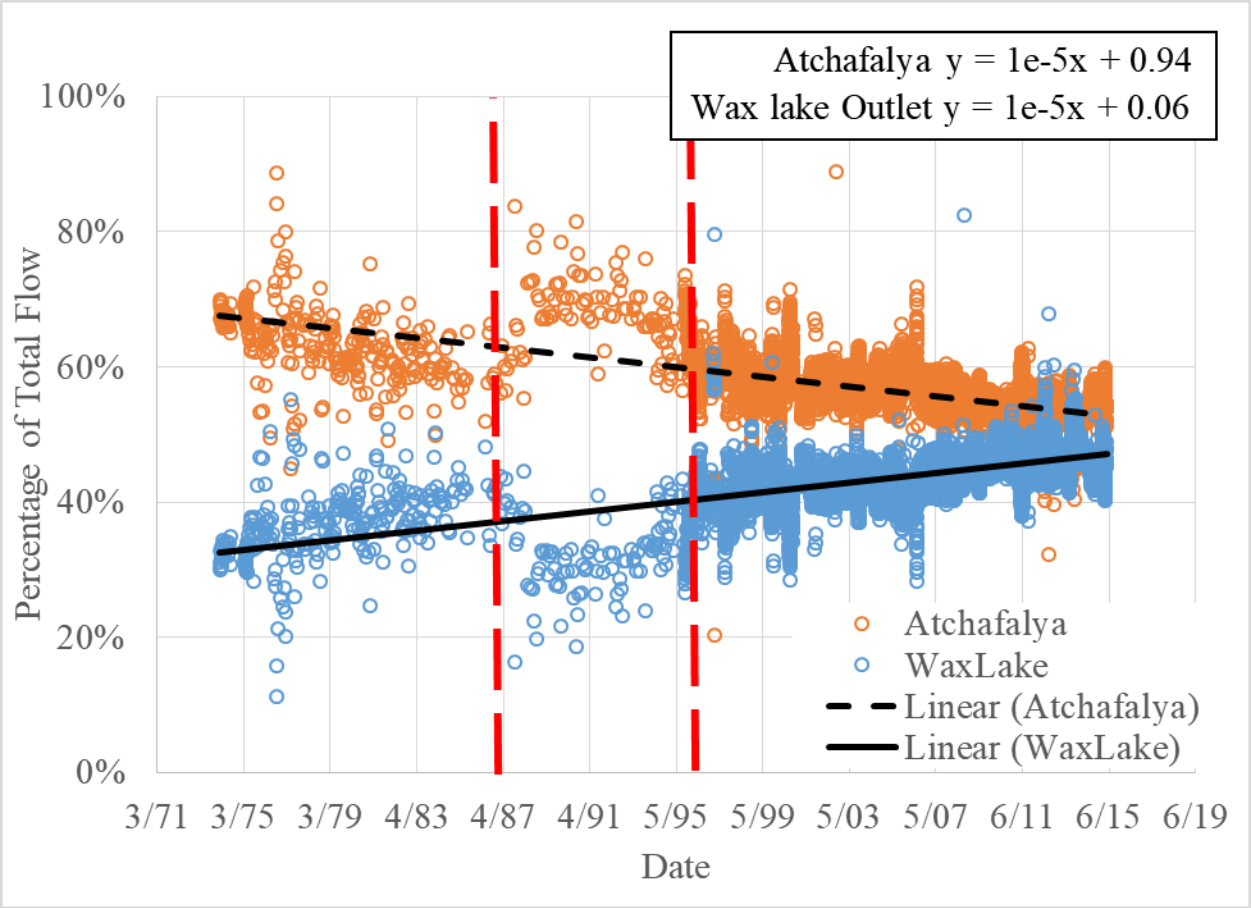

Figure B-4: Proportion of total flow travelling through Atchafalaya Delta and Wax lake Delta from 1972 to present day. The red lines represent a period where a rock weir was emplaced upstream of Wax Lake Outlet, which reduced water discharge. After removal, Wax Lake Delta continues to pull a larger portion of water. Data Collected from USGS Calumet gage for Wax Lake Outlet and Lower Atchafalaya River gage at Morgan City, LA.

Estimated delta angle

The arc length of the entire delta was estimated at discrete radial lengths from the delta apex. Given the arc length and radial distance, one can compute the effective angle for each arc.

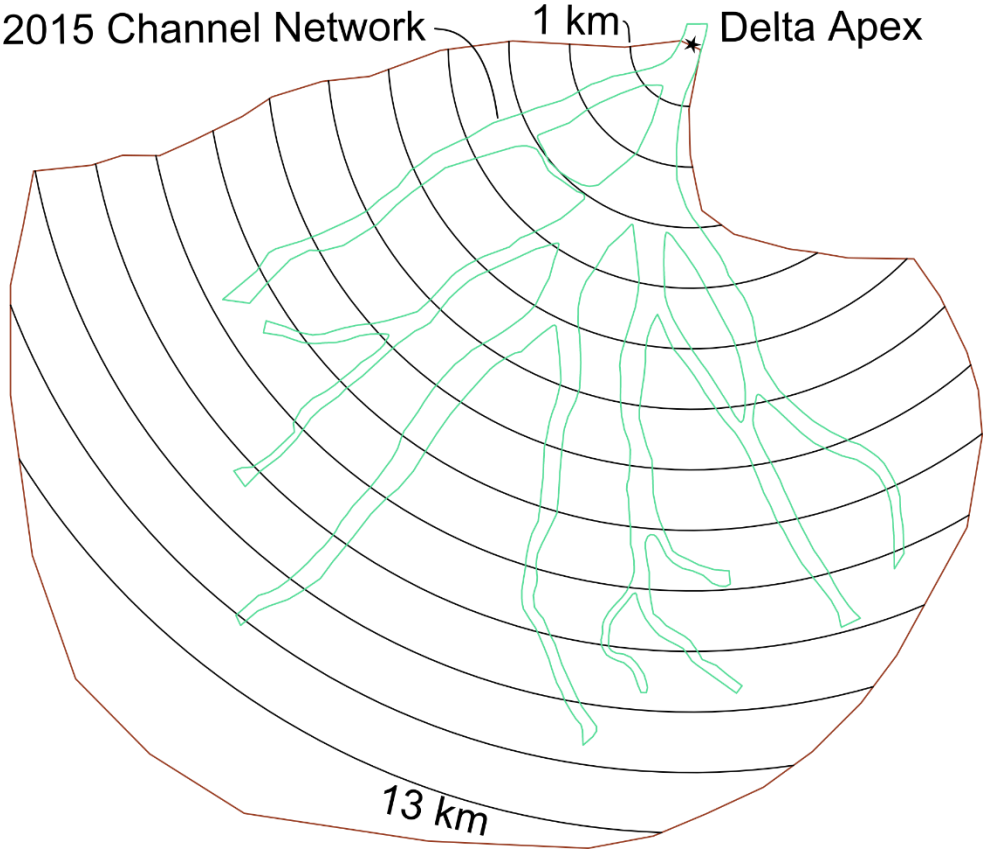

Figure B-5: The extent of the channel network and delta area of WLD in 2015. Channels are estimated from the 2015 DEM and the delta area is approximated by the extent of delta channels.

A single angle value that minimizes the total error across the whole delta is computed as 86 degrees. This value most closely resembles the areal extent of the delta assuming a constant-angle fan-delta within the model. Figure A.6 below shows the relationship between radial length, measured arc length, and effective topset angle. Arc length decreases at the distal end because of uneven sediment distribution at the periphery.

$$\theta_{eff,i} = B_{total,i} / r_i$$

$$\theta_0 = \arg\min \left[\sum_{i=1km}^{13km} \left| r_i \theta - r_i \theta_{eff,i} \right| \right]$$

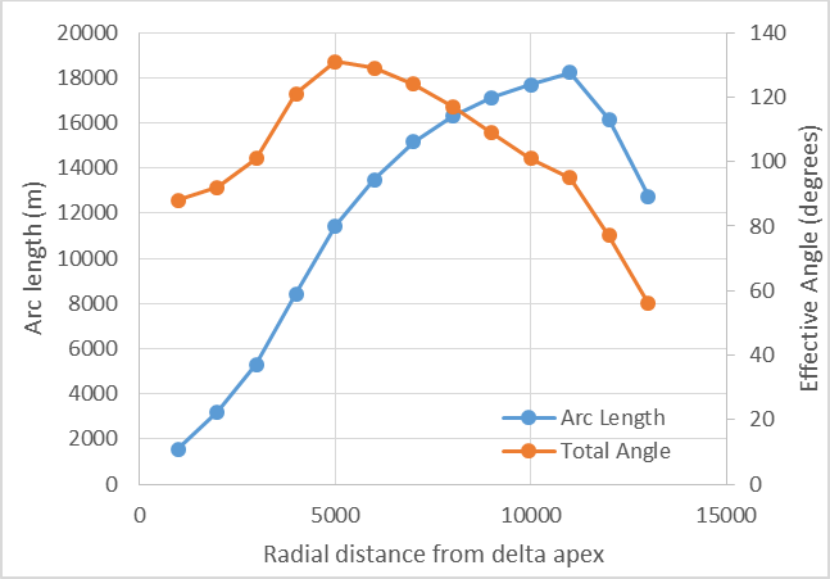

Figure B-6: Estimated topset angle at discrete measurements of distance from the delta apex. We use a topset angle of 86 degrees in the model, as it best represents the total topset area of the current topset at Wax Lake Delta.

Effect of Delta Asymmetry on decreasing total channel width

Measured width in Figure 3-5 shows an increase in width followed by the consistent decrease near the delta periphery. Figure A.7, below, shows a slight decrease in average channel width basinward, but this trend is less severe than total channel width measurements. Measured arc length in Figure A.6 suggests asymmetric delta growth at the delta periphery. Therefore, while individual channels have similar width throughout the delta, asymmetric topset growth leads to fewer channels, which causes rapid decrease in total channel width at the delta periphery. As our model does not account for asymmetric channel growth, this trend should not be compared to our model results.

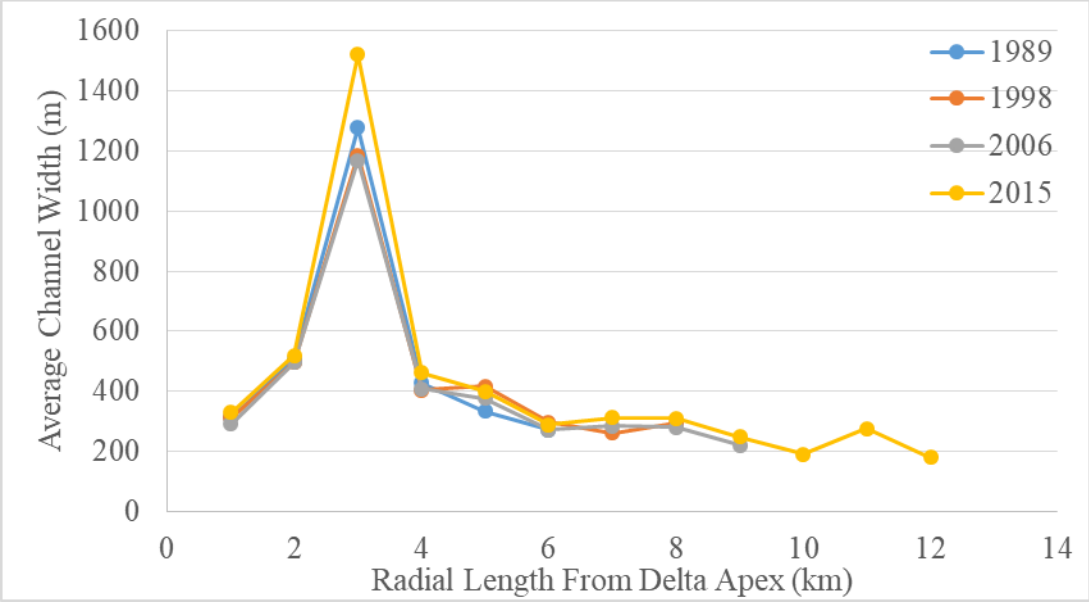

Figure B-7: Average channel width along the delta topset in four measurement years. Beyond the wide section, channel width persistently decreases basinward at an approximate rate of 100 m narrower per every 3-5 km.

Limitations of the models

The framework used herein carries limitations related to simultaneous changes in width and depth. In past self-formed channel models, the change in width is mostly passive. Channel width is only carried into the sediment transport rate equation, while Exner is computed via the total delta topset width. The version presented herein is subject to some oscillations related to the equation setup. Here this is discussed within a single timestep.

Assuming some set of initial conditions, the backwater equation concurrently predicts depth, subject to a fixed downstream elevation; width is also defined relative to the modelled depth, slope and the sediment transport rate, as a function of channel width, is also defined. The Exner equation is computed with representative width and elevation that define the entire delta topset. Changes to channel and floodplain elevations are partitioned relative to the ratio of channel width to topset width. The source of the oscillations lies in this step. The closure for bankfull Shields number implies an equilibrium channel structure, so using it within a time-marching model would be similar to jumping to a steady-state solution instantaneously while solving the temporal evolution toward equilibrium for the other variables. Therefore, changes in channel depth equate to long-term changes in channel width, but are applied immediately in the model. The width change then affects how sediment is distributed between the channel and floodplain. This might make the channel deeper, for example, and in the next timestep, a new width is computed that causes a different sign for $\partial \eta_c / \partial t$. This can cause a feedback loop where channel elevation and channel width oscillate until an equilibrium is reached, after which the model seems to advance smoothly.

The model generally works with the input conditions employed Wax Lake Delta, but within the same model, the constant Shields number equation set, when applied with distributed Exner Equation, is unstable, regardless of time or spatial step. Altering the Czapiga et al. (2018) closure slightly can also result in the same effect version presented here seems to have some oscillation early, when the initial conditions are far from equilibrium, but it is quickly damped and the delta marches forward.

Several approaches have been tried to remedy this issue including: updating width after the Exner equation, only updating width every N time steps, limiting channel width change to a maximum magnitude, and scaling channel width change so the mean magnitude of change equals some prescribed value.

Changing the location where width is updated within a single time step has no long-term effects on model outcome; it only delays effects by a single timestep. Updating width every N timesteps causes massive

change every N timesteps. The last two methods are functional, but they seem to lock the initial conditions in place, which precludes the model's ability to find an equilibrium.

A more advanced version of this model relaxes the assumption of passive floodplain width, i.e. channel width is modeled and the remaining space is allocated to floodplain width. In some cases this version can generate oscillations, but not usually.